Tailored Polymeric Materials to Increase Oil Spill Recovery in Marine Environments

MMS contract number 1435-04-04-CT-36287

Final Report
December 2005

by Victoria Broje and Arturo A. Keller
Bren School of Environmental Science & Management
University of California, Santa Barbara

Table of Contents

	Page
Disclaimer	3
Acknowledgements	3
Executive summary	4
1. Background	6
2. Experimental work	8
2.1 General	8
2.2 Test materials	8
2.3 Seawater	10
2.4 Test oils	10
2.5 Oil weathering	11
2.6 Density, viscosity and surface tension of fresh and evaporated oils	11
2.7 Effect of temperature on oil properties	12
2.8 Contact angle measurements	14
2.8.1 Introduction	14
2.8.2 Contact angle measurements using DCA	16
2.8.3 Effect of roughness on contact angle measurements	18
2.9 Adhesion of oil to contaminated surfaces	21
2.10 Oil recovery at faster speeds using dip-and-withdraw method	22
2.10.1 Experimental setup	22
2.10.2 Results and discussion	24
2.11 Effect of surface pattern on the recovery efficiency	31
2.11.1 Introduction	31
2.11.2 Test surfaces	33
2.11.3 Research method	33
2.11.4 Results and discussion	38
2.12 Effect of oil emulsification on the recovery efficiency	41
2.12.1 Experimental setup	41
2.12.2 Results and discussions	43
3. Conclusions and recommendations	52
4. References	53
Appendix 1. Materials evaluated for this project	54
Appendix 2. Surface pictures of test materials	55
Appendix 3. Contact angle data	71

Disclaimer

This report has been reviewed by the U.S. Minerals Management Service (US MMS) staff for technical adequacy according to contractual specifications. The opinions, conclusions, and recommendations contained in the report are those of the authors and do not necessarily reflect the views and policies of the US MMS. The mention of a trade name or any commercial product in the report does not constitute an endorsement or recommendation for use by the US MMS. Finally, the report does not contain any commercially sensitive, classified or proprietary data release restrictions and may be freely copied and distributed.

Acknowledgements

The project described in this report was funded by the U.S. Minerals Management Service (US MMS) through Contract 0104CT36287. The authors would like to thank MMS for funding this research, personnel of Ohmsett - The National Oil Spill Response Test Facility for oil provided for these experiments, Jeff Kirby for technical support and Eric Liu for help in data collection.

Executive summary

The primary objective of this research was to study the process of oil adhesion to the surface of oleophilic skimmers and to identify parameters affecting the efficiency of the recovery process. This information was used to increase the efficiency of mechanical oil spill recovery equipment by introducing modifications to the shape and material of the recovery surfaces that would result in a greater amount of oil recovery. These changes will result in faster oil spill cleanup and greater environmental protection.

Although oleophilic skimmers are very efficient in separating oil and water and are characterized by a low amount of free water in the recovered product, they nevertheless collect oil at a relatively slow rate, lengthening the recovery process and increasing the cost of response operations. We believe that this is due to the three reasons:

- The selection of the materials used for the adhesion surfaces of oil recovery units has not generally been based on their adhesion properties, but rather on historical practice, price and availability. Significant progress in material and polymer science in the past 10 years now allows us to test materials with a large range of physical properties and tailor them in order to increase their affinity for oil.
- The recovery surface of a smooth disk, belt and drum skimmer has a relatively small surface area that allows only a thin layer of adhered oil to be withdrawn from water. Brush skimmers address this issue by using bristles that significantly increase total surface area of the recovery surface. However, brush skimmers are not very efficient on light oils and petroleum products as only a small portion of the recovered mass can be removed from the bristles. A significant portion of the oil goes back into the water in every pass. For high recovery efficiency, the recovery surface has to have a large surface area and allow close to 100% of recovered product to be scraped into the collector. Ideally, this surface should be able to efficiently recover oils with a wide range of physical properties.
- When oil is withdrawn from the water at 90 degrees (disk skimmer) or at negative angle (most drum skimmers), the recovery surface provides little support for the recovered oil film, allowing the oil to drain freely back into the slick. By recovering oil at a sharp angle to the surface, oil drainage can be slowed down allowing a thicker oil film to remain on the recovery surface and, hence, increasing the amount of recovered product.

A comprehensive study of all aspects of the recovery process allowed us to select the materials with highest oil spill recovery potential; analyze the effects of the initial oil properties, oil weathering and emulsification on the recovery efficiency; and develop a surface pattern that yields a very high recovery efficiency.

The specific goals of the proposed research were to identify:

- The effects of the initial oil properties, oil weathering and emulsification on the amount of recovered oil;
- The physical processes that govern adhesion of oil to various polymeric materials;
- The techniques that would allow comparison of recovery potential of various surfaces;
- The material(s) that have the greatest affinity for different types of oils at various weathering degrees;

- The optimum surface pattern of the recovery surface.

Based on the results of this research, we have determined that:

- Recovery efficiency depends on oil viscosity and, hence, is a strong function of oil properties and temperature. Temperature changes, weathering and emulsification have much greater effects on properties of high viscosity oils than on low viscosity oils;
- Viscous oils above their Pour Point are more easily recovered than light oils, since a thicker slick remains on the surface after withdrawal. The cohesion of viscous oils results in slower oil drainage from the surface;
- Oleophilic elastomers (such as Hypalon® and Neoprene®) have higher oil recovery potential than hard polymeric surfaces, but swelling of some elastomers can reduce their applicability for oil recovery;
- Antistatic Polyurethane and Teflon® can be efficiently used for applications when oil adhesion is not required.
- The Dynamic Contact Angle (DCA) analyzer can provide valuable information about the recovery potential and oleophilicity of various materials. In case of rough surfaces, DCA is less effective in screening materials, although it can still provide some valuable data if rough surfaces are tested with medium viscosity oils rather than with very light or very viscous oils. It was found that for smooth hard plastics and metals, the difference between the advancing and receding contact angles (contact angle hysteresis) is a parameter that can give a reasonable prediction of the material recovery potential. The advancing contact angle indicates the affinity of a material to a test liquid and can give a good description of the wetting/spreading behavior of liquid on solid. The advancing contact angle can be used to evaluate the recovery potential of rough elastomers.
- The dip-and-withdraw technique has higher measurement error than the contact angle technique, but it might be more effective for evaluating rough surfaces or very viscous oils.
- While changing the recovery material can improve the recovery efficiency up to 20%, modifying the recovery surface by introducing a grooved pattern and matching scraper can improve the recovery efficiency up to 100%, compared to a flat surface. The effect of the grooves on oil recovery in a full-scale test with drums may be even more pronounced than the one observed in the laboratory.
- The proposed patterned surface is most efficient on light and medium viscosity oils. In general, a grooved surface is more efficient than a surface covered with bristles except for extremely viscous or semisolid oil.
- Recovery efficiency is higher with decreasing groove angle, although there is a balance between capillary forces holding the oil and the amount of oil within the groove. For viscous oils, the opening of the channel should be wide enough for oil to penetrate inside the groove. For light oils, narrow grooves will perform better.
- A separate detailed study is required to determine optimum recovery surface parameters such as depth and shape of the channels, withdrawal angle and speed.

Through the implementation of the results of this study, a significant improvement in oil spill recovery can be achieved, ultimately leading to faster oil spill cleanup and greater protection of coastal resources.

1. Background

Although pollution prevention must be the primary approach, as long as oil is extracted from offshore oil fields and transported via tankers and pipelines, the potential for oil spills in marine environments exists. According to the Environmental Protection Agency (EPA), almost 14,000 oil spills are reported each year in the United States alone. The largest accidents, such as the tragedy of the Prestige off the shores of northern Spain (2002) and the Exxon Valdez spill in Alaska (1989), make headlines and attract international attention. However, thousands of smaller oil spills occur every day without any publicity. These smaller spills cause significant environmental damage to the local environment. In fact, according to the International Tanker Owners Pollution Federation, routine loading and discharge operations are the main sources of the oil entering the ocean from tankers. Despite preventive measures, oil spills around the world cause significant environmental damage and occur often enough to warrant concern and improvements to current response practices.

The efficiency of oil spill recovery equipment determines the impact of oil spills on coastal ecosystems as well as the time and cost for cleanup. A study of oil spill costs (Etkin, 2000) has shown that when oil is released near sensitive coastlines or resources, the most cost-effective approach is to invest as much equipment, personnel, and energy to keep the oil away from the shoreline or sensitive resource. Once oil has contaminated the intertidal zone, the environmental impact increases substantially. It might take many years before local environments can be restored. Spill experts have estimated that when an oil spill accident impacts a shoreline, as much as 90% to 99% of the cost of cleanup and rehabilitation is associated with shoreline cleanup procedures. The impact on coastal ecosystems, as well as the time and cost of cleanup operations, largely depends on the selected response strategies and the efficiency of recovery equipment. Thus, an immediate response to a spill using optimized contingency techniques can considerably reduce negative environmental and economic impacts.

To select the most efficient oil spill response action, it is important to understand the chemistry and physical behavior of the spilled oil and how its characteristics change over time - in particular its viscosity and emulsion formation. Oil weathering can have significant ramifications with respect to appropriate recovery strategies. Oil is a complicated mixture of many components, and its toxicity, fate and behavior largely depends on its initial properties and composition as well as on specific local environmental conditions. Spreading, evaporation, dispersion, and emulsification can rapidly alter oil properties within several hours, leading to formation of water-in-oil emulsion. During the first 24 hours, different oils can lose from 5 to 50% of light compounds. A major increase in oil viscosity, caused by evaporation of lighter compounds, will occur within hours to a few days. Therefore, the oil that has to be recovered does not have the same properties as the oil that has been spilled. Response measures have a specific “window of opportunity” that is determined by the oil properties, environmental conditions, and properties of the recovery equipment. Past that time, response measures may become ineffective. Failure to consider this fact can dramatically reduce the recovery effectiveness and ultimately the success of the emergency response.

There are a number of contingency measures that are used to respond to the offshore oil spills (Fingas, 2000). Oil slicks can be dispersed, burned, or recovered using mechanical equipment. Natural attenuation is usually inappropriate in coastal waters. Burning and dispersing the oil slick may not be feasible in some cases due to the time required for governmental approval and inability of these techniques to treat emulsified oils. Moreover, in some cases, dispersed oil may cause larger damage than the oil spill itself (e.g. to sensitive fish habitats or fish farms).

Mechanical recovery is the most commonly used oil spill response technique. This technique physically removes oil from the water surface (Fingas, 2000). It usually causes the least environmental impact and therefore is more easily accepted by government agencies and public opinion. Unlike other cleanup techniques, mechanical recovery can be efficiently applied to treat emulsified oils as well as oils of variable viscosities (1,000 – 20,000 cP). The main weakness of mechanical cleanup is the recovery rate. It may be very time consuming and expensive when employed on a large scale. It requires a large number of personnel and equipment. Every additional hour of cleanup time, often due to the inefficiency of the recovery equipment, can increase the cost of the recovery by thousands of dollars.

An adhesion skimmer is probably the most common type of mechanical recovery equipment. It exploits the property of oil to adhere to the rotating skimmer surface in preference to the water. The rotating surface lifts the oil out of the water to an oil removal device (e.g. scraper, roller, etc.). The adhesion surface is the most critical element of the skimmer as it determines the efficiency of recovery. Various shapes of the recovery unit, such as a mop, belt, brush, disc, and drum, have been developed to increase skimmer efficiency. Despite these changes, the materials used to manufacture the surface of adhesion skimmers have remained the same. Steel, aluminum, and general-use plastics had been in use for more than 25 years. Material selection has not been based on the adhesive properties, but rather on historical practice, price and availability. Very little effort has been made to optimize the recovery efficiency by studying the properties of the recovery materials and their influence on the efficiency of the recovery process.

To our knowledge, there have been only two studies of the dependency of oil recovery on material properties. A study by Jokuty et al (1996) aimed to test the adhesive properties of fresh and evaporated oils with a number of materials such as steel, plastic, glass, Teflon, ceramic, and wood. This study indicated that oil adhesive properties vary for different oil weathering degrees and surface material combinations. Ceramic and Teflon were found to pick up twice as much oil as steel.

A study by S. Liukkonen (1995) on plastics, stainless steel and ice, also found some dependence of oil recovery on surface material type and surface roughness. However, there was no attempt to develop new materials for oil recovery in either of these studies.

Both these studies tested fresh and evaporated oils only. The adhesion properties of oil emulsions have not been studied. We believe that information regarding the effect of oil emulsification on the adhesive properties will be extremely useful for understanding the real processes governing oil behavior during the recovery process. Fresh oil exists only during a very short period of time; emulsions start forming within a few hours following a spill. By the time mechanical equipment is deployed on a spill site, it might have to recover an oil emulsion with water content as high as 50-80%. Emulsion formation radically changes oil properties and recovery efficiency. This fact needs to be taken into account when designing the oil recovery process.

The study of adhesion of oil and oil emulsion to the recovery device on a molecular level has not been a subject of comprehensive scientific investigation. Knowledge of the magnitude of forces governing the adhesion will help to find the most effective way to enhance oil recovery rate. Over a past decade, an intensive research on wettability and adhesion properties of various materials has been conducted in the fields of lithography and semiconductors. These studies found that for the same testing liquid, such properties of polymer as composition, surface tension, hydrophobicity and surface charge greatly affect its wettability. Roughness, both on macroscopic and microscopic scale was also found to have tremendous significance. Although, polymeric materials were tested for their affinity for water and various chemicals, their adhesion to oil was not studied.

2. Experimental work

2.1 General

The research process consisted of three phases. During the first phase we studied the adhesion processes at the molecular level. A theoretical model describing the forces and processes influencing adhesion in three-component system (oil-water-solid surface) was developed. More than 30 polymeric materials were evaluated based on their oleophilicity. This preliminary evaluation helped to narrow the list down to 12 materials with the highest oil recovery potential. This work was conducted under a seed grant from the University of California Toxic Substances Research and Teaching Program.

The second phase, funded by the U.S. Minerals Management Service and described in this report, involved a study of oil affinity and adhesion to the surfaces of various properties and shapes. For these tests we used a dynamic contact angle analyzer that utilizes the Wilhelmy plate technique (Cahn Radian 315), manufactured by Thermo Electron Corporation. This advanced equipment is capable of measuring with high accuracy adhesion-related parameters such as dynamic contact angle, surface tension, surface free energy, surface polarity and amount of adhered oil. We also used a "dip-and-withdraw" technique described by Jokuty et al. (1996). All the experiments were carried out in a temperature-controlled room at 25 ± 1 °C to model Gulf of Mexico environment, at 15 ± 1°C to simulate an oil spill in temperate regions and at 5 ± 1°C to simulate an oil spill in cold regions.

Following the detailed laboratory study we selected the most promising materials and surface patterns and used them to manufacture drums that were installed into existing skimmers for full-scale oil spill recovery test at Ohmsett – The National Oil Spill Response Test Facility, which is Phase 3 and is currently completed and reported under separate cover. The Ohmsett facility is capable of simulating an environment that most closely represents the real conditions of oil cleanup at sea. Following the standard procedures developed at Ohmsett for testing mechanical recovery equipment, we tested new materials and surface patterns as well as some materials that are currently being used on oil skimmers in order to determine the effect of surface modifications on oil spill recovery efficiency. Funding for the full-scale oil spill test at Ohmsett was also provided by MMS.

2.2 Test materials

Appendix 1 lists materials that were initially evaluated with respect to key physicochemical properties in order to determine their potential for oil recovery. Only 12 of them were considered fore more detailed study. Two groups of materials were tested.

Hard polymers and metals:

- Stainless Steel
- Aluminum
- Acrylonitrate-Butadiene-Styrene (ABS)
- Polyvinyl chloride (PVC)
- Low Density Polyethylene (LDPE)
- Ultra High Molecular weight Polyethylene (UHMW PE)
- Polypropylene (PP)

Elastomers:

- Ethylene Propylene Diene Monomer (EPDM)
- Ozone resistant Hypalon® rubber
- Styrene-Butadiene Rubber (SBR)
- Epichlorohydrin rubber (ECH)
- Neoprene® rubber

All test materials were purchased from McMaster-Carr (P.O. Box 54960, Los Angeles, CA 90054-0960. http://www.mcmaster.com/) in sheets with a thickness of 1.6 mm. They were cut to equal test strips of 25x25 mm (samples for the contact angle measurements) and 150x25 mm (samples for dipping tests). To smooth the edges of the polymer samples, an endmill was used to remove the edges damaged by the shearing process, leaving smooth edges of homogeneous roughness (Fig 1.).

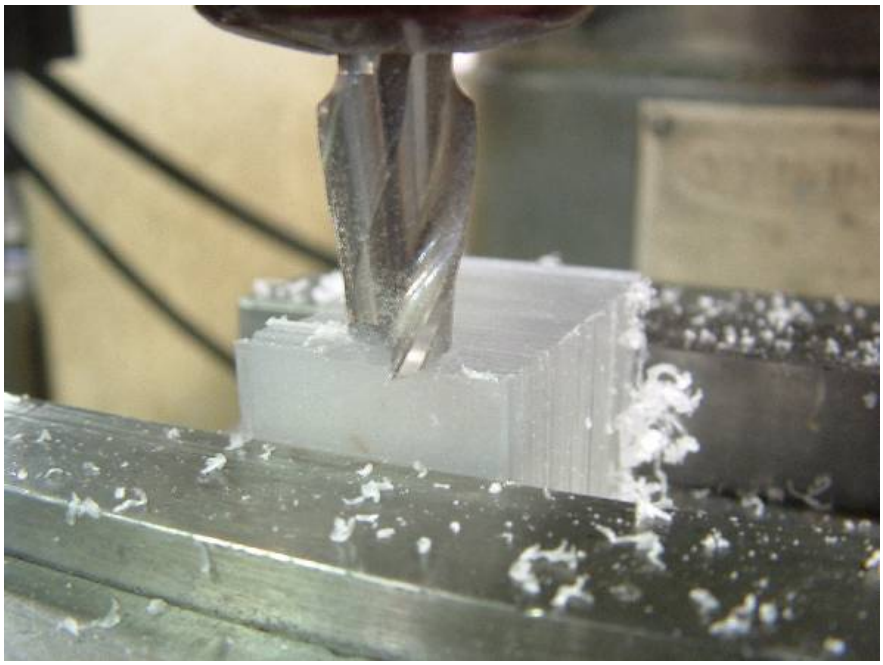

Figure 1. Polyethylene slides installed into endmill.

The roughness of the samples was measured with the Wyko Optical Profilometer (Wyko NT2000). The root-mean-square roughness (as measured at 50x magnification) of the main surface of the plastic samples was less than 100 nm. The roughness of elastomers was on the order of 100-1000 nm. Metals had a very specific surface structure (see Steel in the Appendix 2 as an example), and although their effective roughness was similar to the one of plastics, Using the Wyko profilometer, the surface roughness was estimated to be on the order of 450 nm. Pictures of the samples at 10x and 50x magnification as well as some surface statistics are presented in Appendix 2.

Prior to measuring contact angle or adhesion, all samples were 1) washed in warm water with liquid detergent, 2) rinsed in deionized water, 3) rinsed in ethanol, 4) rinsed with deionized water, 5) blow-dried using nitrogen , 6) placed in a sterile container, 7) left for 12 hours in the temperature controlled room to reach achieve thermal equilibrium. Fresh oil samples and new test surfaces were used for each test. Samples were not reused except for steel and aluminum. Metal samples were pre-

cleaned using chloroform, followed by heptane and methylene chloride to remove all oil residues. Then the metal test strips were subjected to the cleaning process described above.

2.3 Seawater

Seawater used for the experiments was obtained from the intake located several miles offshore in the Santa Barbara channel, to more realistically consider ocean water without the interaction with the shoreline. Salinity of this water is 33.6 ppt. The comparison of physical properties of waters from various sources is presented in Table 1.

Table 1. Physical properties of different water samples at 15°C.

Sample	Density (g/cm^3) ±0.001	Surface Tension (mN/m) ±0.1
Distilled water	1.0002	73.5
Seawater	1.033	74.8
Ohmsett water	1.028	74.0

2.4 Test oils

HydroCal 300 (a hydrotreated naphthenic medium grade lube stock), IFO-120 (Intermediate Fuel Oil), Cook's Inlet and Pt. McIntyre (Alaskan crude oils), were used for this study. The use of various oils helped to determine the effect of chemical composition, viscosity, surface tension, weathering and emulsification degree on adhesion properties.

Every crude oil was analyzed using separation of Saturates, Aromatics, Resins and Asphaltenes (SARA analysis). The SARA separation of crude oil on fractions is based on the solubility characteristics of these groups and involves a combination of precipitation and elution chromatography. When crude oil is diluted with n-heptane, asphaltenes precipitate and are collected using a filtering assembly. The soluble fraction - Maltenes (also called Petrolenes) are then adsorbed onto silica gel (100-200 mesh, pore size 150 Å, pore 1.2 cm^3/g, active surface 320 m^2/g) in a packed chromatographic column and then fractionated into the saturates, aromatics and resins by solvent elution with n-heptane, toluene and 95:5 mixture of methylene chloride and methanol, respectively. The volume of solvent was 40 times larger than a volume of oil sample. These three fractions are then recovered by solvent evaporation using a rotary evaporator (Rotavapor Buchi RE111).

The relative percentage (by weight) of SARA fractions of the test oils are presented in Table 2.

Table 2. SARA composition of tested oils.

fresh oil	Saturates (%wt.) ±1%	Aromatics (%wt.) ±1%	Resins (%wt.) ±1%	Asphaltenes (%wt.) ±1%
IFO-120	32	50	10	8
HydroCal 300	75	25	0	0
Pt. McIntyre	78	16	4	2
Cook's Inlet	80	15	3	2

2.5 Oil weathering

To obtain weathered fractions of crude oils, Cook's Inlet and Pt. McIntyre crudes were evaporated using a Rotavapor Buchi RE111. Oil was heated using a water bath at 90°C. Vacuum was applied to the system to facilitate removal of the lighter fractions and to transfer them into the condensation chamber. Lighter fractions were condensed in a glass container that was cooled down using refrigerated water (at 2°C; closed cycle). A small part of the lighter fractions that was able to escape condensation at 2° C was trapped using a cold vapor trap cooled down to -110°C in order to prevent air contamination and insure complete mass balance. All vapor fractions condensed at this temperature. Figure 2 illustrates the experimental setup.

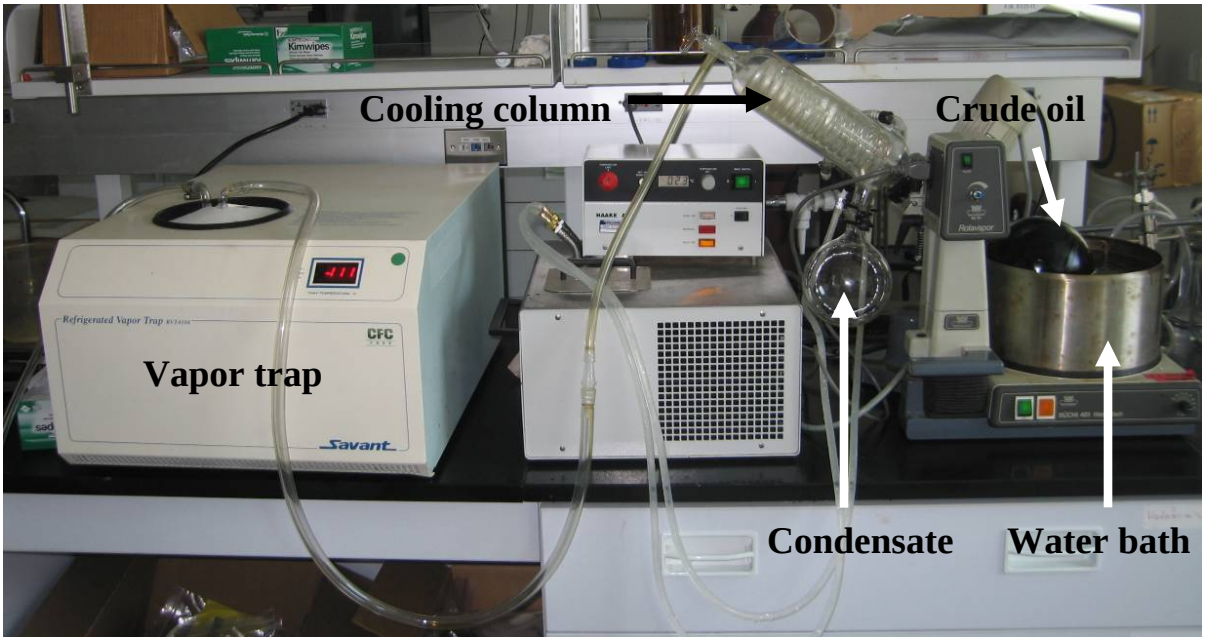

Figure2. Evaporation/weathering system.

To simulate weathered oils, 15% of each crude oil was evaporated for the purpose of the experiments. Condensed lighter fractions were stored for use in future experiments. Oil residue with 15% weight loss was slowly cooled down and stored in a temperature controlled room in a sealed container, to be used for further experiments.

2.6 Density, viscosity and surface tension of fresh and evaporated oils

All measurements were carried out in the temperature controlled room at 25°C, 15°C and 5°C (±1°C). Oil density was measured using a standard Specific Gravity Bottle for viscous fluids according to ASTM D70 and D1429. These methods can be summarized as follows. The test liquid is placed in a pre-weighted glass container of known volume. An opening in the glass stopper allows excess liquid to be removed from the container once the glass stopper is set in place, to achieve a precise liquid volume of 29 ml. Then the container with oil is weighted. Density of liquid is determined by relating mass of liquid to volume. At least 3 measurements are performed for each liquid to ensure quality of data.

Surface tension of the oils was measured using a Dynamic Contact Angle (DCA) analyzer (Cahn Radian 315) following a standard procedure for surface tension measurements using a Du Nouy ring,

as described in the DCA manual. At least 5 measurements were performed to ensure the accuracy of the data.

Oil viscosity was measured using a Brookfield DV-II+ Pro Programmable Viscometer following the standard viscosity measurement procedure described in the manual. At least 3 measurements were performed to ensure the accuracy of the data.

The properties of fresh and weathered oils are presented in Table 3.

Table 3. Properties of fresh and weathered test oils.

	density (kg/m3)			*viscosity (cP)*			*surface tension (mN/m)*		
temperature	5°C	15°C	25°C	5°C	15°C	25°C	5°C	15°C	25°C
Cook's Inlet	0.8724	0.862	0.847	60	9.6	5	28.46	26.6	24.5
Pt. McIntyre	0.8914	0.886	0.871	160	24	14	29.3	28.3	27.3
HydroCal 300	0.9221	0.921	0.905	1296	342	162	33.53	32.5	31.8
IFO-120	0.9669	0.965	0.949	7978	1540	487	34.08	32.4	31.8
weathered Cook's inlet 15 % loss	N/A	0.898	0.882	N/A	32	16	N/A	26.98	24.5
weathered Pt. McIntyre 15% loss	N/A	0.923	0.907	N/A	95	60	N/A	30.7	29.4

The composition of crude oils with respect to their carbon, hydrogen and nitrogen content is presented in Table 4. The analysis was performed using an Organic Elemental Analyzer - CHN (Control Equipment Corp. Model: CEC 440HA).

Table 4. Elemental analysis of test oils

	Weight Percent				*C/N*	*C/H*
Sample	*C*	*H*	*N*	*other components*	*ratio*	*ratio*
Cook's Inlet fresh	75.50	10.59	0.60	13.31	125.51	7.13
Weathered Cook's Inlet	80.77	11.40	0.54	7.28	149.72	7.08
Pt. McIntyre fresh	77.56	10.82	0.55	11.07	140.70	7.17
Weathered Pt. McIntyre	82.52	11.34	0.45	5.69	181.80	7.28
IFO-120	85.71	10.71	0.73	2.86	118.18	8.01
HydroCal 300	87.00	12.44	0.37	0.19	235.22	6.99

2.7 Effect of temperature on oil properties

The effect of temperature on the properties of crude oils and other petroleum products is presented in Figures 3 through 5.

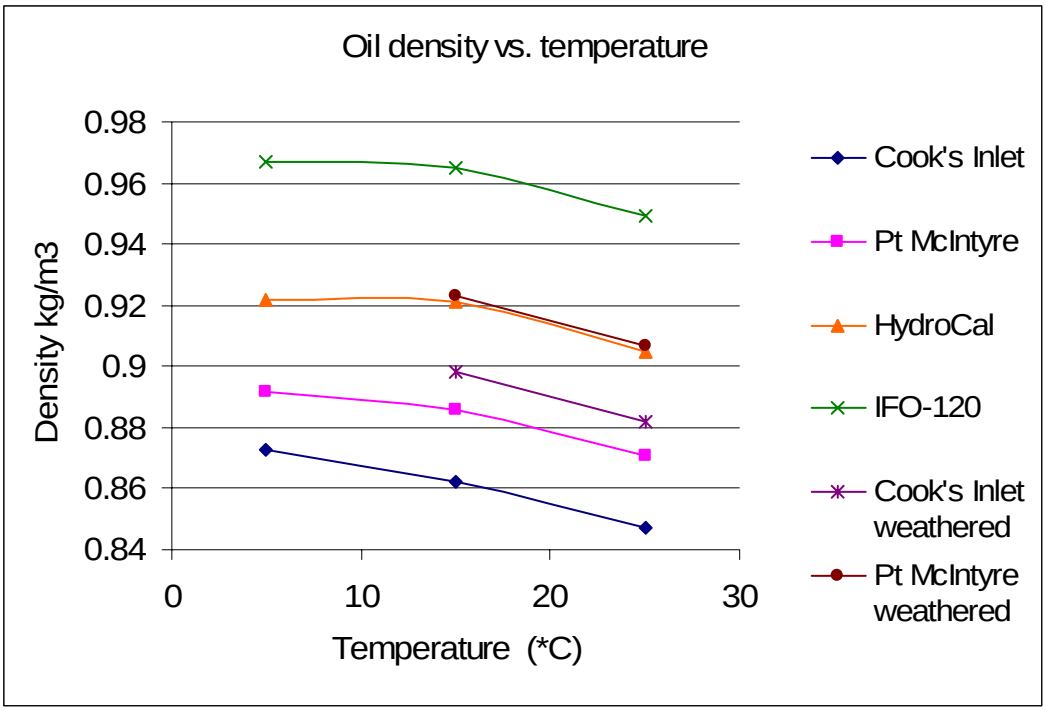

Figure 3. Effect of temperature on the density of crude oils and other petroleum products.

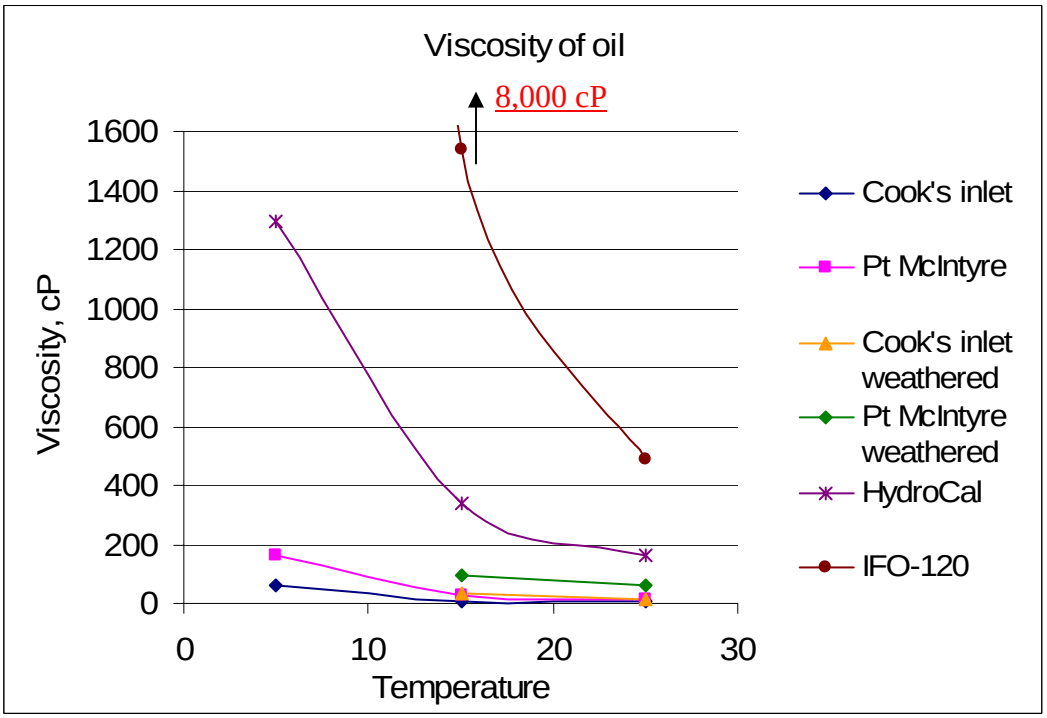

Figure 4. Effect of temperature on viscosity of crude oils and other petroleum products.

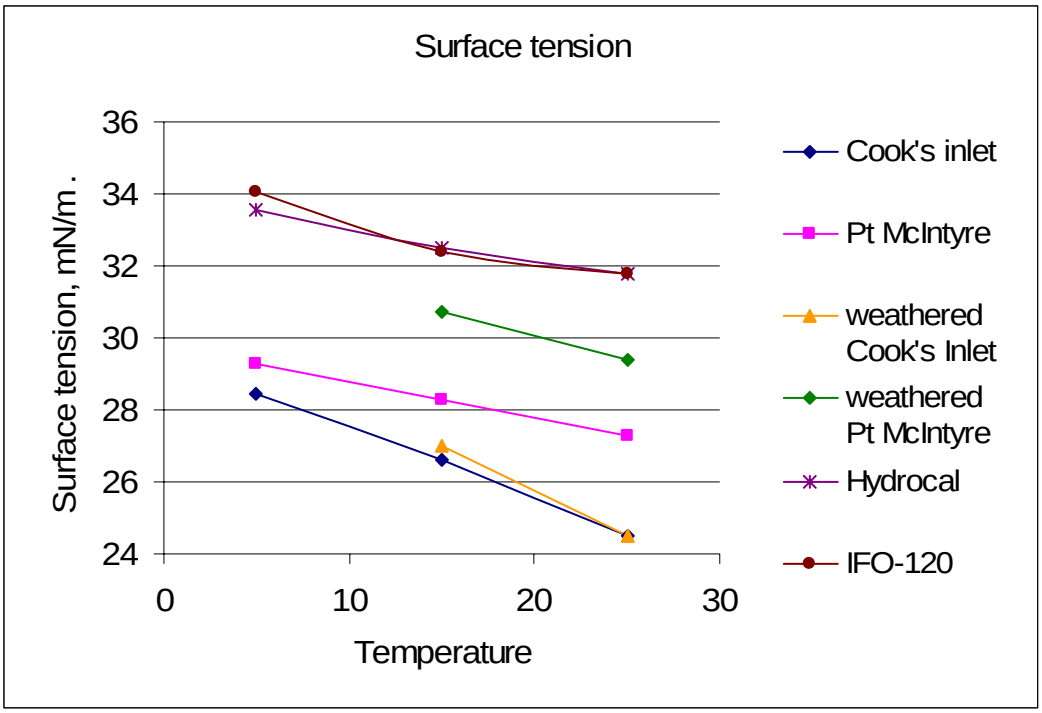

Figure 5. Effect of temperature on surface tension of crude oils and other petroleum products.

As illustrated on Figures 3 and 5, the density and surface tension of all the oils tested decreased with increasing temperature, and the rate of decrease was similar for all oils for each of these properties. The effect of temperature on oil viscosity had a different pattern (Figure 4). More viscous oils exhibited much larger decrease in viscosity than less viscous oils. It indicates that during oil spills in cold waters, viscous oils will exhibit dramatic changes in physical properties and may become semi-solid, which would have a significant effect on oil behavior and oil spill recovery efficiency. These results clearly show the importance of considering the effect of temperature on oil properties and thus on the efficiency of the recovery process.

2.8 Contact angle measurements

2.8.1 Introduction

Contact angles of liquids on polymer surfaces are widely used to predict wetting and adhesion properties of these solids by calculating their solid-vapor surface tension. This method has been widely discussed in the literature (e.g. Wake, 1982). While the theory is based on the equilibrium of an axisymmetric sessile drop on a flat, horizontal, smooth, homogeneous, isotropic, and rigid solid, it is generally found in practice that a static contact angle does not give a correct representation of the wetting process. It is believed that using the Wilhelmy plate technique and measuring a dynamic contact angle provides more accurate values. The Dynamic Contact Angle (DCA) analyzer overcomes the limitations of static contact angle measurement devices by measuring much larger surfaces on liquid solutions rather than single drops on a plate. This eliminates the risk of concentrated contaminants or incomplete profiles. The DCA analyzer operates by holding a plate in a fixed vertical position, attaching it to a microbalance and moving a probe liquid contained in a beaker at constant rate up and down past the plate. A unique contact angle hysteresis curve is produced by the microbalance as it measures the force exerted by the moving contact angle in

advancing and receding directions (Figure 6.). The dynamic contact angle is then calculated from the modified Young's equation (Wilhelmy equation)

$$\Theta = \cos^{-1}(F/\gamma p) \quad (1)$$

where Θ is the contact angle, F is the applied force, γ = surface tension, and p is the wetted perimeter.

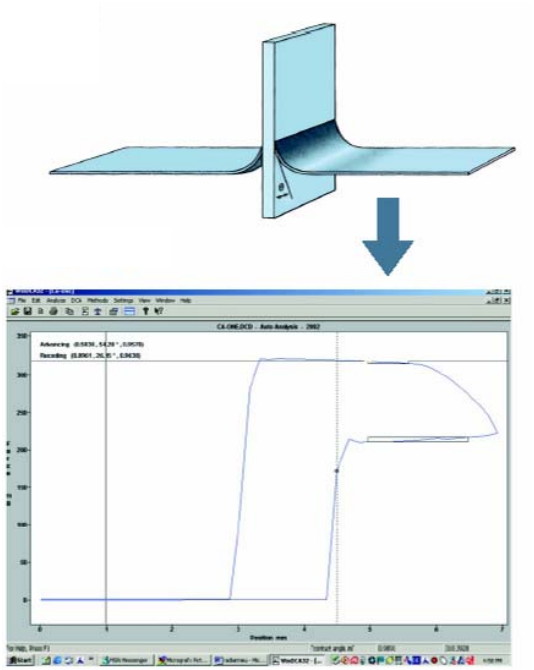

Figure 6. Dynamic contact angle analysis (Thermo Electron Corporation)

The advancing angle illustrates the affinity between the liquid and solid surface (the smaller the angle, the better the spreading). A 180° angle represents complete non-wetting, 0° angle represents complete wetting. The difference between the advancing and receding contact angles is called the contact angle hysteresis. This parameter measures the ability of the solid surface to retain molecules of liquid during the receding phase. If liquid remains on the surface after the surface is withdrawn from the oil, the receding contact angle is 0°.

In addition to the dynamic contact angle, the DCA (Thermo Electron, Radian 315) can also measure surface adsorption by measuring the weight increase of the test surface (plate, fiber or set of fibers) while the sample is withdrawn from the oil. Oil recovery is measured as the weight of adhered oil per unit surface area. This pick-up technique was used in both previous studies of oil adhesion to various materials by Jokuty (1996) and Liukkonen (1995). This method is very reliable for studying oil adhesion properties. Using new advanced equipment allows automating this technique and achieving more consistent and reliable results. The characteristics of the DCA are presented in Table 5.

Table 5. Characteristics of Cahn Radian Dynamic Contact Angle Analyzer

Surface Tension Range	Contact Angle Range	Surface Tension Precision	Contact Angle Precision	Balance Precision	Max Sample Weight	Max Sample Diameter	Min Fiber Diameter
1-1000 mN/m	0-180 degrees	± 0.001 mN/m	± 0.01 degrees	1 μgram	100 grams	75 mm	0.1 mm

The Dynamic Contact Angle analyzer has been successfully used by other researchers studying wetting and adhesion properties of various surfaces (e.g. Lee et al., 1998 and Della Bona, 2004).

2.8.2 Contact angle measurements using the DCA

In general, the contact angle measurement process can be summarized as follows:

The size of the test surface (≈25x25 mm) is measured using an electronic micrometer with a precision of ± 0.1 mm. Then, the sample is placed in the test chamber above the test liquid (oil or water), making sure that its lower surface is parallel to the liquid surface. The test surface is automatically submerged into the test liquid at a rate of 80 μm/sec until 20 mm are submerged, and then the test surface is withdrawn at the same speed. The instrument measures the force on the test surface as it enters the liquid, is submerged and then is retracted. The software calculates the corresponding advancing and receding angles as well as the amount of the residue remaining on the surface at the end of the experiment. Five to ten measurements are made for each liquid-test surface combination to ensure the accuracy of the data.

The relation between contact angle hysteresis and recovered mass for plastics and metals is presented on Figure 7. Every line on this graphic represents values of a contact angle hysteresis for all solid surfaces and one test oil. Every dot represents a hysteresis value for each individual type of hard polymer or metal.

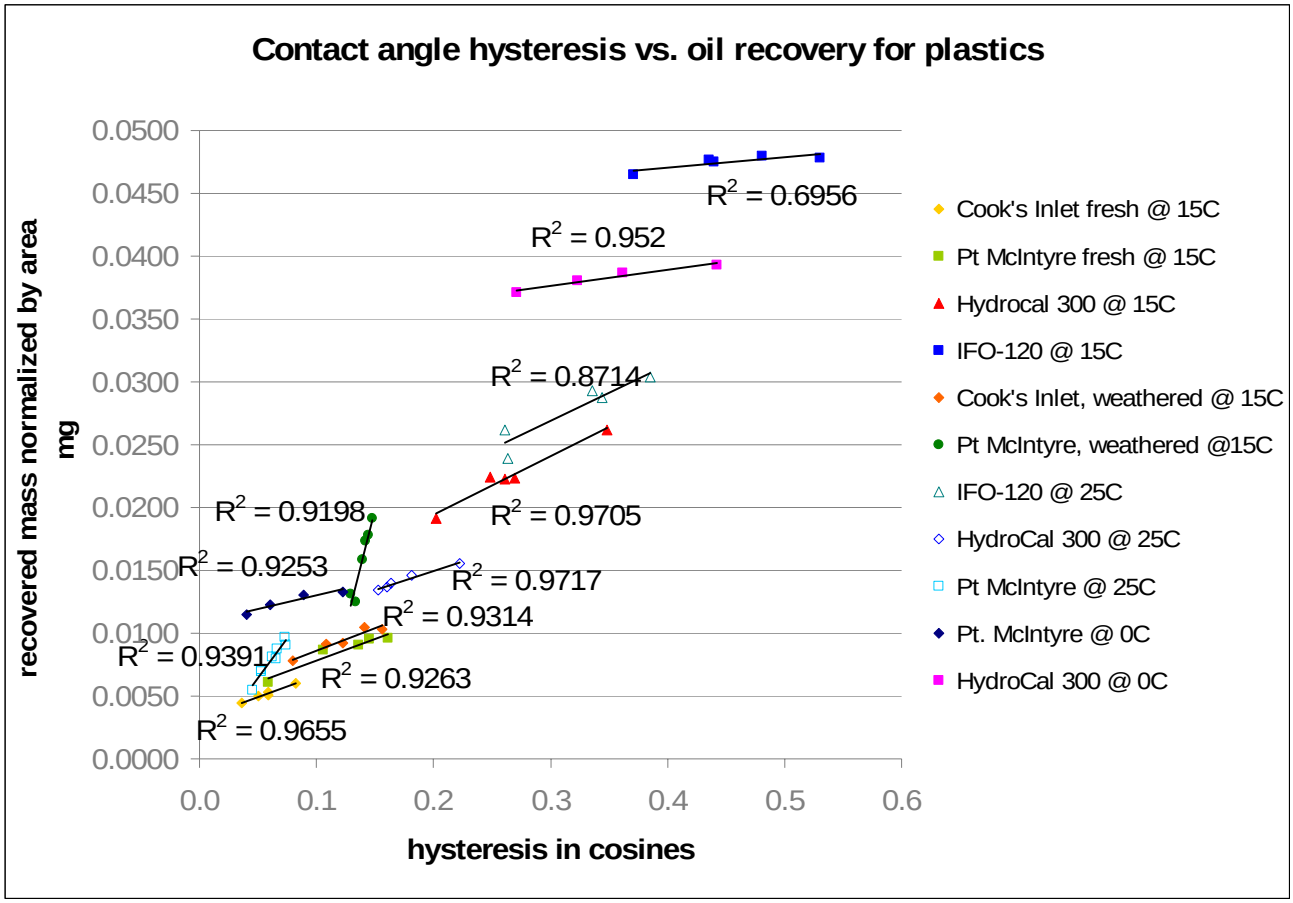

Figure 7. The relation between contact angle hysteresis and recovered mass for polymers and metals

Because of the sensitivity of contact angle measurements to the surface roughness of the test materials, data for hard polymers can not be directly compared with data for elastomers. All materials were compared only to materials within the same roughness group. Contact angle experiments using hard polymers and metals (with low roughness) showed that the best criterion for comparing materials is the difference between advancing and receding contact angles, also denominated the contact angle hysteresis. For the analysis, we assumed that the cosine of receding angle is equal to 0, since an oil film remains on the surface, representing a complete wetting.

Spreading of oil on the test surface is determined by the affinity of the surface for the test liquid: a higher cosine of an advancing contact angle increases spreading. When the objective of the study is to determine the penetration of oil into certain materials such as soils or sorbents, only the advancing angle should be used for the comparison between materials as it represents wetting ability of a liquid towards a test material in the advancing direction. Recovery of oil is more complicated than that. Not only should the test surface have a reasonably high affinity for the oil to allow spreading, but most importantly, it must be able to retain the oil film on the surface, slowing drainage during the withdrawal process.

Figure 7 shows that plastics and metals with higher hysteresis tend to recover more oil. The difference in the recovered amount of oil can vary up to 30% between tested materials. In general, polypropylene and aluminum were found to have higher oil spill recovery potential in a water-free environment, while polyethylene had the lowest recovery efficiency. It must be noted though, that this situation might change in the presence of water, because high surface energy materials have also

high affinity for water which would have certain ramifications on the recovery process. It is somewhat challenging to study oil spill recovery in water-wet environment at the laboratory due to the significant influence of a scale effect on the results of the experiments.

Figure 7 shows that the amount of recovered oil is strongly affected by the oil properties. More dense and viscous oils (IFO and HydroCal) form a thicker film on the test surface leading to higher recovered mass. Less viscous oils form thinner films which yield a lower recovered mass. As oil weathers and becomes more viscous, it forms thicker films and the total recovered mass increases. As Figures 4 and 7 show, increasing temperature causes a decrease of the contact angle hysteresis and viscosity, resulting in a thinner oil film and decreasing the amount of oil remaining on the surface.

Variations in the contact angle measurements were most likely caused by the imperfections in the surfaces of the industrially manufactured polymers, variations in roughness and errors in the measurement of sample weight. The variation in weight measurements were about 1- 13 % (reaching 20 % for oleophobic materials), while variations in contact angle measurements were less than 3 %.

It must be noted that recovered oil mass measured by DCA cannot be directly translated into oil recovery by skimmers. Laboratory experiments involving surface withdrawal are done at a very slow rate and may not fully represent the large scale process. At this phase, the aim was to study the affinity of materials to oil.

Measurements of contact angles had shown that hydrophobicity is not related to oleophilicity. Hydrophobic materials such as Teflon® and Antistatic Polyurethane are also oleophobic. Some oils may adhere to polyurethane if they remain in contact for a long enough time, but the oil can be easily removed, unlike the interaction between oil and other polymers. These materials may be used for applications where oil adhesion is not desired.

2.8.3 Effect of roughness on the contact angle measurements.

The amount of oil recovered by various surfaces varies not only due to the chemical properties and hydrophobicity of the surface, but also due to their roughness. Elastomers have significantly larger surface roughness compare to hard polymers and metals. Elastomers don't allow the precise measurement of a contact angle, as the measured angle is predominantly determined by the local surface roughness and not by the affinity of material for the test oil. For future experiments, a special surface with a very low roughness should be made from the polymeric mold. This would allow better analysis of the material affinity for various oils. It must be noted though that in this case, only oleophility of the material can be studied. DCA data for smooth elastomers will not be able to describe the recovery (oil retaining) potential of the materials as their oil retention mechanism is determined by their roughness. Recovery tests such as dip-and-withdraw technique can be used for rough elastomers and will provide a meaningful comparison between the recovery potential of various materials for as long as they are compared using the amount of recovered oil.

Current DCA measurements for rough elastomers provided a relative comparison of selected elastomers, which allowed the selection of the materials with the highest recovery potential. These contact angle data should not be compared directly to the contact angle data obtained for hard plastics and metals. The oil retention mechanism of elastomers is predominantly determined by their roughness, while hard polymers and metals retain oil due to their ability to rearrange the molecules of liquids close to the surface. That's why a contact angle hysteresis is used to describe the recovery potential of hard plastics and metals, while a cosine of advancing angle is used to describe the affinity of oils to elastomers. If oil can penetrate into the elastomeric structure, it will be retained there during the withdrawal. In this case, smaller advancing angle (higher affinity of oil to the material) corresponds to the higher recovered mass. The difference between the surface structures of

hard polymers and elastomers is illustrated on Figure 8 using an example of polypropylene and Hypalon®.

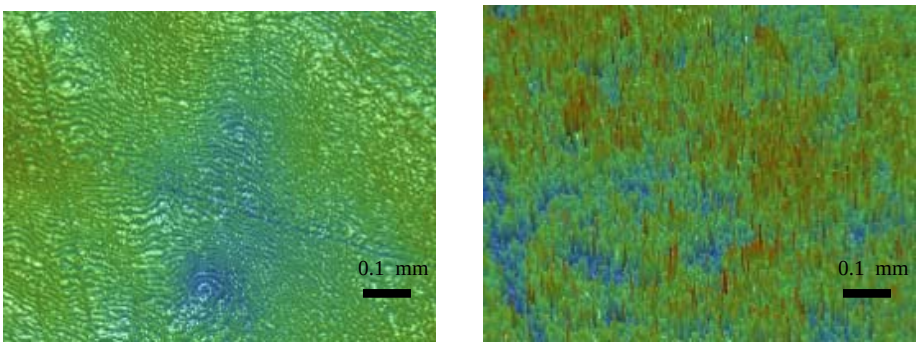

a) b)

Figure 8. Surface profiles of (a) polypropylene and (b) Hypalon®.

Only oils of medium to high viscosities were used for DCA analysis of rough elastomers, since low viscosity oils penetrate too deep into the elastomeric structure. In this case "an effective roughness" of the surface is much higher, and the contact angle is affected more by the local roughness than by the selection of the material. Very viscous oils cannot be used for this analysis, as the selected speed of advancing (80 microns/sec) doesn't allow the meniscus of viscous oil in the contact with a rough surface to achieve an equilibrium condition. Hence it is not recommended to use liquids with very high or very low viscosity for contact angle measurements with rough elastomers.

For oleophobic elastomers, roughness of the surface decreases spreading and adhesion of oil due to air trapped in the crevices of the surface, which prevents oil from penetrating into the surface structure and decreases the total contact area. For oleophilic elastomers, roughness increases oil adhesion, allowing oil to penetrate deeper inside the surface structure and preventing drainage. The relation between the cosine of advancing angle and the amount of recovered oil for elastomers is presented in Figure 9.

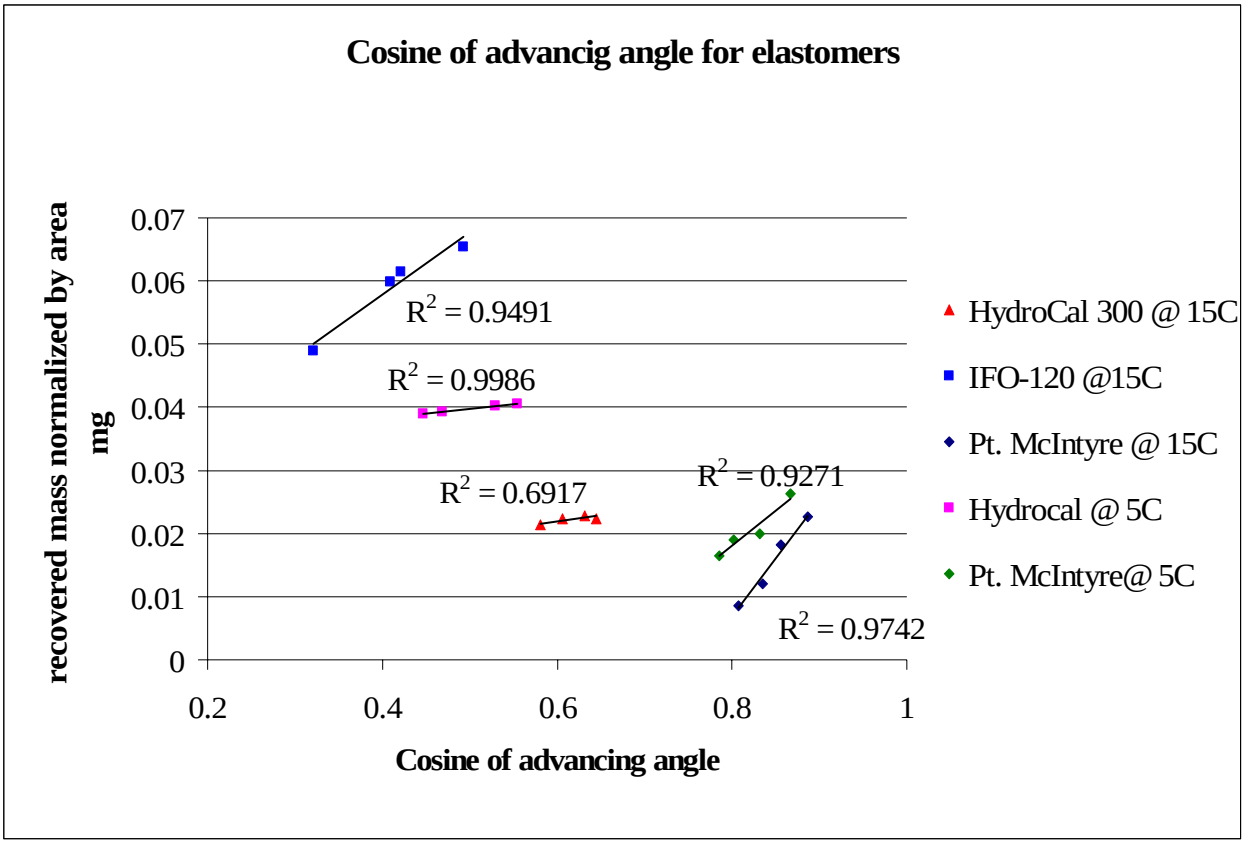

Figure 9. Relation between the cosine of advancing angle and recovered mass for elastomers.

Experiments had shown that Hypalon® and Neoprene® have the largest oil recovery potential, while Epichlorohydrin had the lowest oil recovery rate among the oleophilic elastomers tested. Teflon® and Antistatic Polyurethane have very low affinity for oils and recovered almost no oil. Overall, the oleophilic elastomers showed a higher recovery potential than the hard polymers and metals. This is illustrated in Figure 10. Since a comparison of contact angles between surfaces with different roughness is not correct, we used the amount of oil recovered during DCA test to compare various materials. Figure 10 represents the amount of recovered oil for Polypropylene, Low Density Polyethylene, Hypalon® and Neoprene® corresponding to each tested oil. Each oil type was assigned a number (1 through 11) according to its viscosity. The viscosity of oil increases from left to right. In all cases, Hypalon® and Neoprene® were found to recover higher amounts of oil compared to hard polymers. This is due to the fact that these two elastomers have a high affinity to oil combined with significant surface roughness which allows them to retain higher amounts of oil. This is mechanism is especially effective on oils with low viscosity. Figure 10 also shows the importance of temperature and oil viscosity on the amount of recovered oil. Oils with higher viscosities (above their Pour Point) and at lower temperatures can be recovered faster than oils with low viscosities.

It was found that although EPDM has the highest affinity for oil among the elastomers we tested, it has a high swelling rate, so EPDM was excluded from further study. Hypalon® and Neoprene® were found to have good affinity for oil combined with sufficient resistance to swelling. In addition, they can be modified (crosslinked) if needed to decrease their swelling rate while retaining their oleophilic properties.

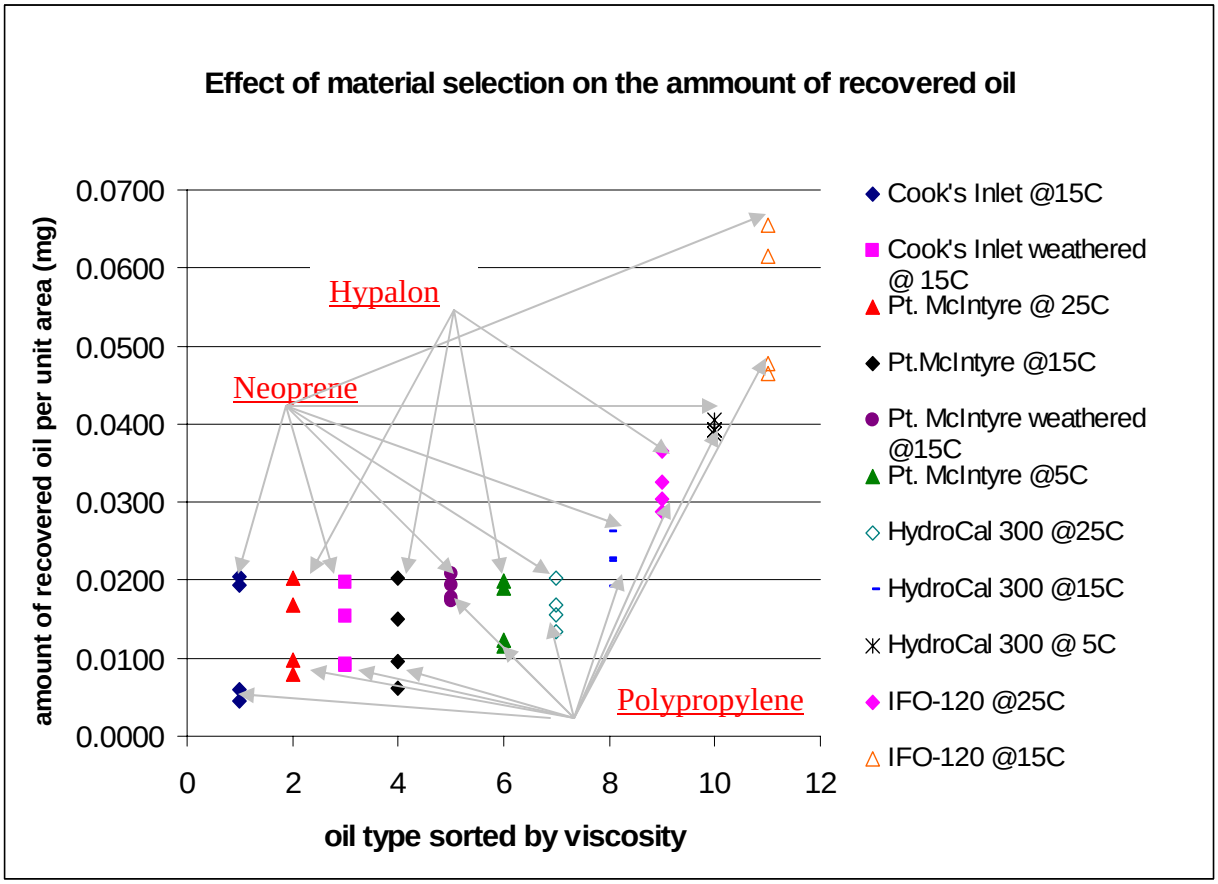

Figure 10. The effect of material selection, oil type and temperature on the amount of recovered oil.

Based on the results of these experiments, five materials were selected for the field-scale tests at Ohmsett:

- Polypropylene
- Polyethylene
- Aluminum
- Hypalon®
- Neoprene®

A number of drums were manufactured from these materials. They were installed on the existing skimmer and used to study the effect of material on the recovery efficiency. The results of these experiments will be published in a separate report.

2.9 Adhesion of oil to contaminated surfaces

A set of tests was conducted in order to determine whether or not the selected test materials can maintain their ability to recover oil for several consecutive cycles, once they have been in contact with oil a first time. The results of this test might have a significant effect on the selection of appropriate materials. Materials that can only recover oil while pre-cleaned in laboratory conditions may not be recommendable for the recovery equipment since most of the time the drum surface interacts with oil already with a thin oil film on its surface, since the scraper cannot remove all oil molecules from the surface.

This test was performed using the DCA following the procedure developed for pre-cleaned samples. Since the contact angle value cannot be accurately measured for materials that have already been exposed to oil, only the recovered mass of oil was measured. The materials were tested as received from the manufacturers without pre-cleaning. After the first run, oil that adhered to the surface was removed using a paper tissue, leaving a visible oil layer on the surface. The sample was then installed back in the DCA test chamber for the second run. The amount of oil recovered after each run was calculated. The results of this test are presented in Figure 11. Each number on the x-axis corresponds to specific test material. Recovered mass is shown on the y-axis.

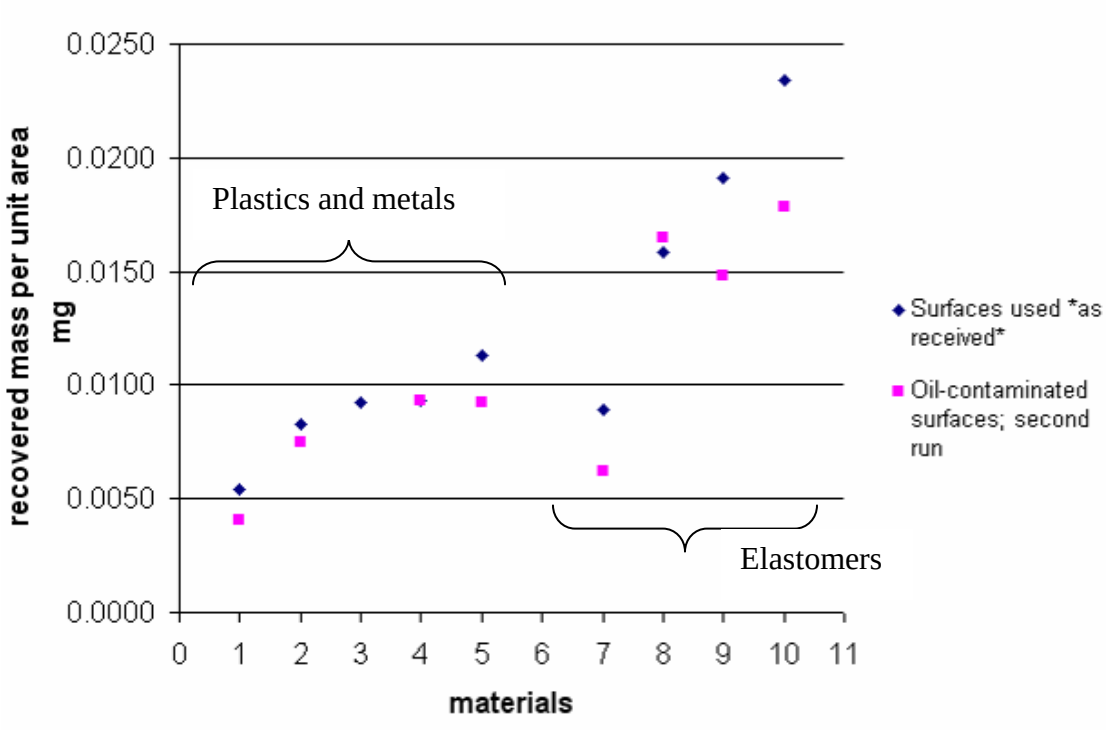

Figure 11. Recovery efficiency of previously-oiled test surfaces.

Figure 11 shows that the materials that were selected for the further testing at Ohmsett are likely to retain their ability to recover oil during consecutive recovery cycles.

2.10 Oil recovery at faster speeds using dip-and-withdraw method

2.10.1 Experimental setup

Oil recovery at fast speed was performed using a stepping motor. The experiment setup is presented in Figure 12.

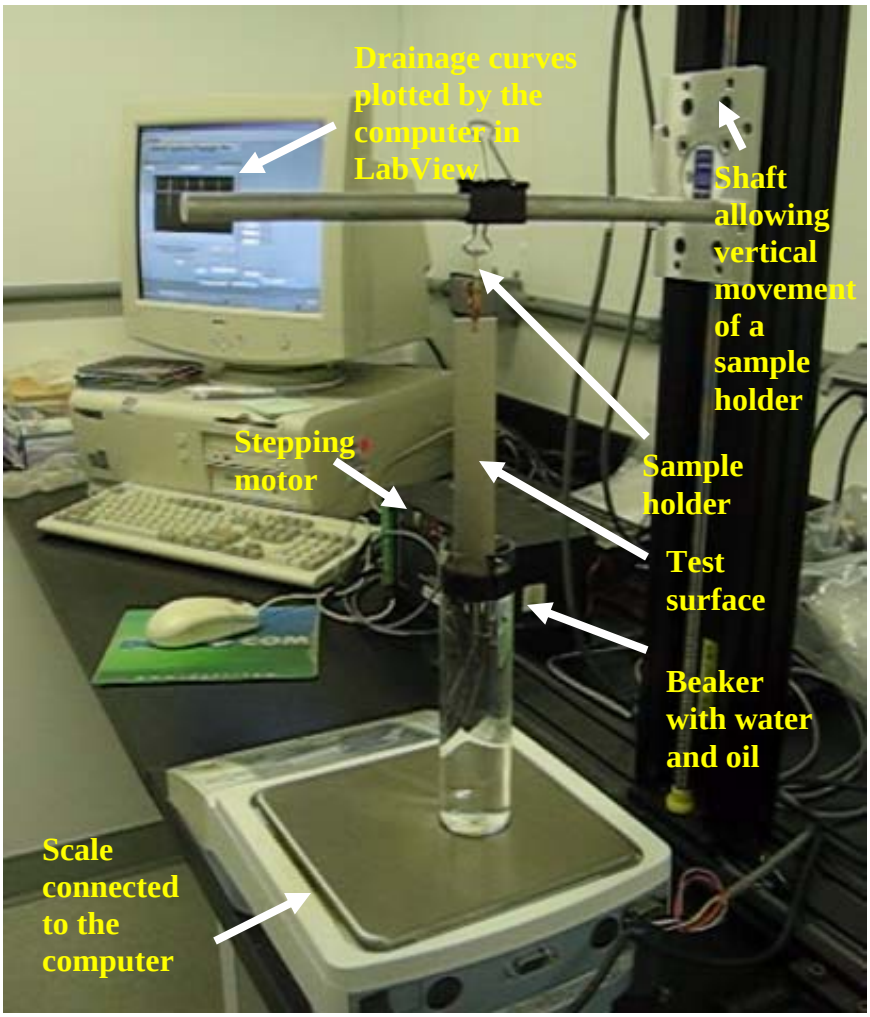

Figure 12. Dip-and-withdraw test setup.

These experiments were carried out in the temperature controlled room at 5°C, 15°C and 25°C (±1°C). The test procedure was similar to the dip-and-withdraw test described by Jokuty (1996). Test samples were cut in strips (15 x 2.5 cm) and cleaned according to the procedure developed for DCA samples. Dipping tests curried out with clean and previously oiled test surfaces showed that the amount of recovered oil doesn't change significantly between clean and contaminated surfaces of the same material. In order to simulate a real-life oil recovery and eliminate an error that might be caused by the higher amount of oil being recovered by the clean elastomers (due to their rougher structure) all dipping tests were curried out using previously oiled surfaces, that were carefully cleaned only using a paper tissues.

A beaker was filled with 150 ml of filtered seawater from Santa Barbara Channel (salinity of about 33.6 ppt). Then 15 ml of test oil was carefully added on top of the water surface. The beaker with seawater was placed on a scale connected to a computer. A test surface was placed in a sample holder above the oil surface. The sample holder was moved vertically using a programmed stepping motor such that the test surface was submerged into the oil-water mixture by exactly 14 mm and then withdrawn. The speed of withdrawal was 74 mm/s. Once the oiled surface was withdrawn from the beaker, the scale measured the maximum oil loss and then generated the signal to plot the increase of oil mass in the beaker caused by the oil drainage from the plate and droplets of oil falling

back into the beaker. From the shape of these curves, the effect of different materials and oils on the recovery was analyzed. For each material 5 to 10 tests were performed to ensure accuracy of data. New oil was used for each test.

2.10.2 Results and discussion

Drainage curves for a range of oils, temperatures and materials are presented in Figures 13 through 25. The curves correspond to the weight loss from the water/oil beaker detected by the scale once the test surface was withdrawn. The lowest point of each curve corresponds to the maximum mass recovered by the test surface immediately after withdrawal. As oil drained back into the beaker, total recovered mass decreased.

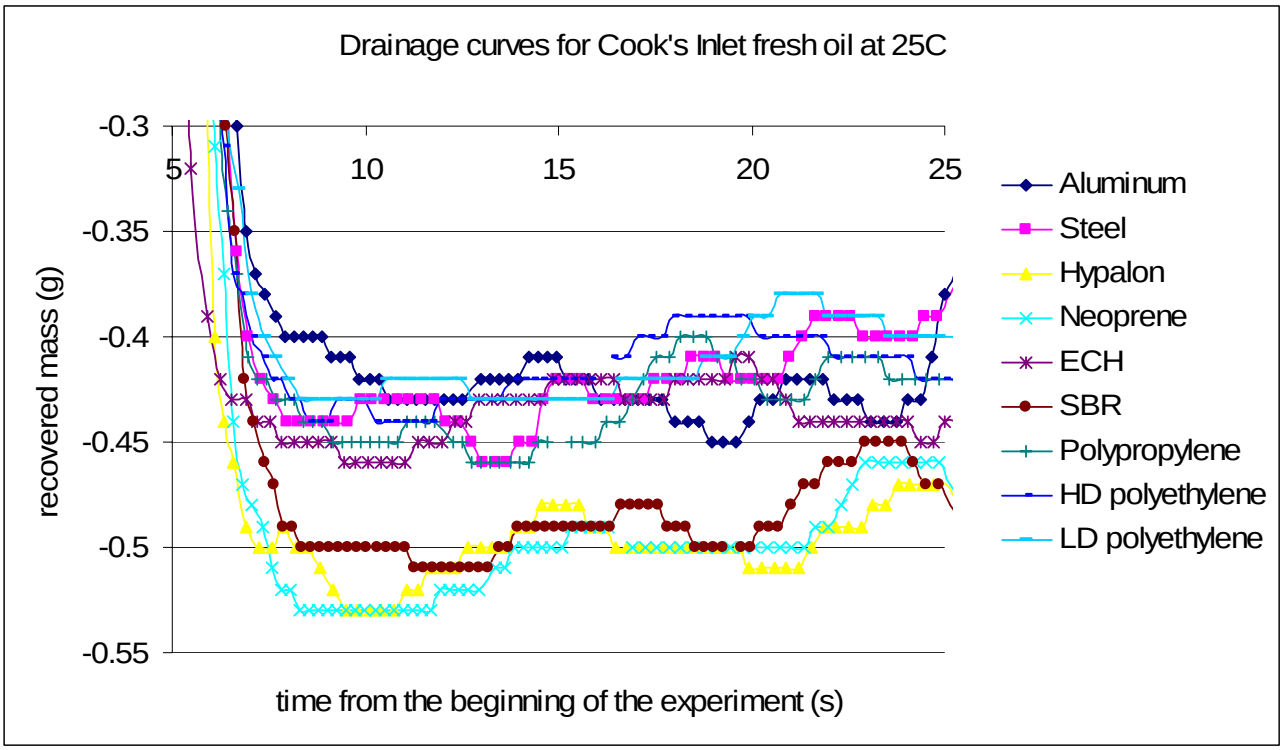

Figure 13. Drainage curves for Cook's Inlet fresh oil at 25°C.

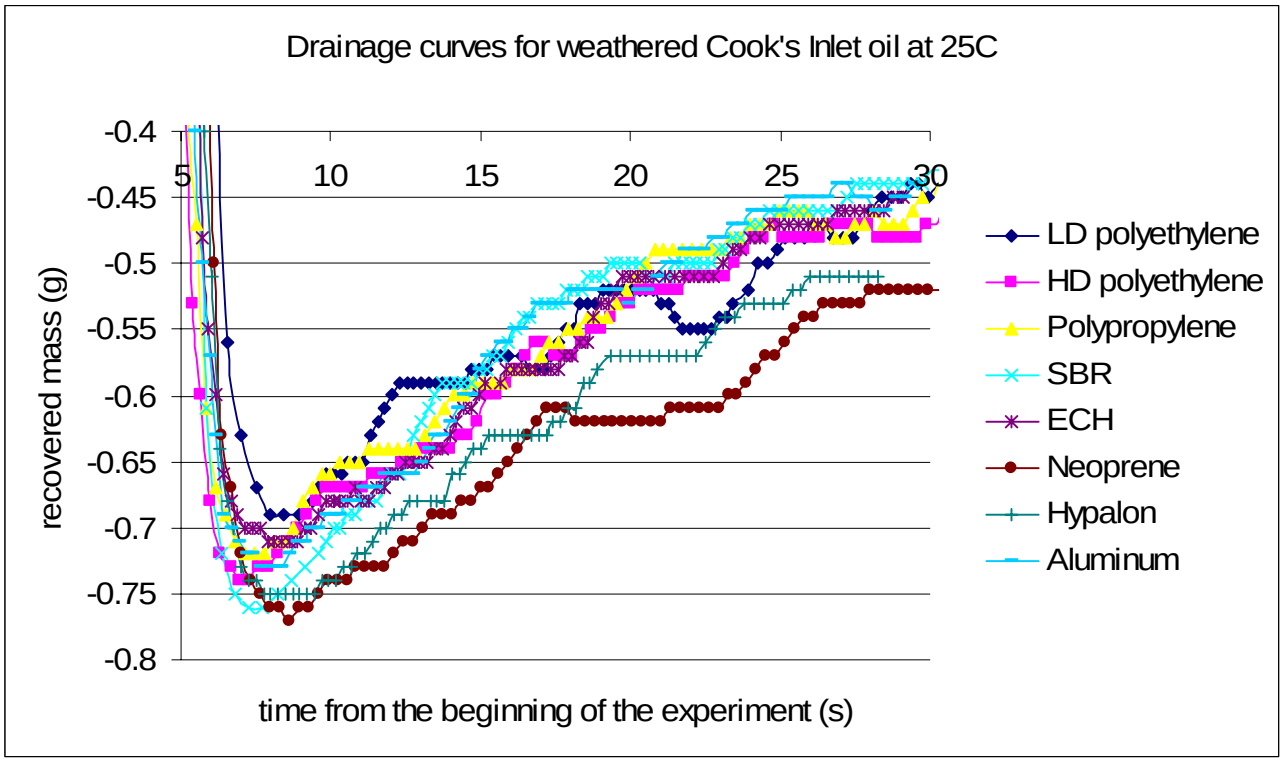

Figure 14. Drainage curves for weathered Cook's Inlet oil at 25°C.

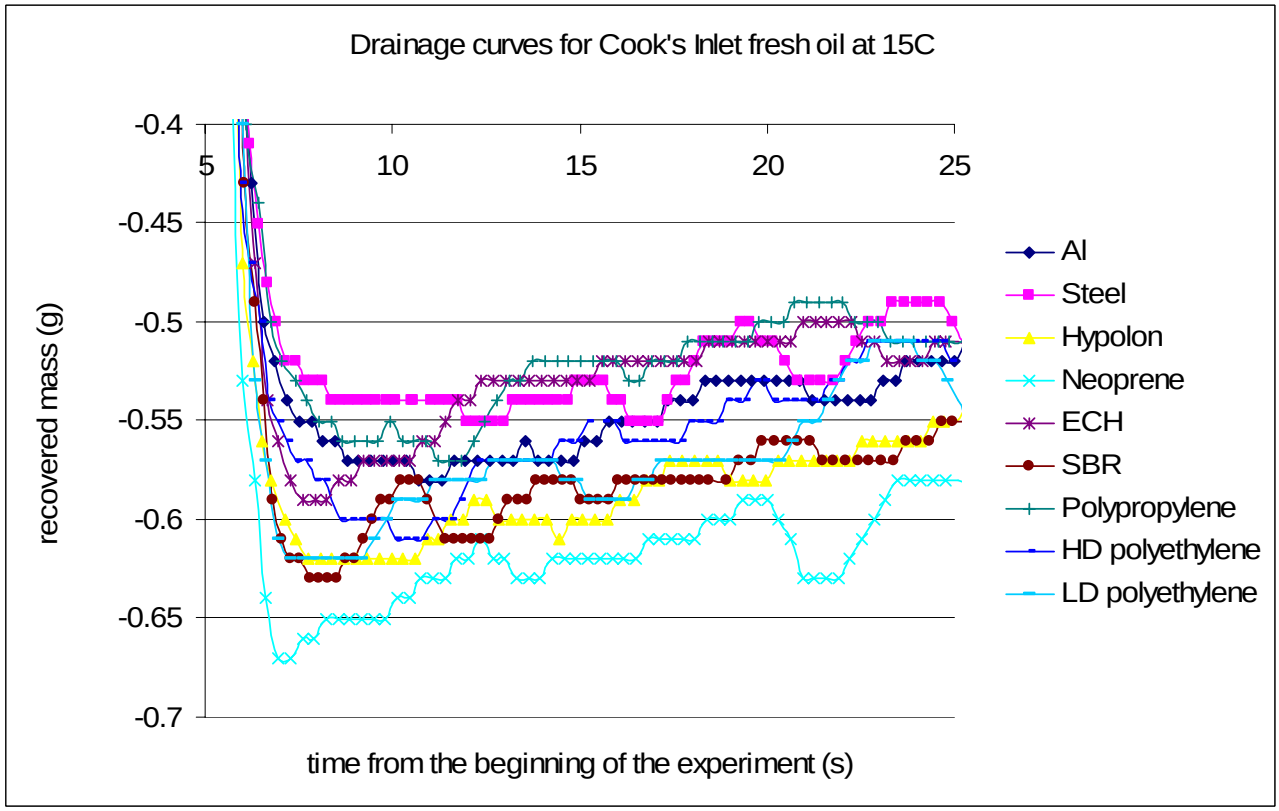

Figure 15. Drainage curves for Cook's Inlet fresh oil at 15°C.

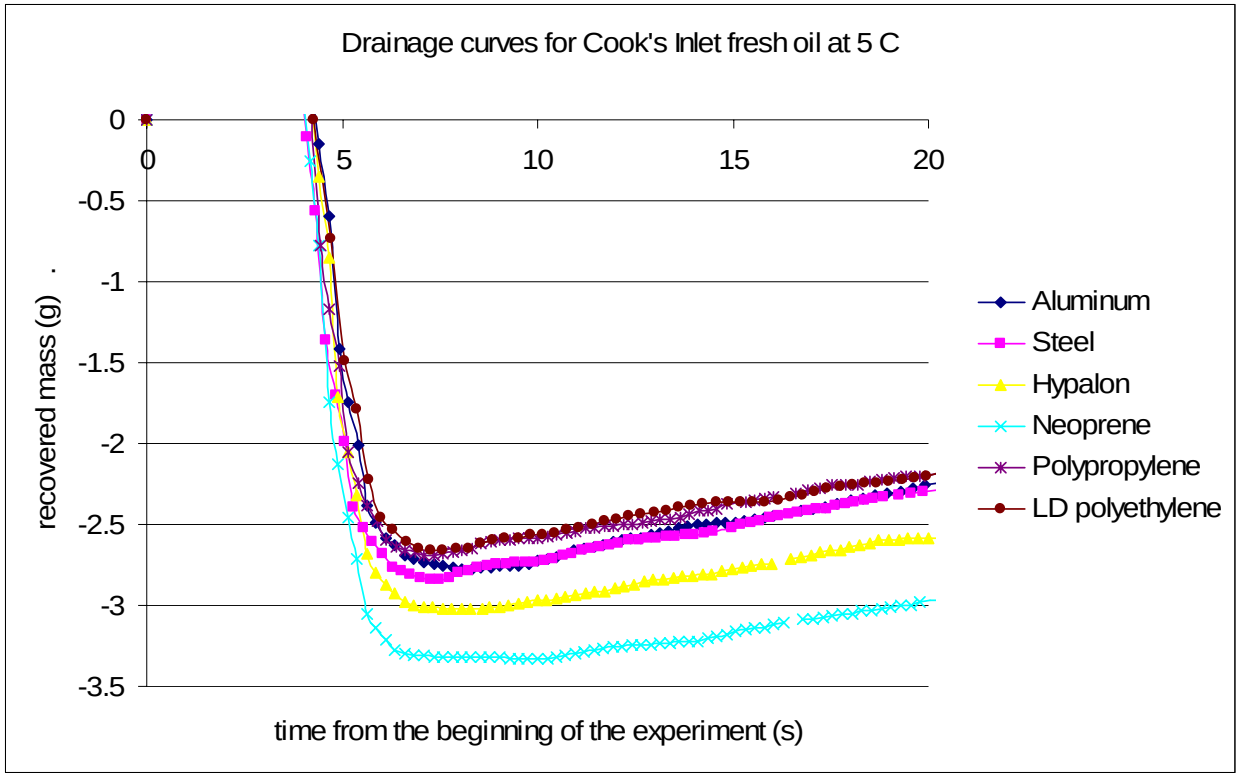

Figure 16. Drainage curves for Cook's Inlet fresh oil at 5°C.

Pt. McIntyre drainage curves at 25, 15 and 5ºC.

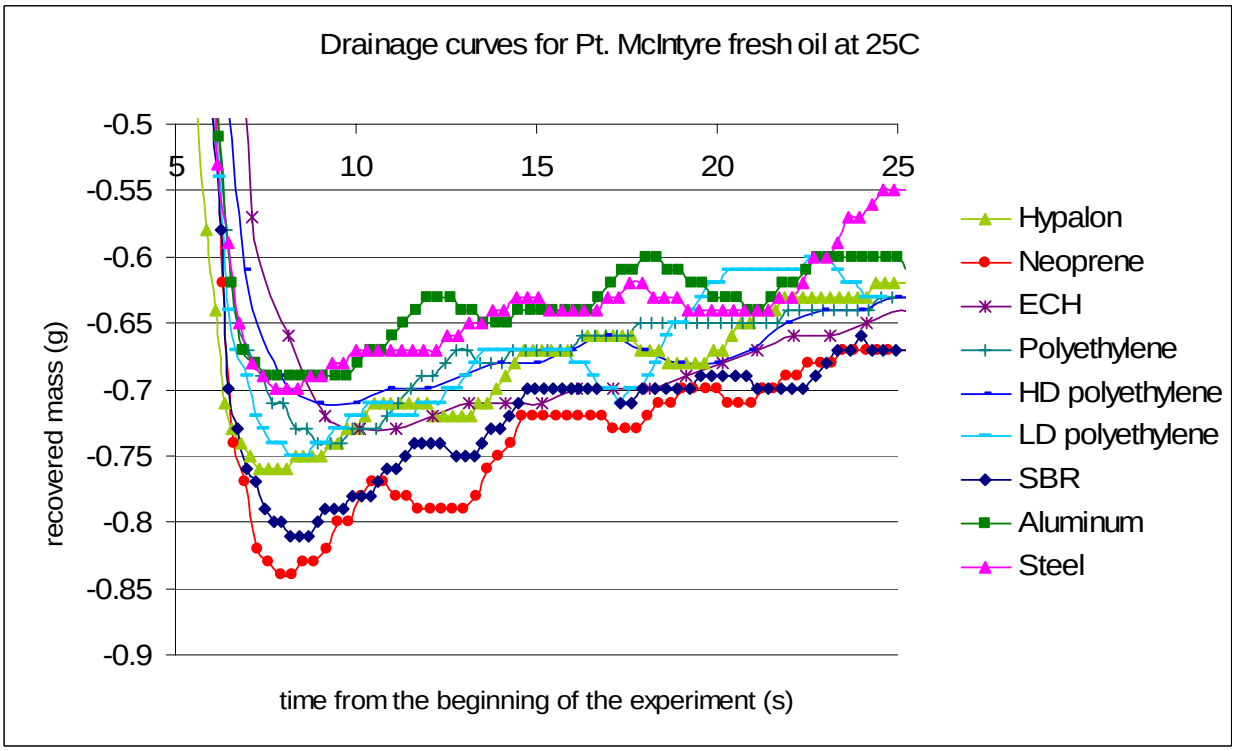

Figure 17. Drainage curves for Pt. McIntyre fresh oil at 25°C.

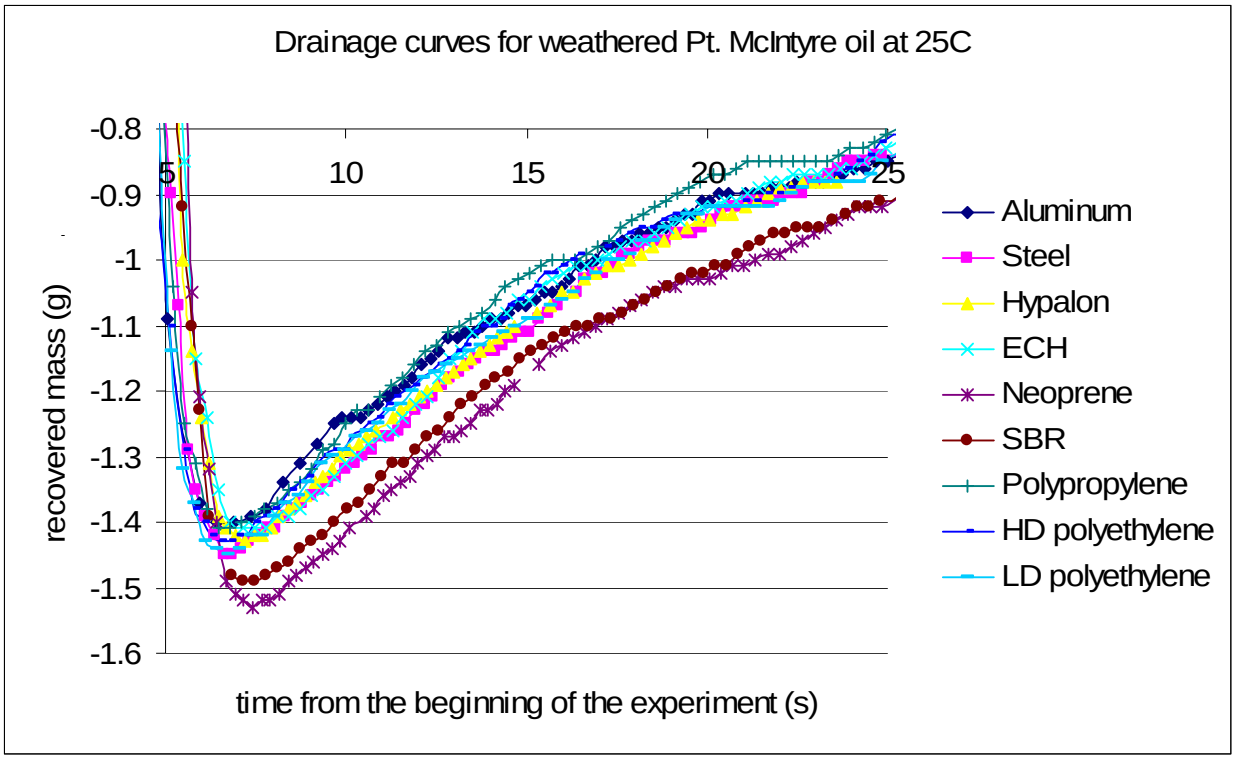

Figure 18. Drainage curves for weathered Pt. McIntyre oil at 25°C.

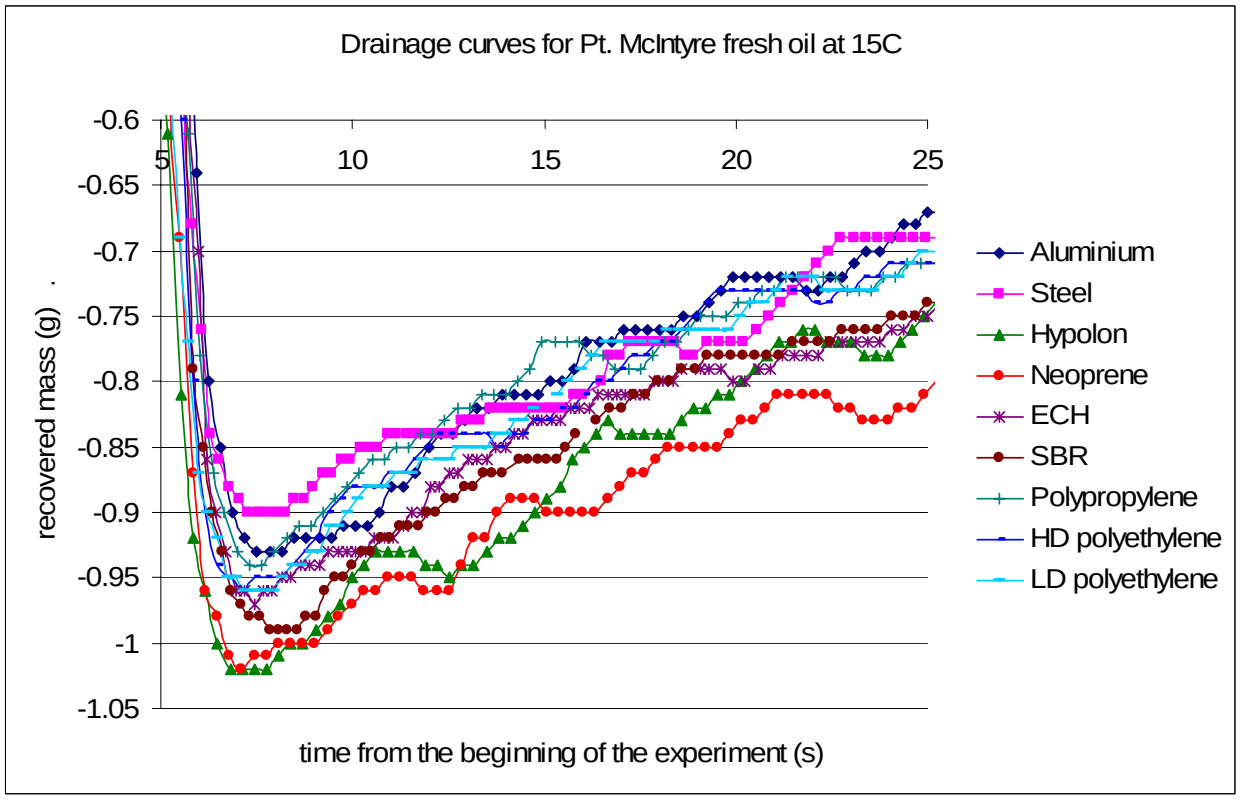

Figure 19. Drainage curves for Pt. McIntyre fresh oil at 15°C.

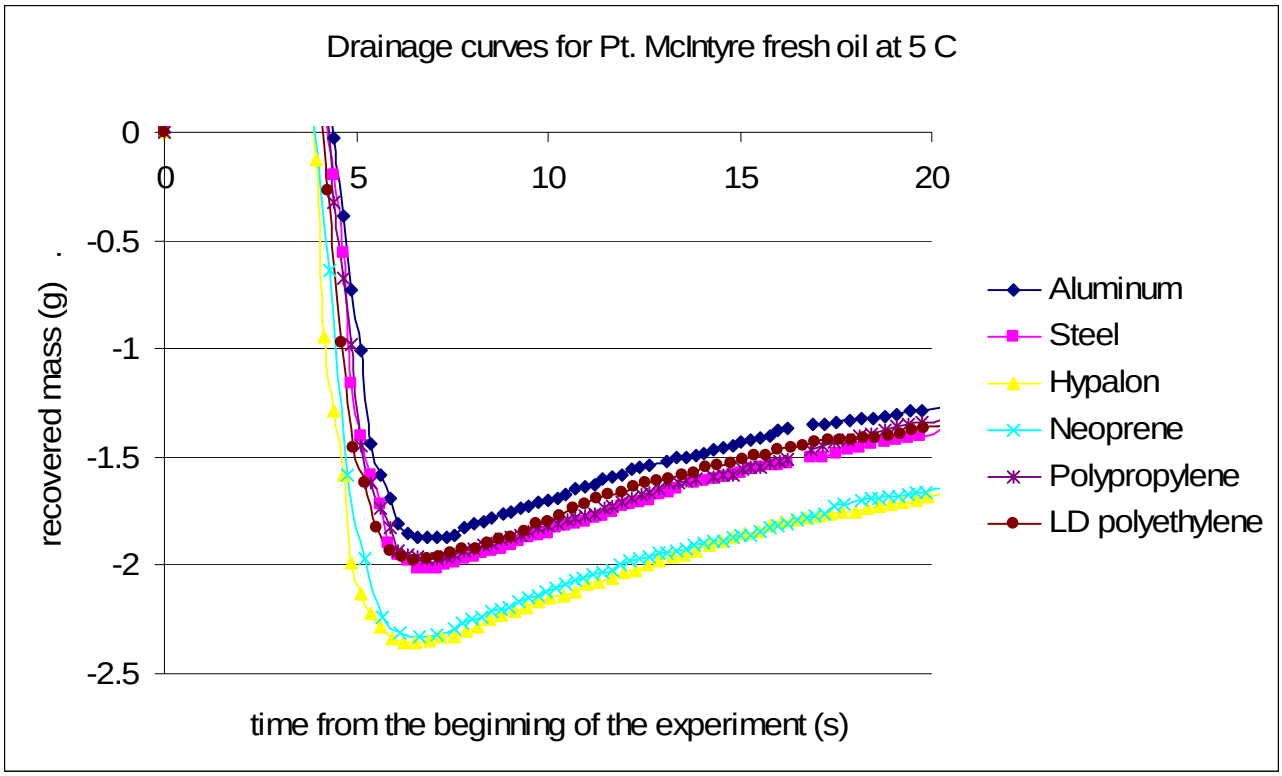

Figure 20. Drainage curves for Pt. McIntyre fresh oil at 5°C.

HydroCal 300 drainage curves at 25, 15 and 5ºC.

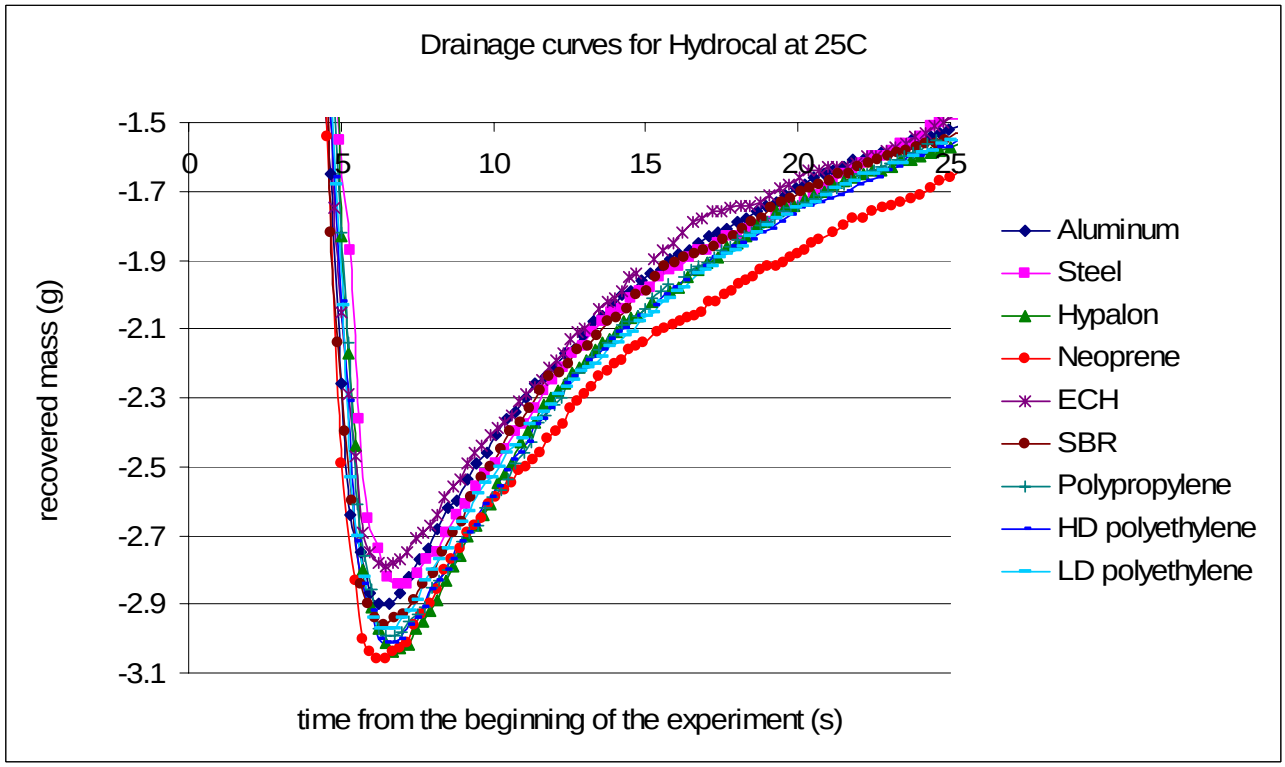

Figure 21. Drainage curves for HydroCal 300 at 25°C.

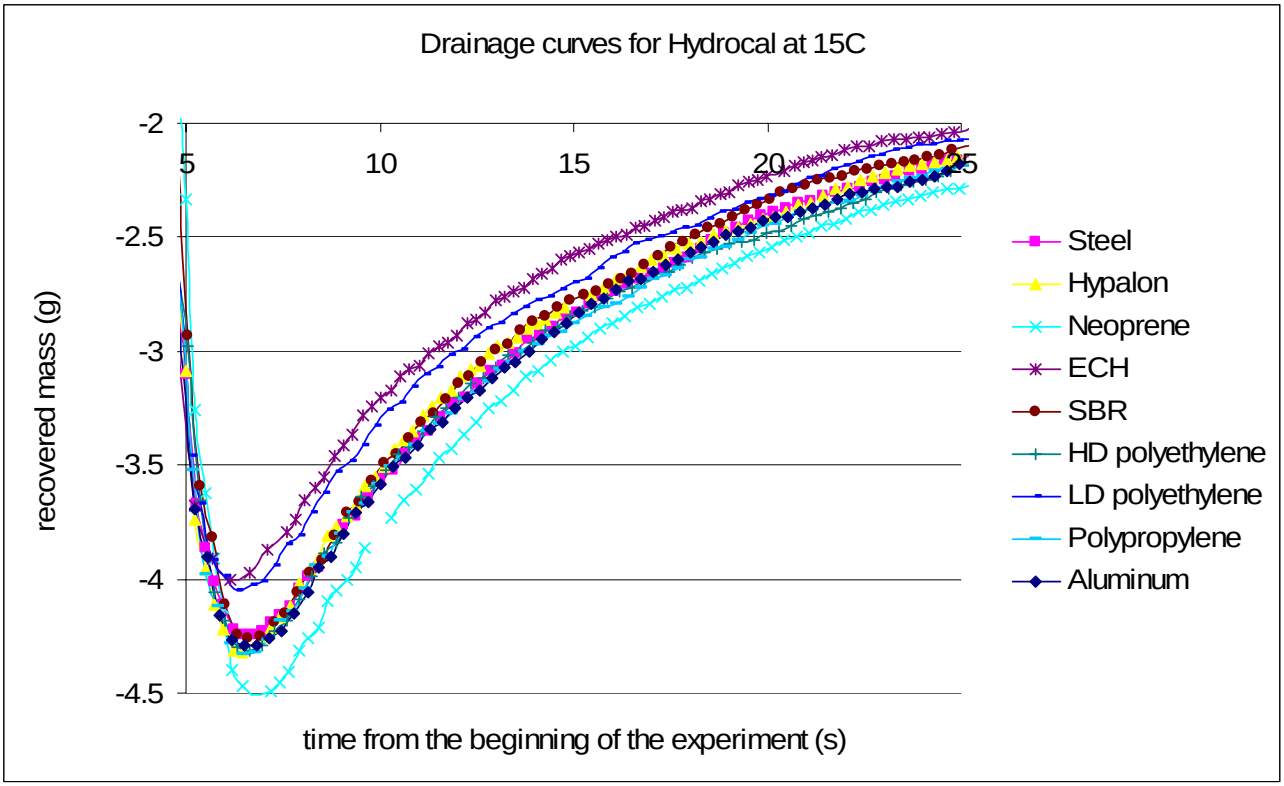

Figure 22. Drainage curves for HydroCal 300 at 15°C.

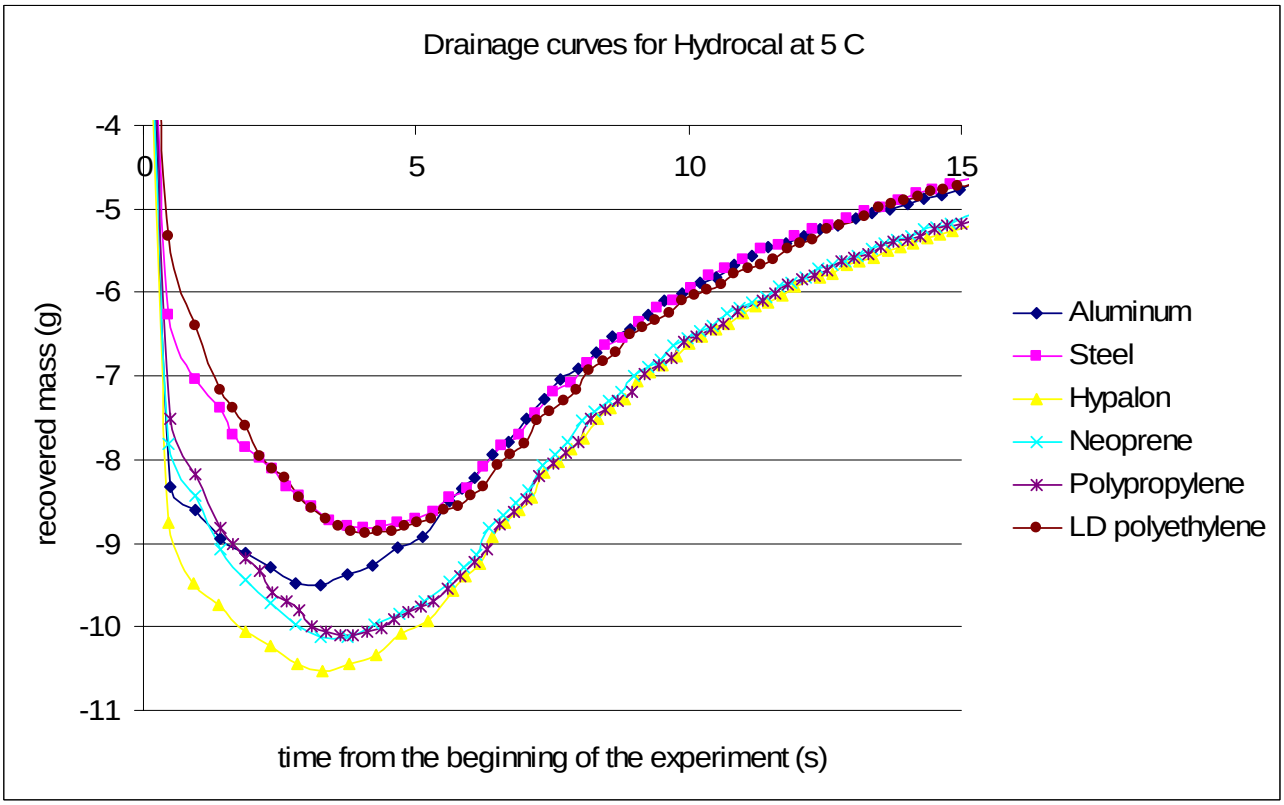

Figure 23. Drainage curves for HydroCal 300 at 5°C.

IFO-120 drainage curves at 25 and 15 ºC.

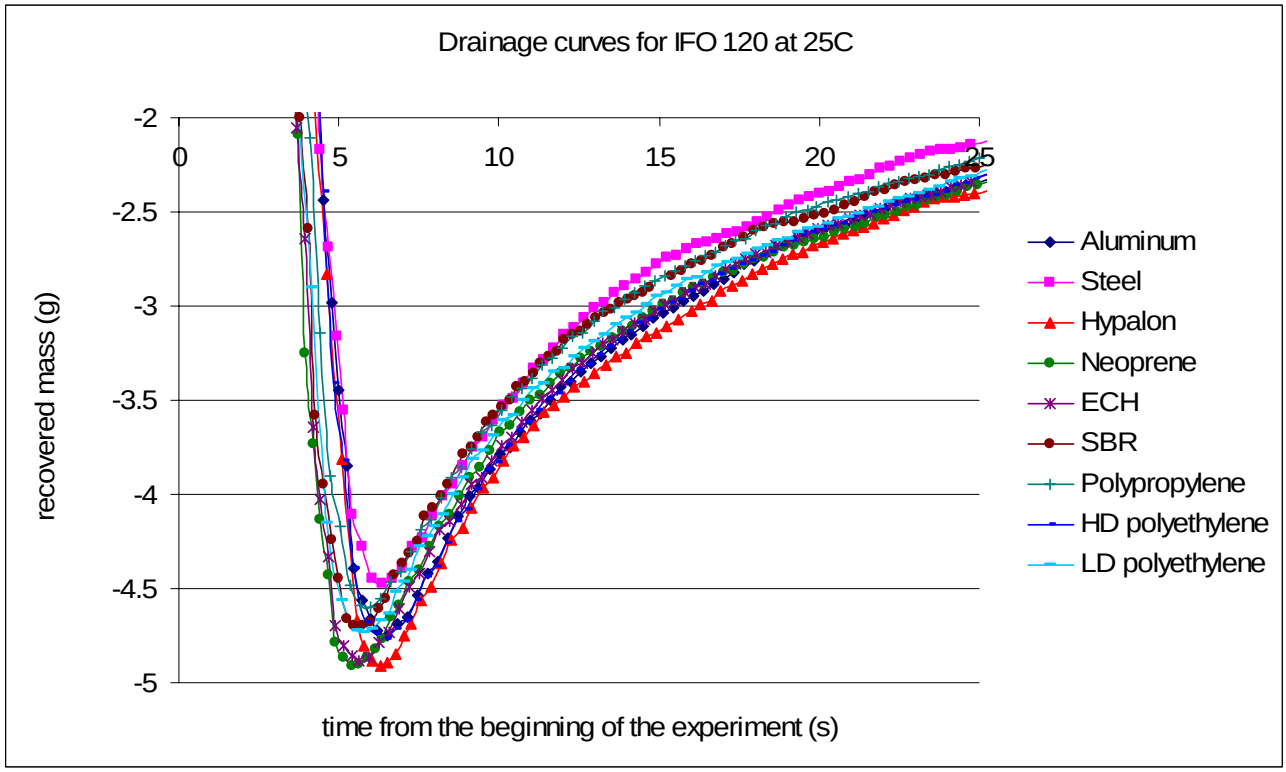

Figure 24. Drainage curves for IFO-120 at 25°C.

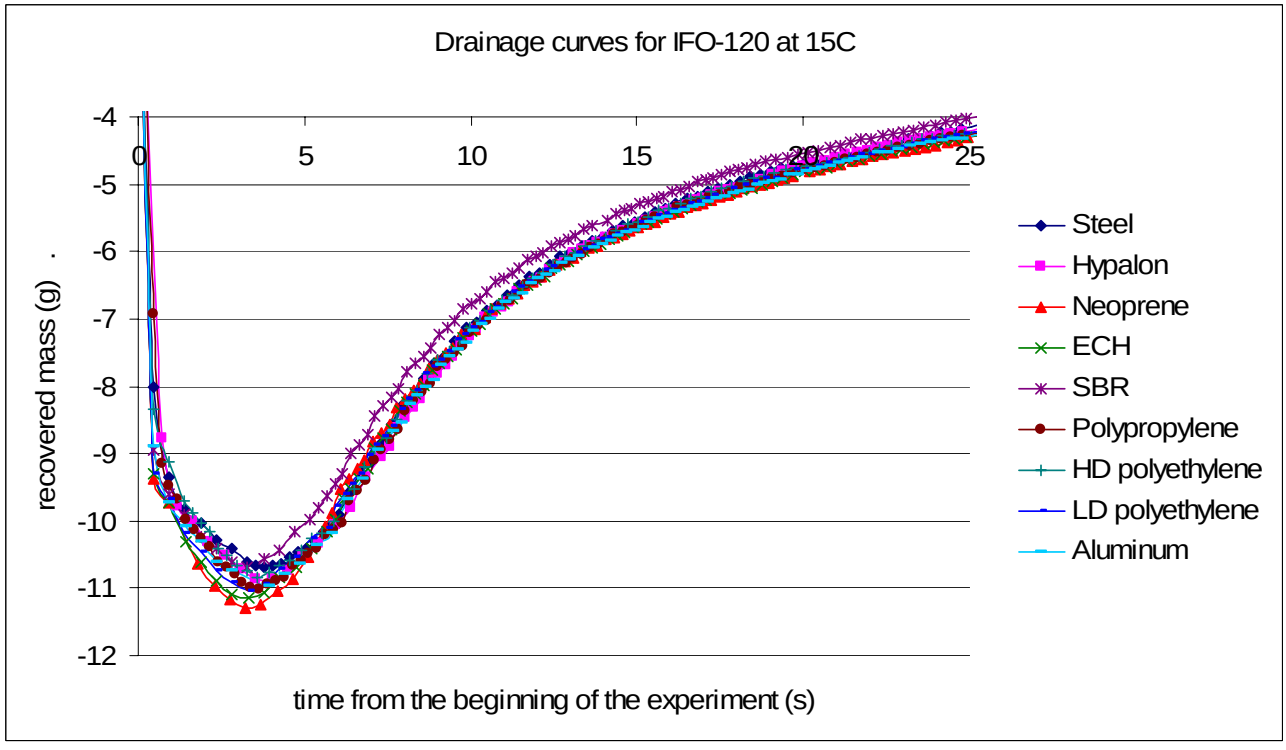

Figure 25. Drainage curves for IFO-120 at 15°C.

The results show that speed of withdrawal has an important effect on the amount of recovered oil. Up to 50% of recovered oil drained back into the beaker after 15 seconds. So, the recovery efficiency can be significantly increased by decreasing oil drainage from the recovery surface. This can be achieved by faster rotation (withdrawal) of the recovery surface, using rough soft materials such as elastomers, creating surface patterns to slow the oil drainage or by a combination of all of these. It must be noted though, that the increase of rotation speed must be balanced by the hydrodynamic behavior of oil in the contact with the recovery surface. When the rotation speed reaches a critical level, water entrainment occurs, preventing oil from a contact with the recovery surface. This critical speed will be determined empirically in future studies. The optimum rotation speed was determined during the field-scale experiments at Ohmsett. These data are described in the separate report.

As illustrated by Figures 13 through 25, there is up to a 20 % difference in the recovery efficiency of various materials. Dip-and-withdraw tests confirmed the results of the contact angle measurements by showing that Hypalon® and Neoprene® have higher oil recovery efficiencies than other materials. This is especially true for lighter oils. More viscous oils form a thicker film on the surface and diminish the effect of the recovery material properties. The recovered mass measured for Cook's inlet crude oil at 5°C seems to be slightly higher than it would have been expected. This is due to the fact that this sample of crude oil started showing some signs of weathering and appeared to have some free water. This changed its physical properties, lead to a slight increase in viscosity and hence to the higher amount of recovered oil.

The results also clearly show the effect of oil viscosity and its change with temperature on the recovery process. Cook's Inlet fresh oil at 15°C yielded a 15% larger recovered mass than at 25°C. HydroCal yielded 25% more at 15°C and IFO yielded 100% larger recovered mass at 15°C compared to 25°C. This was due to the rapid viscosity increase with decreasing temperature for viscous oils (Figure 4 and Table 3).

Drainage experiments confirmed the earlier observation that although the current dip-and-withdraw technique is closer to the full scale system than DCA tests, it has a rather low accuracy. This is due to the formation of a drop attached to the lower edge of the test surface after the test material is withdrawn from the liquid. This complicates comparison between various materials. As many as 10-15 tests have to be done for each recovery surface in order to obtain consistent drainage curves. For an "endless" surface such as a rotating drum, one would not expect to observe the "hanging drop" effect.

2.11 Effect of surface pattern on the recovery efficiency

2.11.1 Introduction

Two types of recovery surfaces patterns are usually used for adhesion oil skimmers. Smooth flat surfaces are used on drum, disk and belt skimmers. Drum and belt skimmers might also have a surface covered with brushes. The later configuration has an obvious advantage due to the much higher surface area (oil covering every bristle) and formation of oil meniscuses between the bristles, but the difficulty of oil removal from the brushes may result in a lower overall recovery. Brush surfaces tend to pick up debris together with oil, which may affect the recovery efficiency and oil-transfer process. The smooth surface area of a drum, disk and belt doesn't usually recover debris, but this configuration picks up less oil than a brush surface due to the smaller surface area.

The oil spill recovery process is composed of two equally important goals. The first one is to remove oil from the water surface and the second one is to remove oil adhered to the recovery surface and transfer it into the collector. The recovery efficiency depends on the achievement of both

of these goals. In case of a smooth surface, the amount of recovered oil is relatively low, but close to 100% of it can be removed by a scraper. In the case of a brush surface and light to medium oils, oil covers every bristle and forms small menisci between the bristles, preventing oil from draining back into the slick. Unfortunately, the configuration of this surface doesn't allow for scraping every bristle individually and removing all adhered oil. Hence, a significant amount of oil remains on the surface after scrapping, reducing the overall recovery rate. A brush configuration works much more efficiently on high viscosity and semi-solid oils. In this case, oil doesn't cover the bristles or penetrate inside the brush. It is merely being lifted from the water by the tips of the bristles and physically transported to the collector. This process is not exactly related to oil adhesion and spreading properties. This explains the ability of a brush surface to recover more debris than a smooth surface.

The characteristics of an adhesion skimmer that can significantly increase oil recovery efficiency can be summarized as follows:

- It should have the maximum surface area possible for a given width of the recovery surface (drum, belt, or disk).
- A configuration allowing the formation of oil menisci is desirable as it allows thicker layer of oil to be recovered and slows oil drainage back into the oil spill.
- Close to 100% of the oil adhered to the recovery surface should be removed by the scraper.
- It should be able to adjust to the changes of oil properties as it weathers over the time and efficiently recover oil with wide range of properties. This would allow the same recovery surface to be used for the whole period of the recovery process.

With these goals in mind, we found a configuration that would satisfy all the criteria. The configuration of the recovery surface and method of recovery is shown on Figure 26.

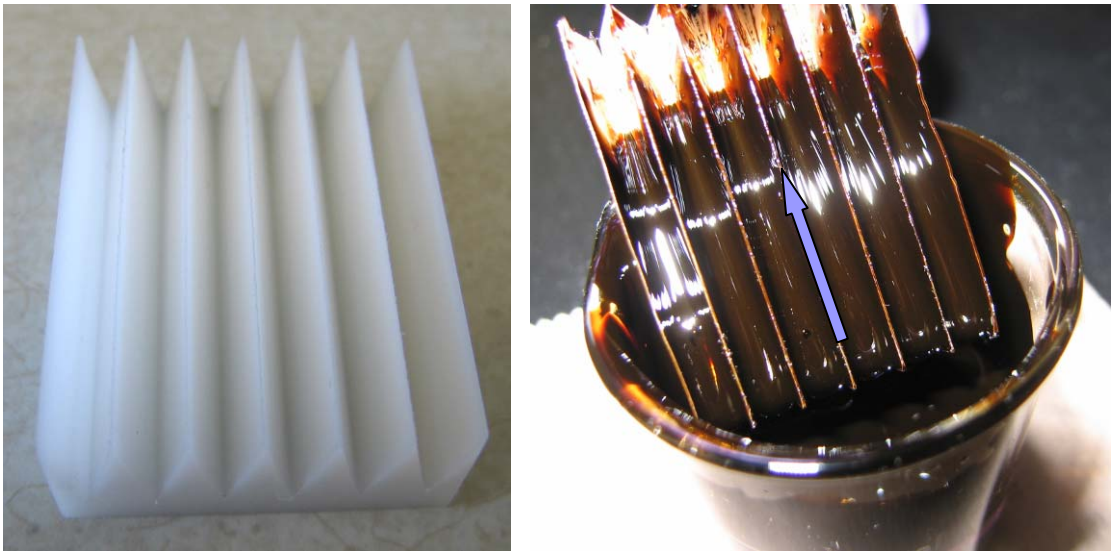

Figure 26. V-patterned recovery surface.
U.S. Provisional Patent Application (serial no. 60/673,043) by UCSB
The arrow indicates the direction of oil recovery.

A V-patterned surface maximizes the surface area of the drum. Depending on the angle and the depth of the channels, the surface area can be increased 2-4-fold for the same width of recovery

surface. It also allows menisci to be formed in the depth of the channel, increasing the amount of recovered oil and slowing down oil drainage. The variation of channel opening with channel depth allows it to be efficiently used on oils with a wide range of viscosities. The lighter oils will be collected in the depth of the channels, while viscous oils can be collected in a wider part of the channel allowing water drainage in the deeper part of the groove. The scraper should be made to match the recovery surface. If V-patterned surfaces with a matching scraper are used, close to 100% of adhered oil can be removed and transferred into the oil collector.

The angle of oil withdrawal from the oil spill has a significant effect on the formation and thickness of the adhered oil film. If oil is withdrawn at a sharp angle (0-90 degrees), it forms a thicker film on the surface because the effect of gravity is reduced by the presence of the recovery surface underneath the film. In this case, drainage of oil is relatively slow. If oil is withdrawn at the angle larger than 90 degrees, gravity force is not compensated by the substrate and the rate of oil drainage from the surface is significantly higher. This leads to formation of much thinner oil film and, hence, lower recovery efficiency. Although a 90 degrees withdrawal angle allows more efficient oil recovery than a wider angle, it is recommended that a V-patterned surface (or any recovery surface for that matter) be used to withdraw oil at angles of less than 90 degrees to maximize the thickness of recovered film.

2.11.2 Test surfaces

A number of surface patterns were manufactured from the aluminum plates in order to study the effect of surface pattern on the recovery efficiency. Test surfaces are presented on Figures 27 through 29.

The surface area can be significantly increased by introducing the grooves with sharper angles, as illustrated in Table 6.

Table 6. The effect of a groove angle on the surface area.

Angle of surface grooves	Surface area (mm^2)- grooved side
180° - flat surface	1453
90° grooves	2005
60° grooves	2896
30° grooves	4663

The surface area of the grooved side can be increased up to 3 times if a flat surface is replaced with a surface with 30° grooves. This will not directly translate to a 3-times higher recovery rate, as oil collected in the depth of the channel is attached to two sides of the grove at the same time. Nevertheless, the V-patterned surface has significantly higher surface area compared to the flat surface, and hence it will allow higher oil recovery rate for the same width of the drum/belt.

In addition to V-shaped grooves, one can also have other configurations, as shown in Figure 29. Some configurations may lend themselves to easier machining on a drum or belt skimmer, and thus we are exploring all the possible geometric configurations. Further research into the advantages and disadvantages of each geometry would be useful.

2.11.3 Research method

The experiments were carried out in the temperature controlled room at 25°C (±1°C). The test procedure was similar to the dip-and-withdraw test described by Jokuty (1996). The experimental setup was similar to the one shown in Figure 12.

Test samples were pre-cleaned with soapy water, ethanol and de-ionized water, blow-dried under a stream of nitrogen and left in the temperature controlled room for at least 24 hours prior to the test. A beaker was filled with 50 ml of filtered seawater from Santa Barbara Channel (salinity of about 33.6 ppt). Then 5 ml HydroCal 300 was carefully added on top of the water surface. The beaker was installed on the scale connected to the computer.

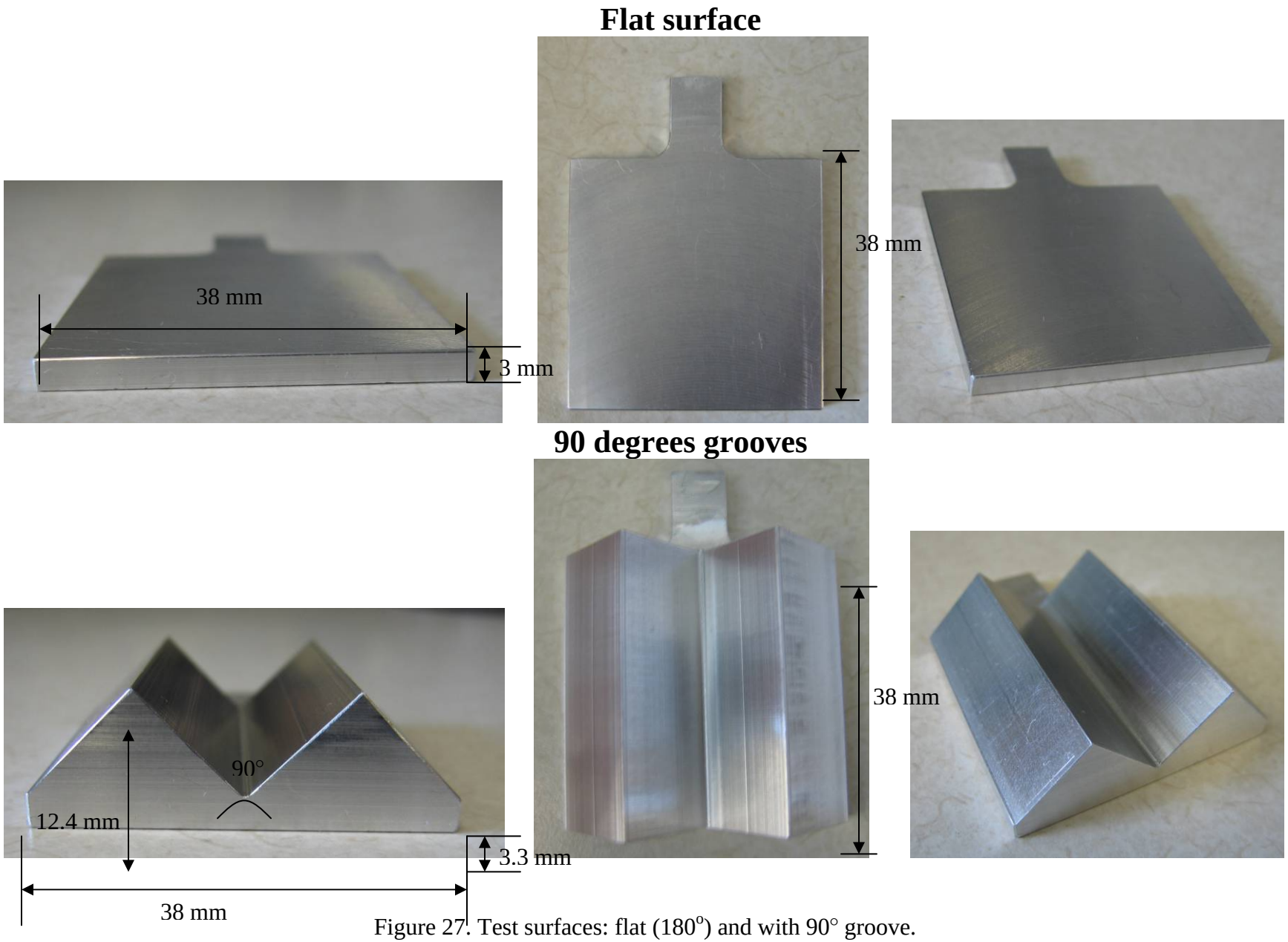

Figure 27. Test surfaces: flat (180^{o}) and with 90° groove.

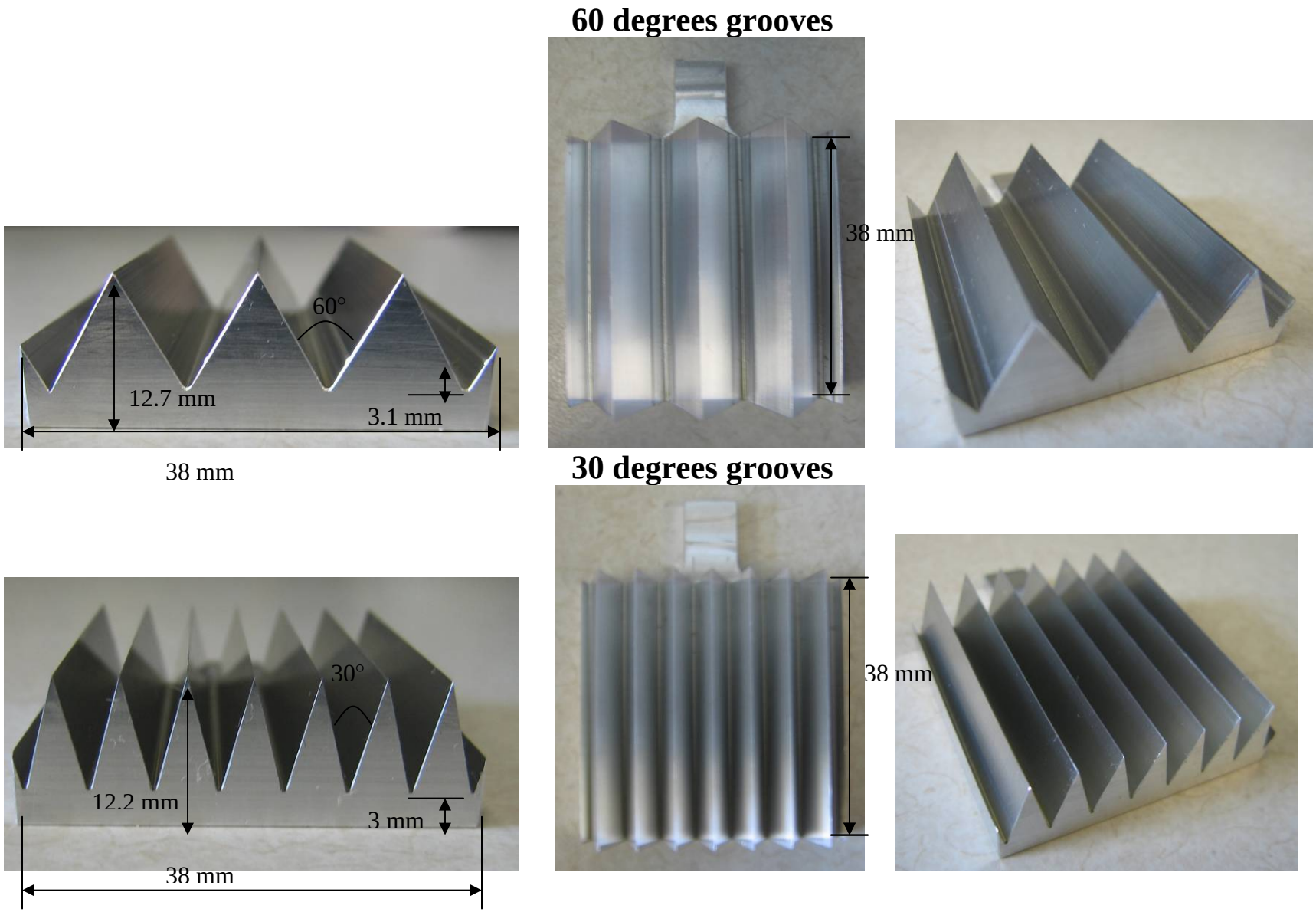

Figure 28. Test surfaces with 60° and 30° grooves.

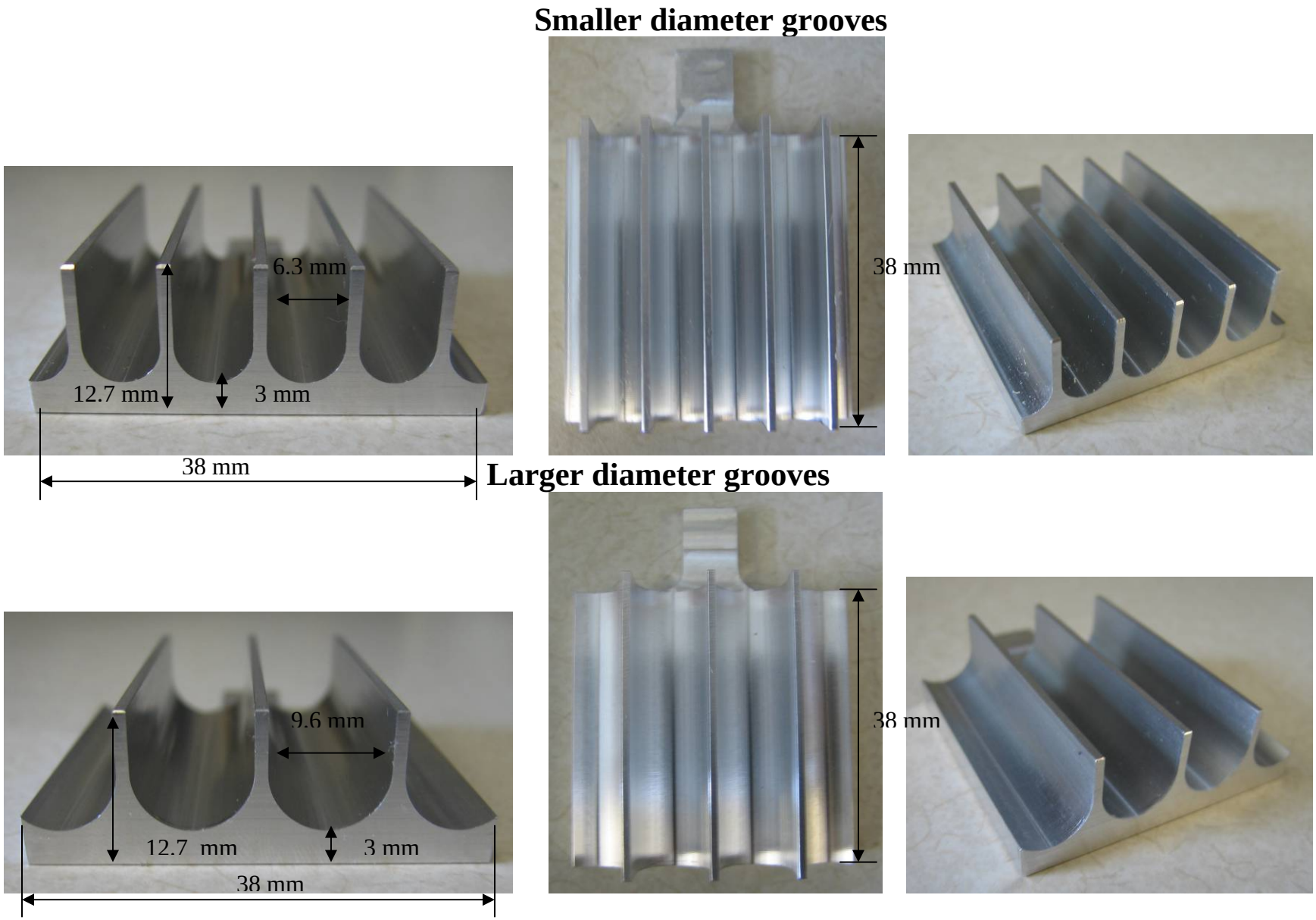

Figure 29. Tested surfaces with round grooves.

A test surface was placed into the sample holder above the oil surface. A sample holder can be moved using a programmed stepping motor in a way that test surface is submerged into oil-water mixture on 20 mm and then withdrawn. The speed of withdrawal was 74 mm/s. Once the oiled surface was withdrawn from the beaker, the scale detected the maximum oil loss and then generated the signal to plot the increase of oil mass in the beaker caused by oil drainage from the plate and droplets of oil falling back into the beaker. From the shape of these curves, the effect of the recovery and oil properties was analyzed. From 5 to 10 tests were performed for each test surface to ensure accuracy of data. New oil was used for each test.

2.11.4 Results and discussion

Drainage curves for the various patterned surfaces are presented in Figure 30, compared to a flat surface. The initial weight of the beaker with seawater and the oil layer was zeroed out. Oil recovery was thus measured as a negative change in mass. Zero time represented the start of the withdrawal process. At around 4 seconds the test surface was completely removed from the beaker. That point represented the maximum mass of oil adhered to the test surface, before oil began draining back to the beaker as oil droplets. After about 25 seconds, oil drainage stopped in most cases. The final recovered mass was found by averaging the data at the end plateau section of the curve.

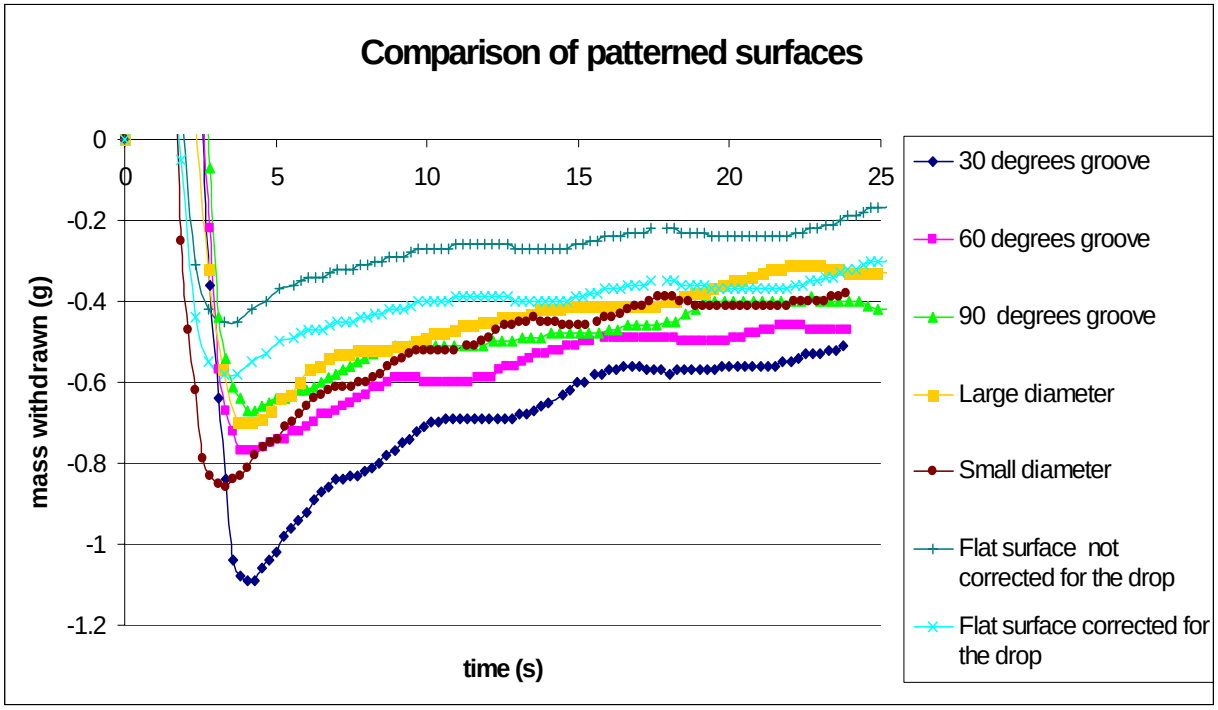

Figure 30. Drainage curves for patterned surfaces.

The data presented in Figure 30 shows that there is a significant difference between the amount of oil recovered by the patterned surfaces. The flat surface data had to be corrected to accommodate the fact that the flat surface had a smaller surface area of the bottom part than grooved surfaces. The grooved surfaces had comparable size of bottom areas. By calculating the weight of the drop corresponding to the bottom surface area of grooved samples allowed to shift a curve for a flat sample to a new position that allows comparing recovery properties of the recovery surfaces and exclude the effect of presence of the drop at the bottom of the samples after withdrawal. Figure 30

shows that recovery efficiency can be doubled with a 30-degree surface pattern instead of a flat surface. Recovery increases with decreasing angle, but at some point there is a limit to the amount of oil in the groove, which we did not explore. Grooves with rounded cross-sections appeared to be less efficient than the triangular-shaped grooves. The effect of groove angle for triangular grooves is presented in Figure 31. Decreasing angle increases the oil recovery for a given oil.

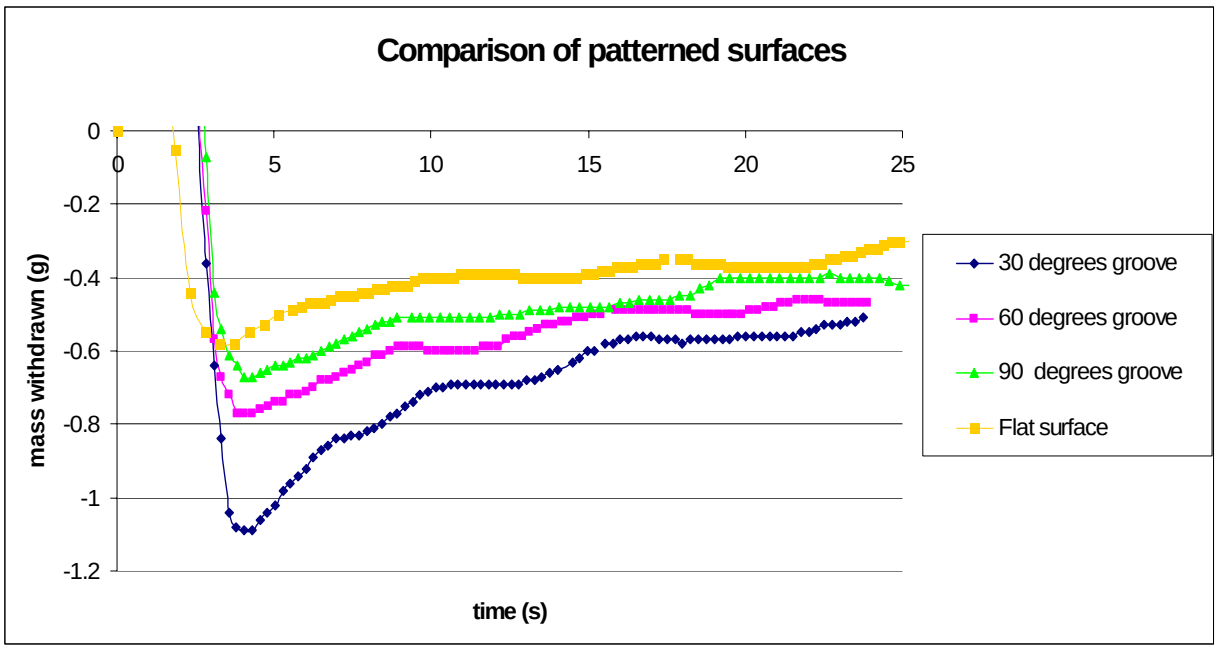

Figure 31. Comparison of oil recovery by triangular-shaped grooves.

Figure 32 summarizes the initial (maximum) oil removal from the water surface, and the final removal after the oil drained back to the beaker, for the various surface patterns. The blue line corresponds to the maximum amount of oil that can be recovered at a withdrawal speed of 74 mm/s, while the pink line corresponds to the final oil remaining on the surface after drainage. The former illustrates the recovery at faster speeds and the later illustrates the recovery at the very slow speed. Overall recovery efficiency increases with decreasing groove angle since a smaller angle retains a larger meniscus in the channel and slows down oil drainage. However, for very viscous oils and emulsions, the opening of the channel should be wide enough for oil/emulsion to enter the groove. There is thus a minimum groove angle that may be dependent on oil properties. Grooves with smaller angle also increase the surface area of the drum per unit width allowing more oil to attach to the surface (Table 6.)

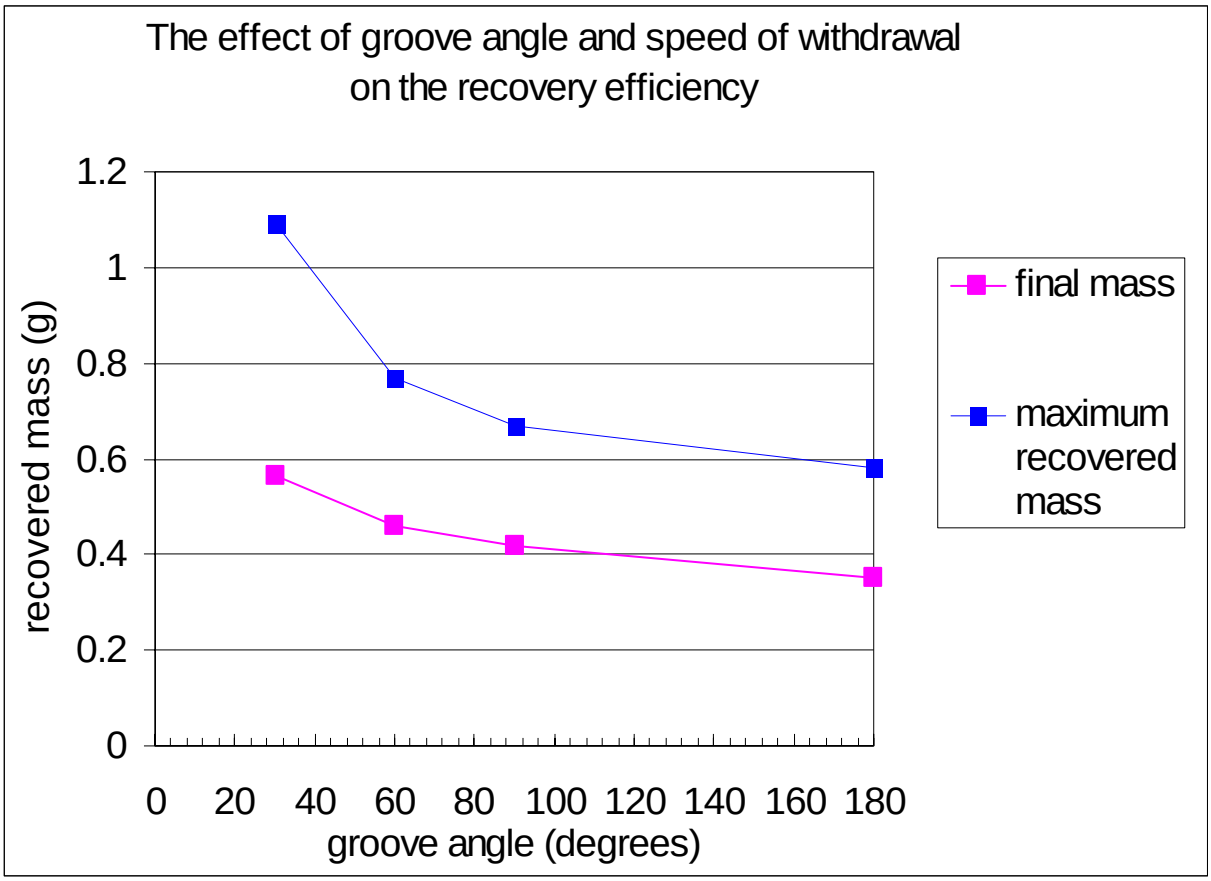

Figure 32. Maximum initial oil recovery and final oil recovery after drainage.

It must be kept in mind that vertical withdrawal of oil from a beaker is a convenient laboratory test, but is an incomplete representation of the oil recovery process with a skimmer. The skimmer rotational speed may also play an important role. The effect of the grooves on oil recovery by drums in a full-scale test may be even more pronounced than the one observed in the laboratory and oil recovery efficiency may be higher, due to the difference in the hydrodynamics of the process.

A separate detailed study would be required to determine optimum recovery surface parameters such as angle, depth and shape of the channels, withdrawal angle and speed. The recovery speed has to be high enough to bring the maximum amount of collected oil to the scraper and prevent it from draining down. The limiting factor is water entrainment at high speeds, which can break the oil film. Once the oil film is broken, the contact between oil and recovery surface at very high rotational speeds can be lost, resulting in decreasing recovery. High rotational speeds can also emulsify the oil, which results in higher water uptake and may reduce the overall oil recovery rate. The critical rotational speed can be determined experimentally with a full-scale test, and is likely to depend on

(1) surface material;
(2) withdrawal angle;
(3) oil properties; and
(4) temperature.

2.12 Effect of oil emulsification on the recovery efficiency.

2.12.1 Experimental setup

The emulsification mechanism is presented in Figure 33. It can hold up to 6 emulsification funnels.

Figure 33. Emulsification mechanism.

The emulsification procedure is similar to the one developed by SINTEF (www.sintef.no) and can be summarized as follows:

Funnels with a volume control orifice were filled with 500 ml of seawater from the Santa Barbara Channel. Then, 50 ml of oil was carefully added to the surface, resulting in a film thickness of about 14 mm. The hermetically closed funnels were installed into the emulsification mechanism and left in the temperature-controlled room for at least 12 hours prior to the experiment.

To simulate the emulsification process caused by braking waves, the funnels were rotated at a speed of 30 rpm for 17 hours and were stopped periodically for observation and measurements. After the emulsification was completed the funnels were opened and the amount of free water was measured. Water uptake by the oil samples after emulsification was calculated. Figure 34 shows emulsions obtained from different oils.

Emulsions obtained from each test oil were used to measure the affinity of test materials for emulsified oil. The test procedure was similar to the one described in section 2.10.1 with the exception of HydroCal and IFO emulsions. Unlike emulsions of Alaskan crude oils that were tested in the presence of free water, HydroCal and IFO emulsions were tested without free water due to their high viscosity. This is illustrated in Figure 34.

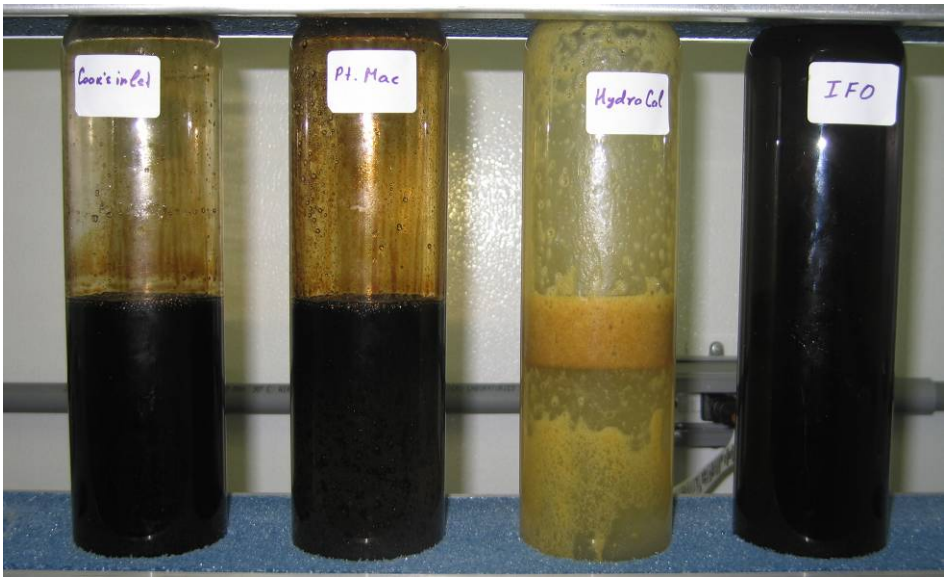

Figure 33. Emulsified oils and petroleum products.

Figure 34. Dip-and-withdraw test for emulsified HydroCal.

2.12.2 Results and discussions

The emulsification patterns of tested oils were quite different. During the same emulsification time of 16-17 hours at 15 or 25 ºC, Cook's Inlet and Pt. McIntyre crude oils formed an emulsion with a water content of less than 10%, while IFO-120 and HydroCal formed an emulsion with a water content of about 55-60%. At 5ºC, the water content of two crude oils emulsions was similar to the one at 15 and 25ºC (less than 10%). The water content of HydroCal emulsion decreased to 50-55% while the water content of IFO-120 emulsion decreased to 40-45%. Unlike other test oils, HydroCal formed a very unstable emulsion due to the lack of polar fractions in its chemical structure. Table 7 shows the viscosities of fresh and emulsified oils at three temperatures.

Table 7. The effect of emulsification and temperature on oil viscosity (measured in cP).

temperature	**5°C**		**15°C**		**25°C**	
oil type	fresh	emulsified	fresh	emulsified	fresh	emulsified
Cook's Inlet	60	65	9	12	5	9
Pt. McIntyre	160	n/a*	24	33	14	16
HydroCal 300	1296	13200	342	3790	162	1600
IFO-120	7978	17600	1540	18600	487	1400

* n/a – Not Applicable. Viscosity of this emulsion was not measured.

Table 7 illustrates the importance of emulsification process on the behavior of oils. Emulsification led to an increase in viscosity for all tested oils. Temperature decrease had similar effect. The increase in viscosity due to emulsification and temperature decrease was especially significant for viscous oils. The viscosity of light crude oil emulsions didn't increase at lower temperatures as much as the viscosity of heavier oils did. Figure 35 shows the effect of temperature on the viscosity of fresh and emulsified IFO-120 and HydroCal 300. The viscosity of emulsion was higher than the one of the fresh oils at all three temperatures. It was observed that at 5ºC, the viscosity of IFO-120 was very high which resulted in a slower water uptake and the reduction of emulsion water content down to 40%. The resulting viscosity of IFO-120 emulsion at 5ºC was slightly lower than viscosity at 15 °C, due to the higher (55%) water content.

The results of dipping tests with emulsions at 25, 15 and 5ºC are presented in Figures 36 through 45. The experimental procedure was similar to the dipping tests with fresh oils, so these graphics can be directly compared to the ones presented in section 2.10.2. It must be kept in mind, that although the amount of recovered product is higher for the emulsified oils, it contains water that was recovered together with oil.

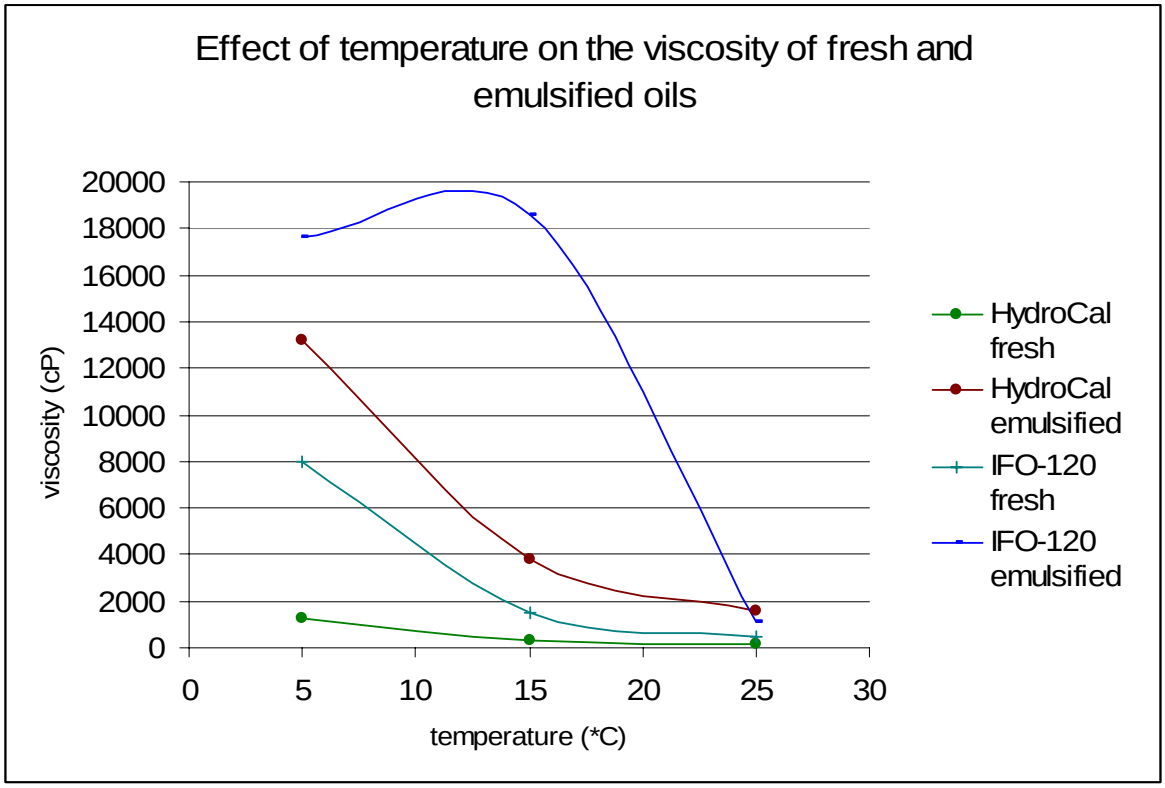

Figure 35. Effect of temperature on the viscosity of fresh and emulsified HydroCal and IFO.

Drainage curves for Cook's inlet emulsified oil at 25, 15 and 5ºC.

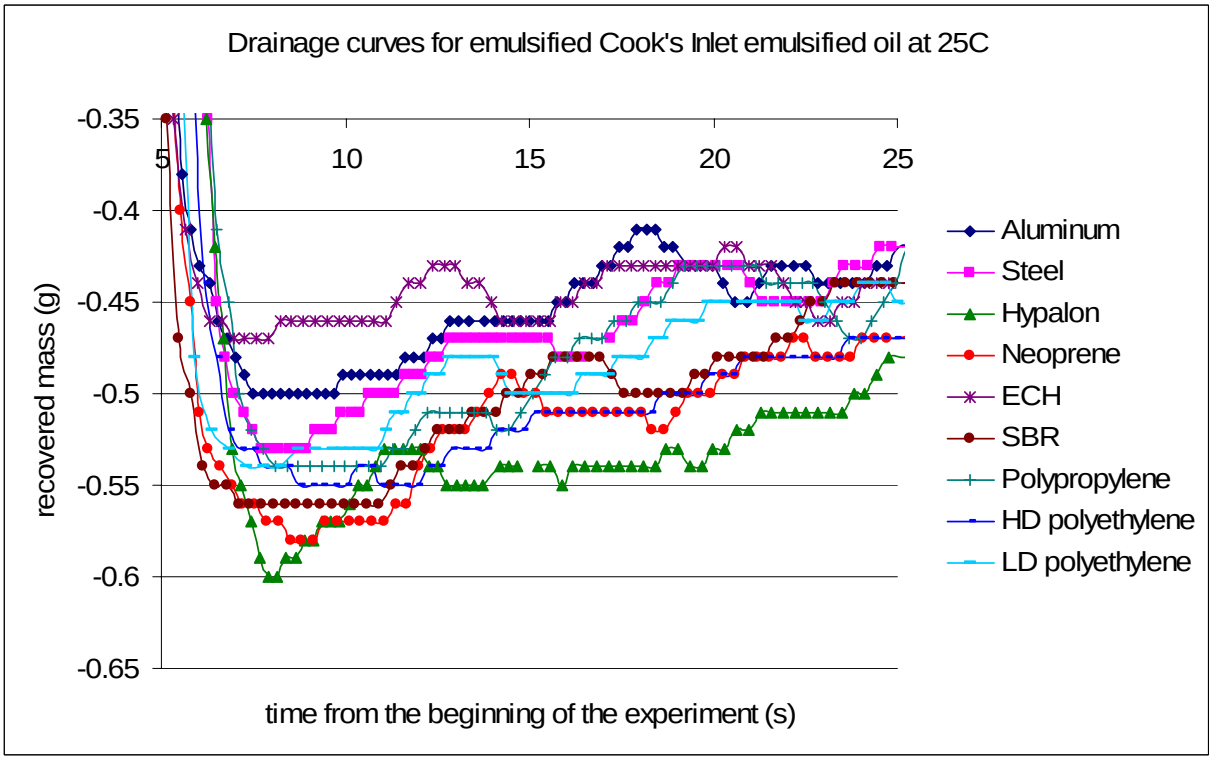

Figure 36. Drainage curves for emulsified Cook's Inlet oil at 25ºC.

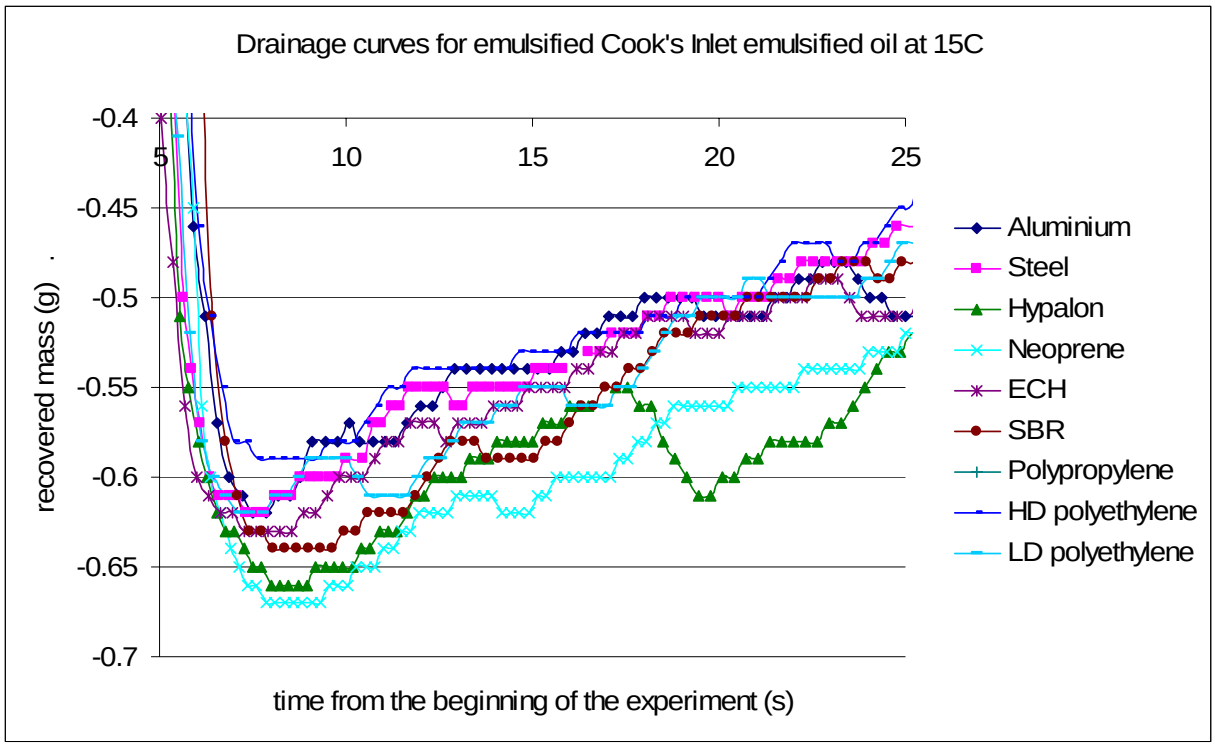

Figure 37. Drainage curves for emulsified Cook's Inlet oil at 15ºC.

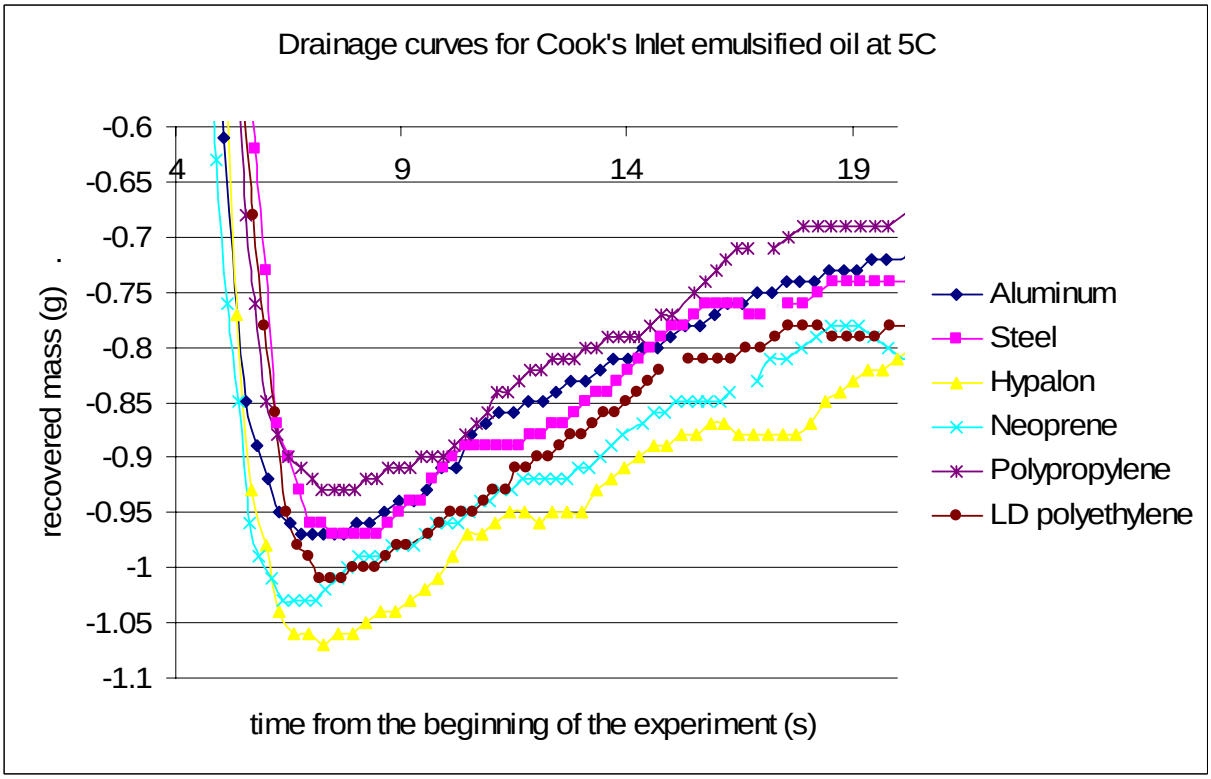

Figure 38. Drainage curves for emulsified Cook's Inlet oil at 5ºC.

Drainage curves for Pt. McIntyre emulsified oil at 25, 15 and 5ºC.

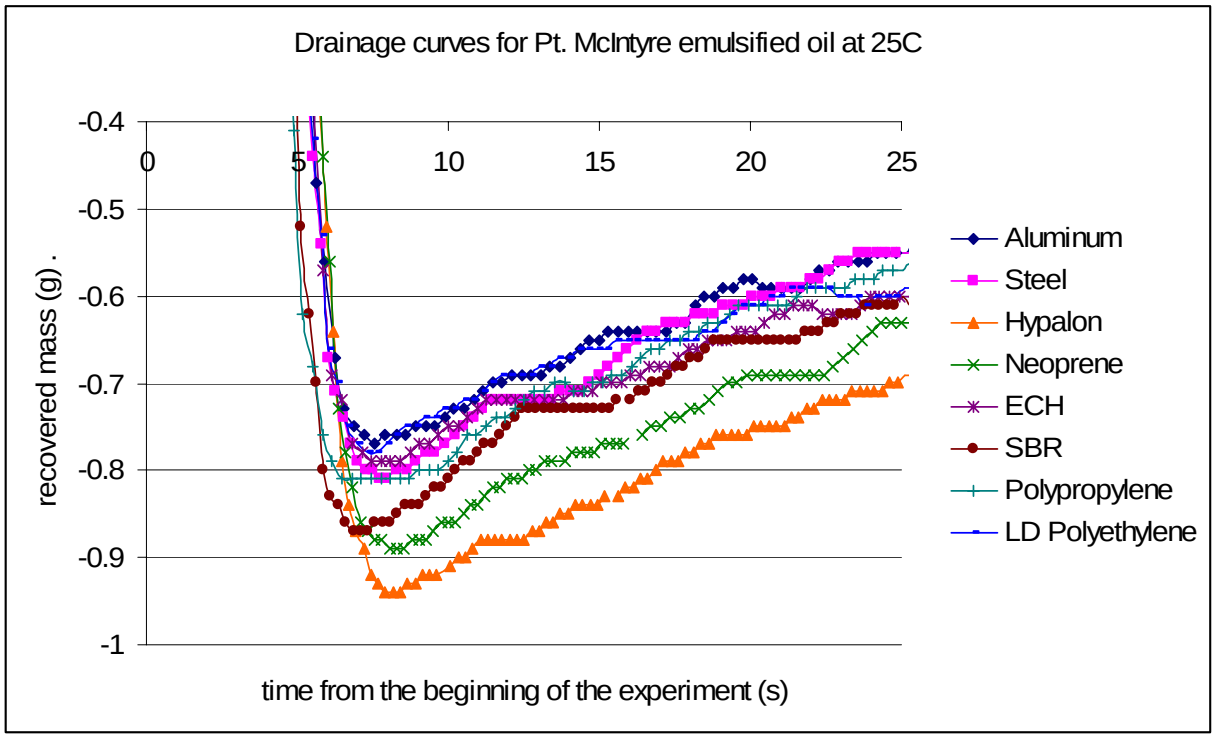

Figure 39. Drainage curves for emulsified Pt. McIntyre oil at 25ºC.

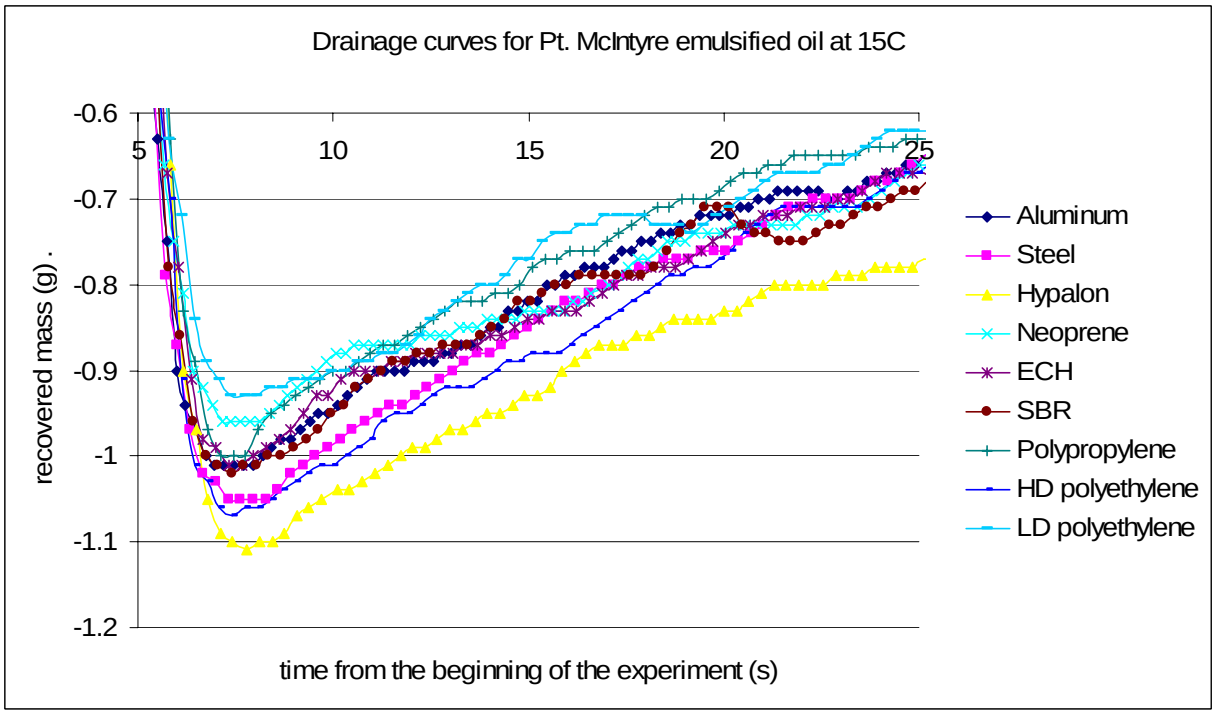

Figure 40. Drainage curves for emulsified Pt. McIntyre oil at 15ºC.

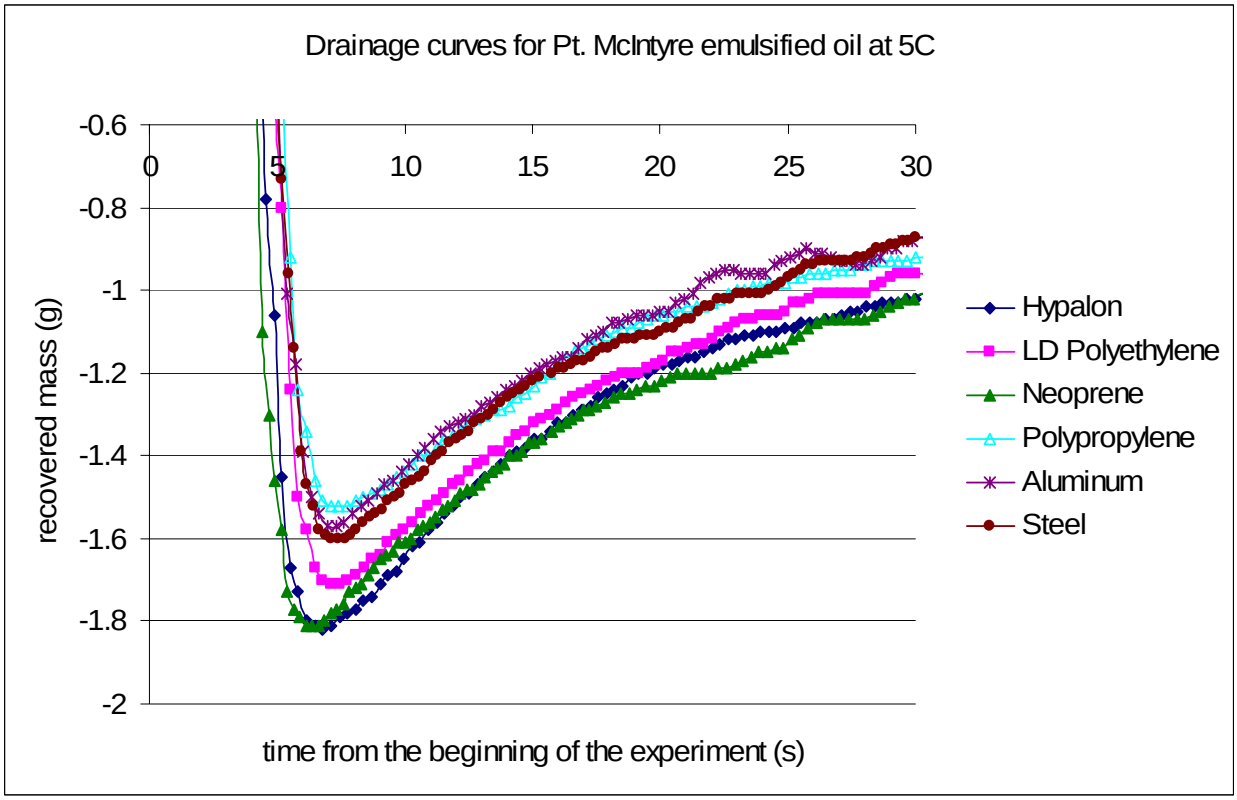

Figure 41. Drainage curves for emulsified Pt. McIntyre oil at 5ºC.

Drainage curves for HydroCal 300 emulsified oil at 25 and 15ºC.

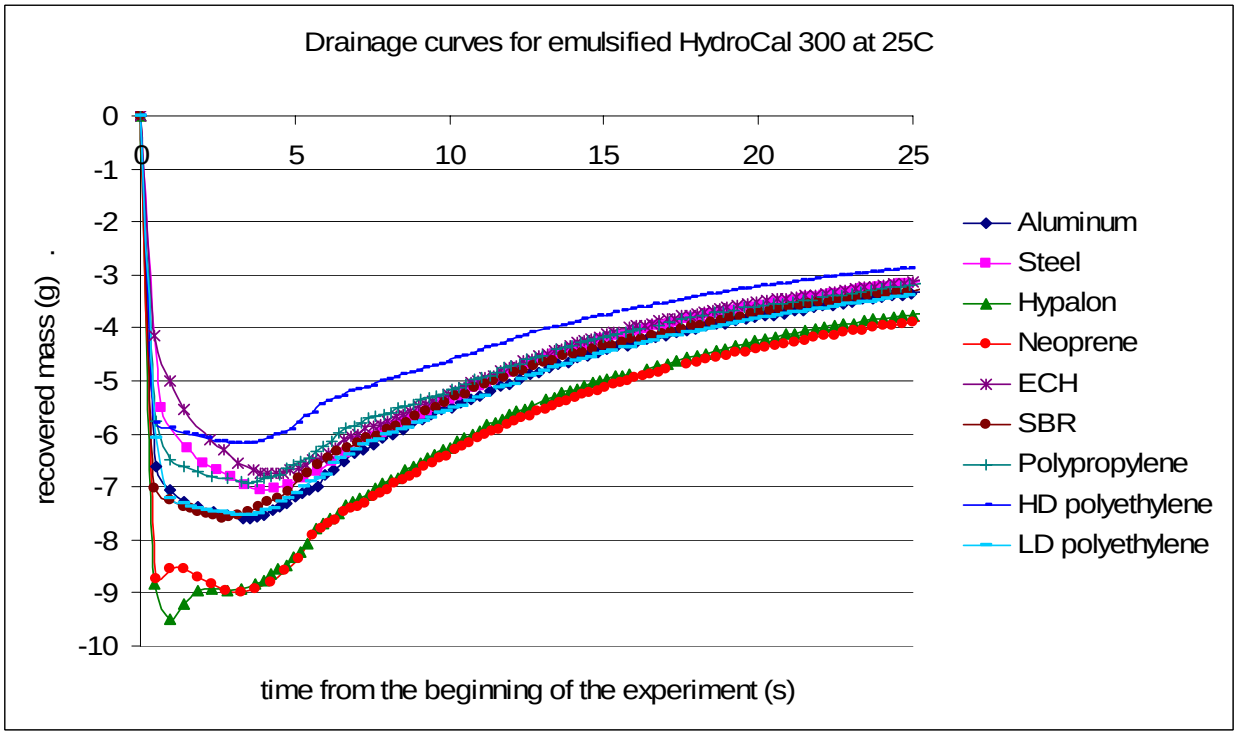

Figure 42. Drainage curves for emulsified HydroCal 300 at 25ºC.

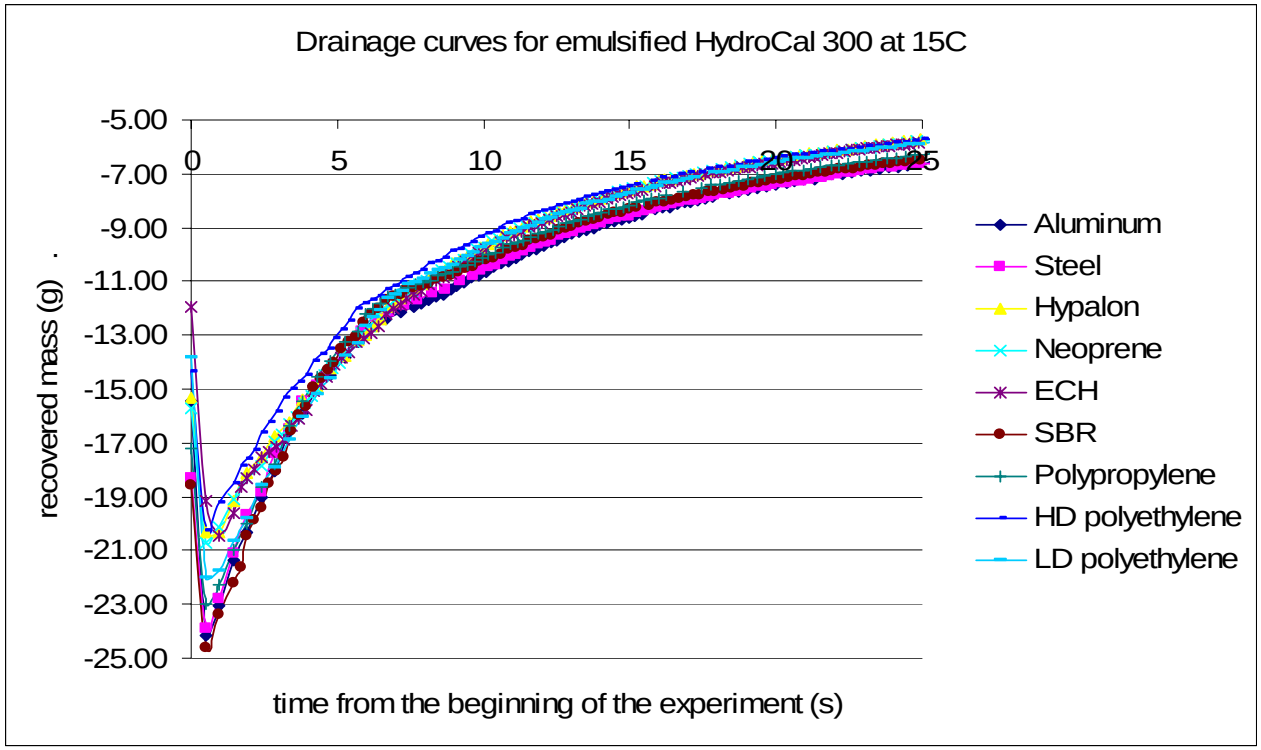

Figure 43. Drainage curves for emulsified HydroCal 300 at 15ºC.

Drainage curves for IFO-120 emulsified oil at 25 and 15ºC.

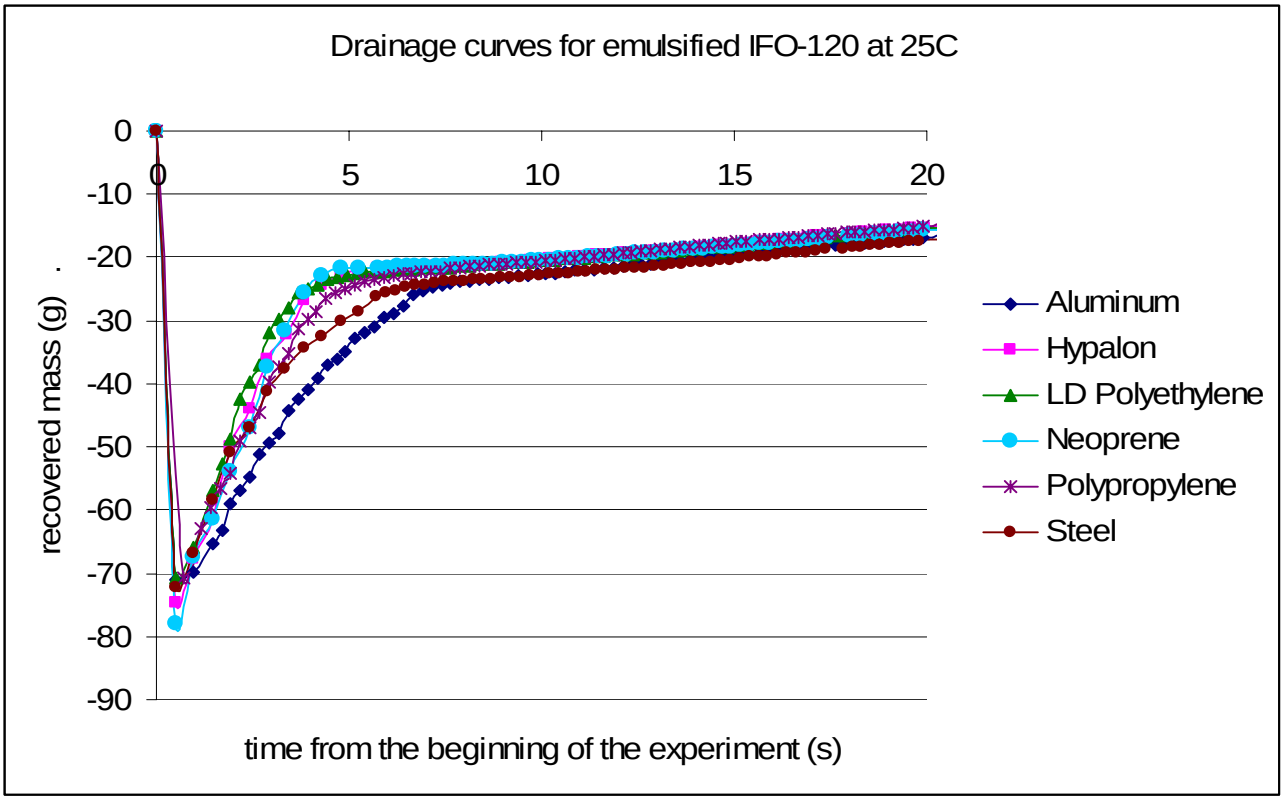

Figure 44. Drainage curves for emulsified IFO-120 at 25ºC.

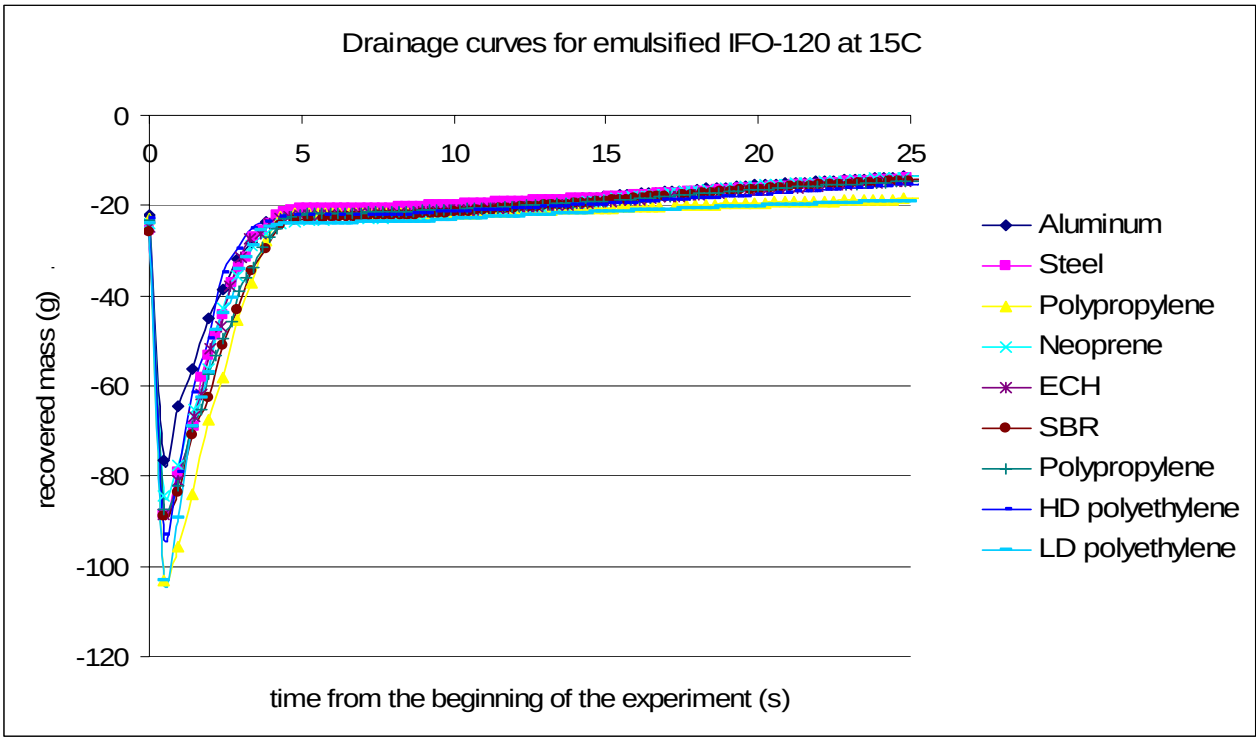

Figure 45. Drainage curves for emulsified IFO-120 at 15ºC.

The data presented in Figures 37 through 46 confirmed the previous observation that increased viscosity (either due to temperature or oil type) results in a higher recovered mass. Hypalon® and Neoprene® were found to recover more oil than other tested materials.

A summary of the effect of temperature, oil type, weathering and emulsification degree on the amount of recovered oil is illustrated in Figure 47. All data plotted on this graphic correspond to the tests with aluminum plates with HydroCal 300 and Pt. McIntyre crude oil.

Figure 47 shows that the amount of recovered oil is proportional to its viscosity. That was valid for fresh, evaporated and weathered oils. For Pt. McIntyre crude oil, weathering (loss of 15% of light components) had grater effect on the increase of viscosity and hence on the amount of recovered mass, than decreasing of ambient temperature from 25 to 15ºC. Emulsification at 25 and 15ºC caused a minor increase in the recovered mass, while at 5ºC, larger mass was recovered for fresh oil. An emulsification and temperature decrease increased the amount of recovered HydroCal. It was observed that emulsification of HydroCal had greater effect on the amount of recovered product than the temperature decrease from 25 to 15Cº. Overall, oils with higher viscosity had much greater changes in their behavior and viscosity than lighter oils.

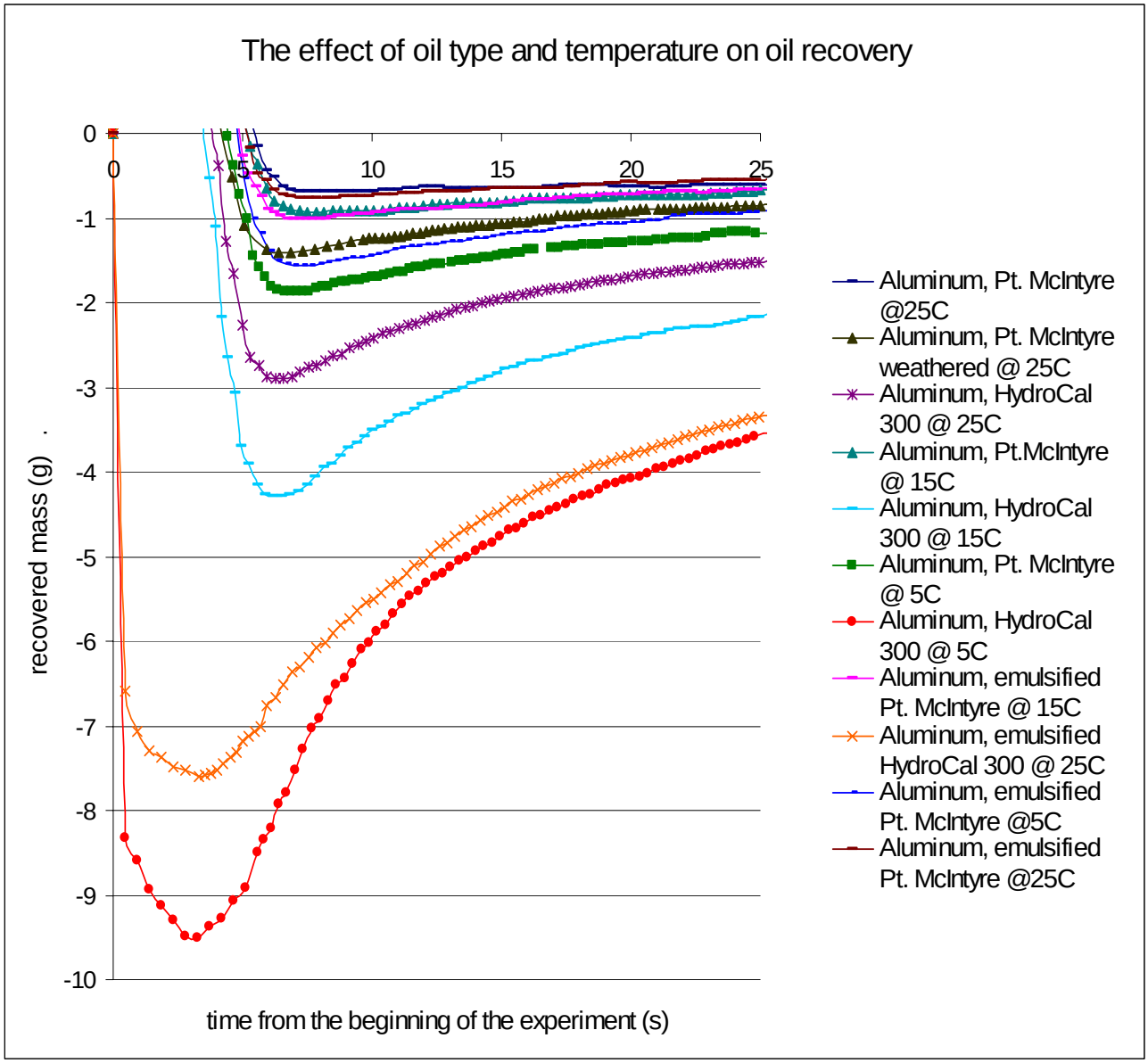

Figure 46. The effect of oil type, temperature and emulsification on the amount of recovered oil.

Figures 47 and 48 represent the comparison of the recovery potential of some of the tested materials. The amount of oil recovered by each material was plotted against oil viscosity. Figure 47 shows data for light oils. Figure 48 shows data for viscous oils. Both Figures confirm that the recovered mass is a strong function of oil viscosity and that the recovery potential of Neoprene® and Hypalon® was highest for all tested oils.

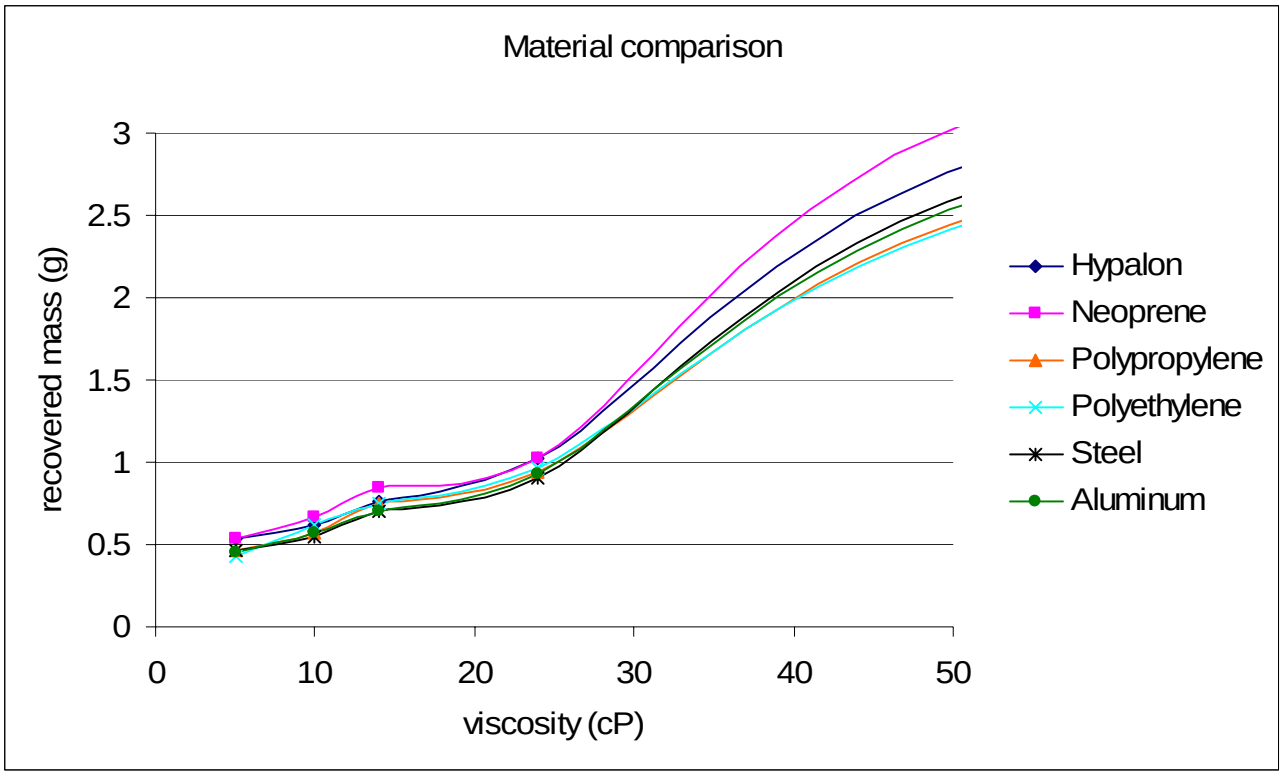

Figure 47. Recovery potential of various materials as a function of oil viscosity. Light oils.

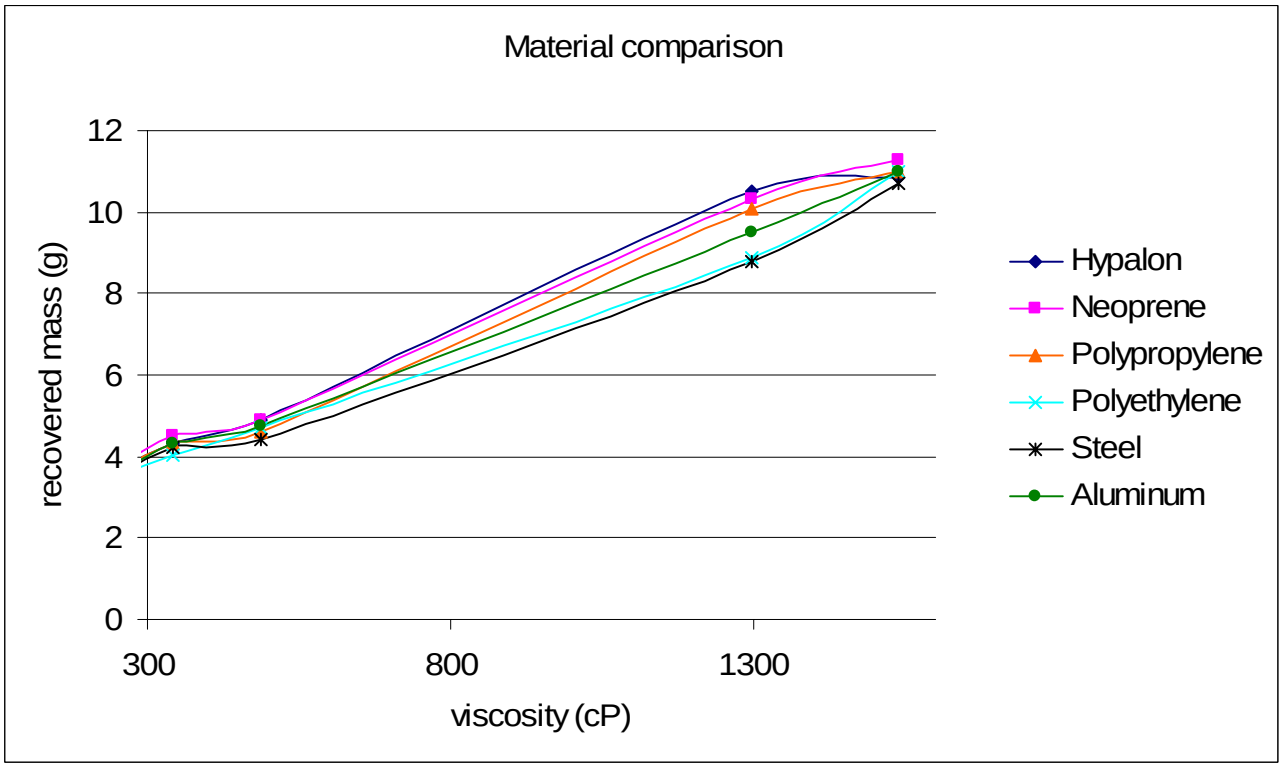

Figure 48. Recovery potential of various materials as a function of oil viscosity. Viscous oils.

3. Conclusions and recommendations

Based on the results of this research, we have determined that:

- Recovery efficiency depends on oil viscosity and, hence, is a strong function of oil properties and temperature. Temperature changes, weathering and emulsification have much greater effects on properties of high viscosity oils than on low viscosity oils;
- Viscous oils above their pour point are more easily recovered than light oils, since a thicker slick remains on the surface after withdrawal. The cohesion of viscous oils results in slower oil drainage from the surface;
- Oleophilic elastomers (such as Hypalon® and Neoprene®) have higher oil recovery potential than hard polymeric surfaces, but swelling of some elastomers can reduce their applicability for oil recovery;
- Antistatic Polyurethane and Teflon® can be efficiently used for applications when oil adhesion is not required.
- The DCA can provide valuable information about the recovery potential and oleophilicity of various materials. For rough surfaces, DCA is less effective for screening than a dipping test, although it can still provide some valuable data if the rough surfaces are tested with medium viscosity oils rather than with very light or very viscous oils. It was found that for smooth hard plastics and metals, the difference between the advancing and receding contact angles (contact angle hysteresis) is a parameter that can give a reasonable prediction of the material recovery potential. Advancing contact angle indicates the affinity of a material to a test liquid and can give a good description of a wetting/spreading behavior of liquid on solid. Advancing contact angle can be used to evaluate the recovery potential of rough elastomers. In this case, if liquid can wet the surface, it will be retained there by the surface roughness during the withdrawal;
- The dip-and-withdraw technique has higher measurement error than the contact angle (DCA technique), but it might be more effective for evaluating rough surfaces or very viscous oils.
- While changing the recovery material can improve the recovery efficiency up to 20%, adding a grooved pattern to the recovery surface with a matching scraper can improve the recovery efficiency up to 100%, compared to a flat surface. The effect of the grooves on oil recovery in a full-scale test with drums may be even more pronounced than the one observed in the laboratory and oil recovery efficiency may be higher, due to the difference in the hydrodynamics of the recovery process;
- The proposed patterned surface is most efficient on light and medium viscous oils. In general, it is more efficient than the surface covered with bristles except for the cases of extremely viscous or semisolid oils;
- Recovery efficiency is higher with decreasing groove angle, although there is a balance between capillary forces holding the oil and the amount of oil within the groove. For viscous oils, the opening of the channel should be wide enough for oil to penetrate inside the groove. For light oils, narrow grooves will perform better; and
- A separate detailed study is required to determine optimum recovery surface parameters such as angle, depth and shape of the channels, withdrawal angle and speed.

4. References

ASTM D70. Standard Test Method for Specific Gravity and Density of Semi-Solid Bituminous Materials (Pycnometer Method). ASTM International, 2003.

ASTM D1429. Standard Test Methods for Specific Gravity of Water and Brine. ASTM International, 2003.

Etkin, D. S., Cleanup Costs for Oil Spills in Ports. Port Technology International, 2000.

Fingas, M., Basics of oil spill cleanup. 2nd edition. Edited by J. Charles. Lewis Publishers, 2000.

Jokuty, P., Whiticar, S., McRoberts, K., Mullin, J., Oil adhesion testing – recent results. Proceedings from the Nineteenth Arctic Marine Oil spill Prog. Tech. Seminar. Canada. 1996.

Liukkonen S., Koskivaara R., Rytkonen, J., Lampela, K., Adhesion of oil to plastics, stainless steel and ice. Proceedings from the Eighteenth Arctic Marine Oilspill Program Technical Seminar. Canada. 1995.

Wake W.C., Adhesion and the formulation of adhesives. Applied Science Publishers, London, 1982.

Della Bona A., Shen C. and Anusavice K.J., Work of adhesion of resin on treated lithia disilicate-based ceramic, Dental Materials, Volume 20, Issue 4, May 2004.

Lee Y., Fang T., Yang Y. and Maa J., The enhancement of dropwise condensation by wettability modification of solid surface, International Communications in Heat and Mass Transfer, Volume 25, Issue 8, November 1998.

Appendix 1. Materials evaluated for this project.

Materials evaluated for this project:

1. Epichlorohydrin resin (ECH)
2. Polyethylene glycol (PEG)
3. Polytetrafluoroethylene (PTFE)
4. Polyvinylidene fluoride (PVDF)
5. Polyethylene (Low density PE)
6. Polypropylene (PP)
7. Polyetheretherketone (PEEK)
8. Polyurethane (Antistatic)
9. Acrylonitrile Butadiene Styrene (ABS)
10. Cast Acrylic
11. Acetate
12. Delrin
13. Teflon (Virgin electrical Grade)
14. Nylon 6/6
15. Polycarbonate
16. Polyester
17. Polyethylene (Ultra High Molecular Weight)
18. Polystyrene (High-Impact)
19. Polyvinyl Sulfate (PVC)
20. Vinyl rubber
21. Comercial grade Viton rubber
22. Silicone rubber
23. Hypalon ® ozon-resistant rubber
24. Comercial grade Neoprene® rubber
25. Butyl rubber
26. Comercial grade Buna-n rubber
27. Latex rubber
28. Gum rubber
29. Styrene-Butadiene Rubber
30. Neoprene® Rubber
31. Aluminum
32. Stainless steel
33. Ethylene Propylene Diene Monomer (EPDM)

Appendix 2. Surface pictures of test materials.

Aluminum 10x magnification

Surface Statistics:

Ra: 499.52 nm

Rq: 609.55 nm

Rz: 4.15 um

Rt: 4.56 um

Set-up Parameters:

Size: 640 X 480

Sampling: 966.80 nm

Processed Options:

Terms Removed:

Tilt

Filtering:

None

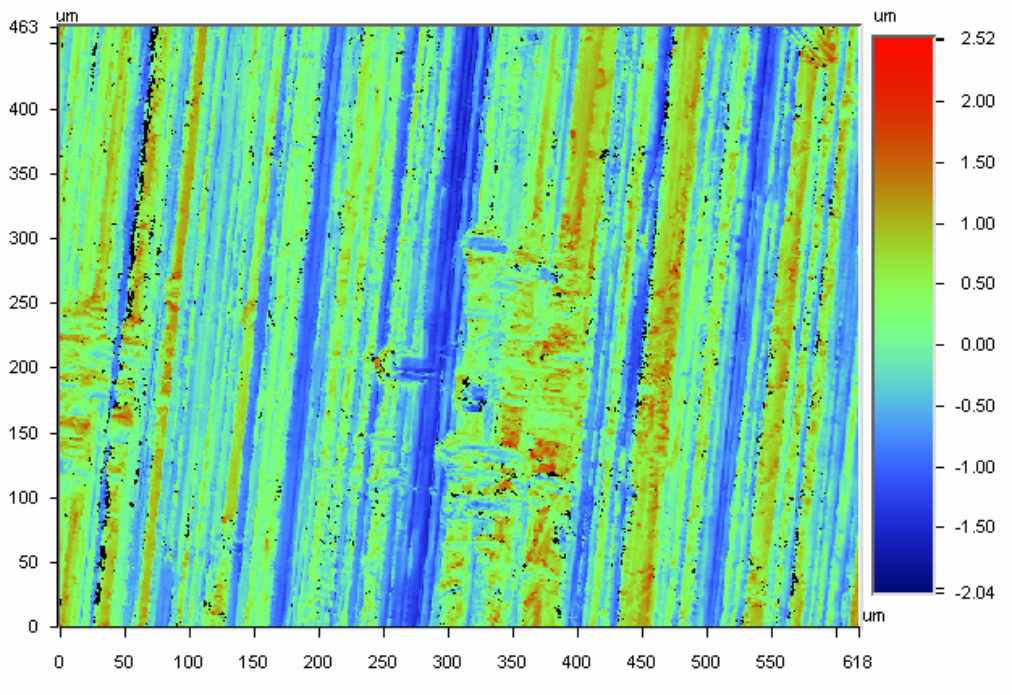

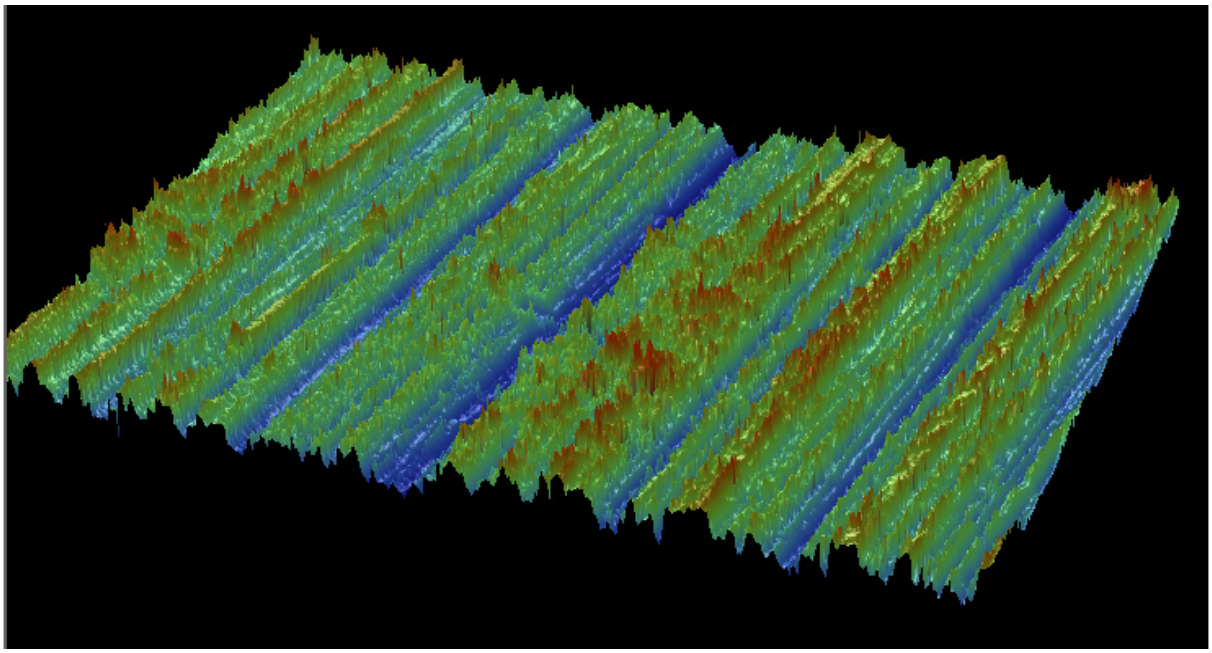

Aluminum 50x magnification

Surface Statistics:

Ra: 377.69 nm

Rq: 449.83 nm

Rz: 2.92 um

Rt: 3.30 um

Set-up Parameters:

Size: 640 X 480

Sampling: 193.36 nm

Processed Options:

Terms Removed:

Tilt

Filtering:

None

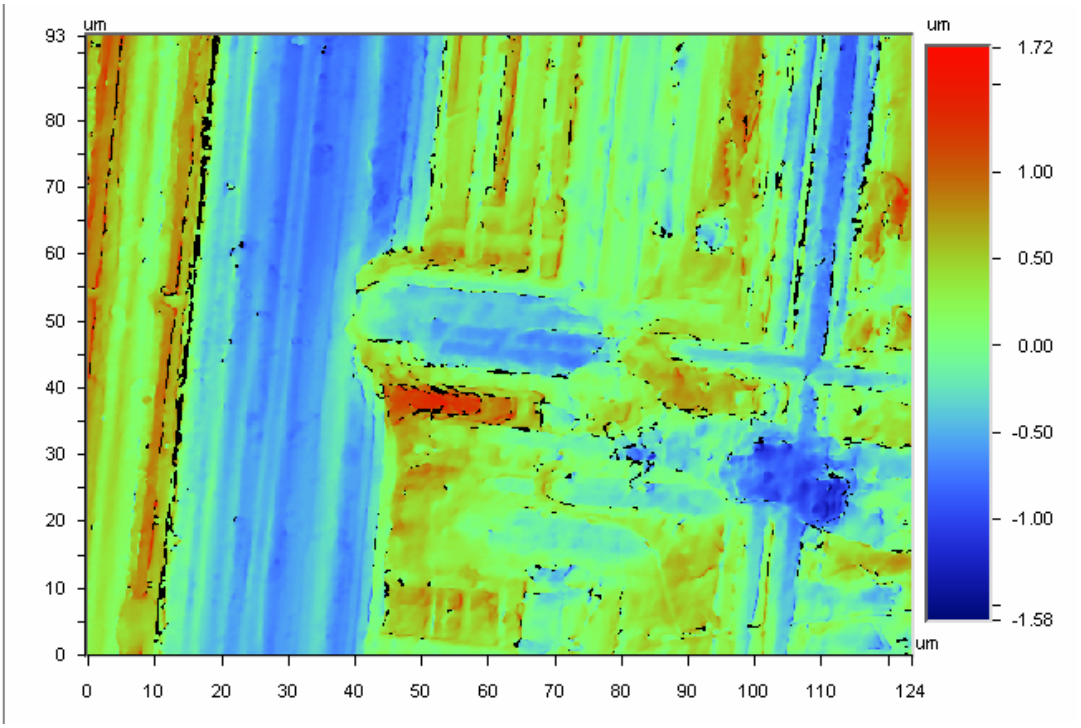

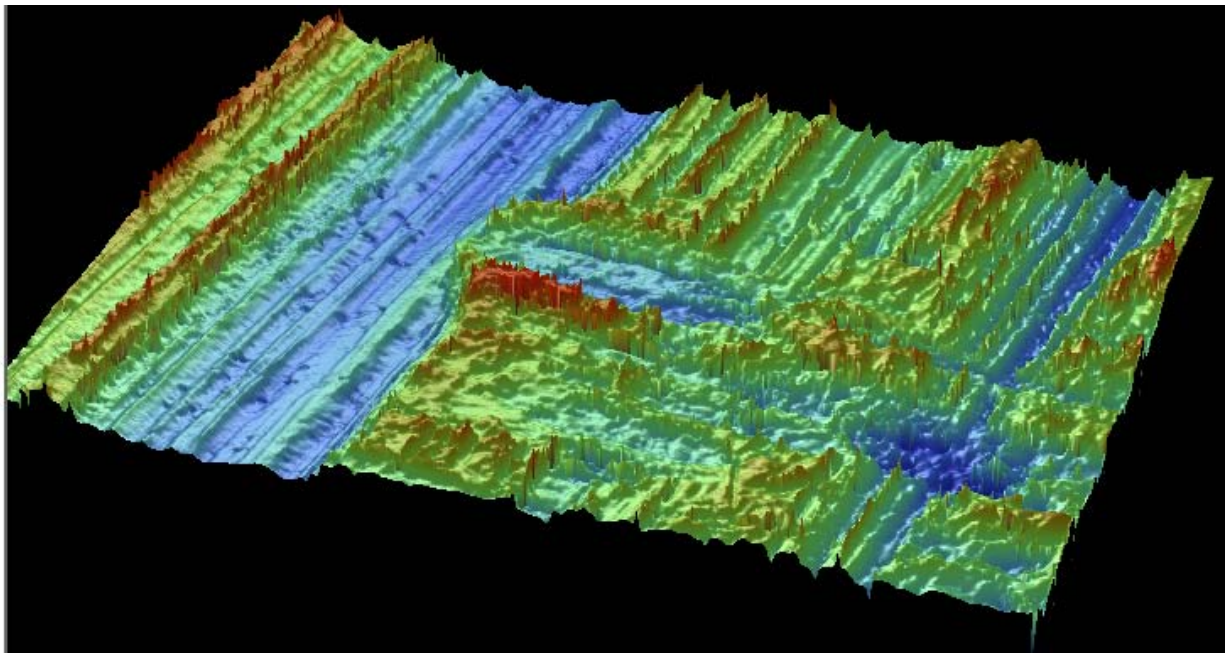

Epichlorohydrin resin (ECH) 10x magnification

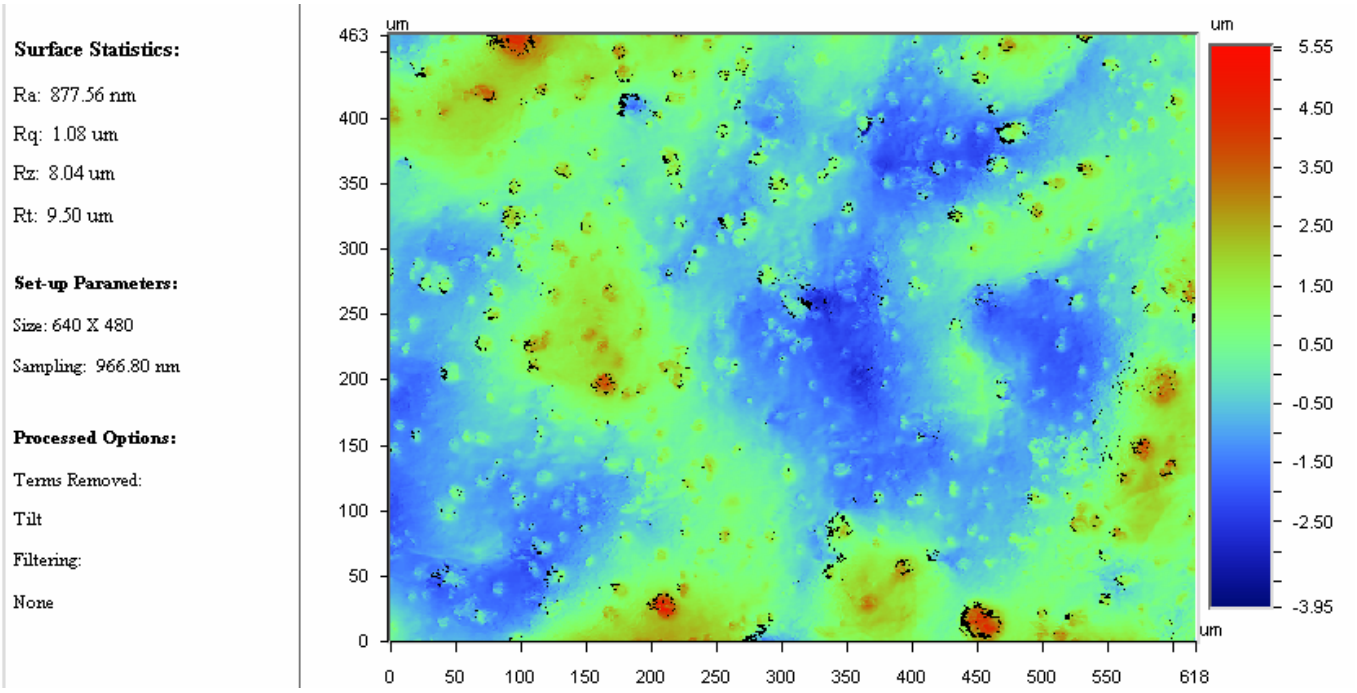

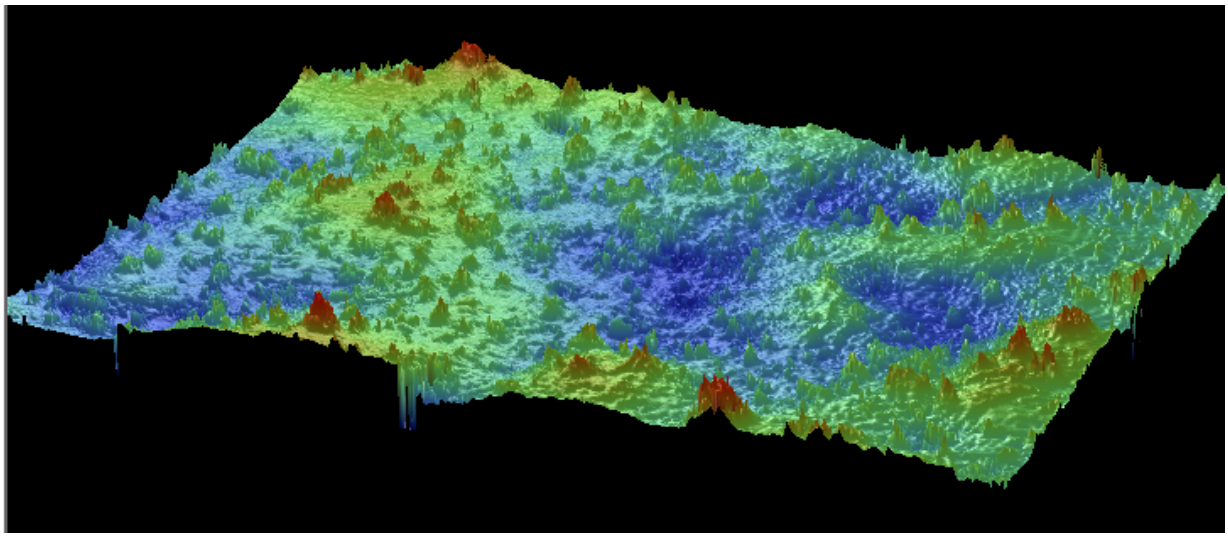

Epichlorohydrin resin (ECH) 50x magnification

Surface Statistics:

Ra: 367.26 nm

Rq: 451.00 nm

Rz: 3.01 um

Rt: 3.49 um

Set-up Parameters:

Size: 640 X 480

Sampling: 193.36 nm

Processed Options:

Terms Removed:

Tilt

Filtering:

None

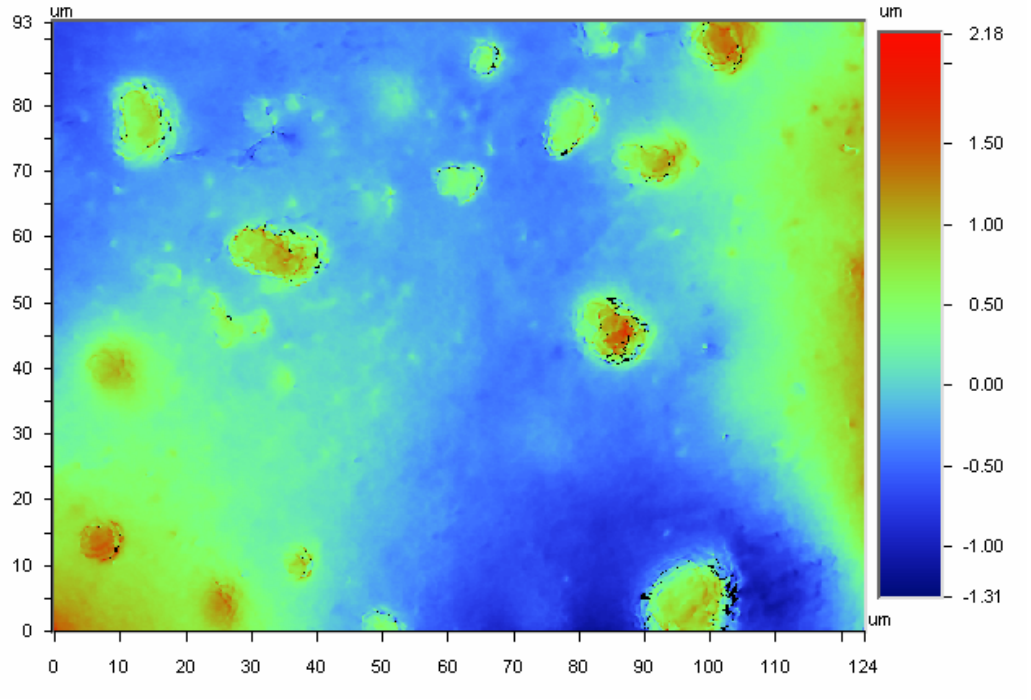

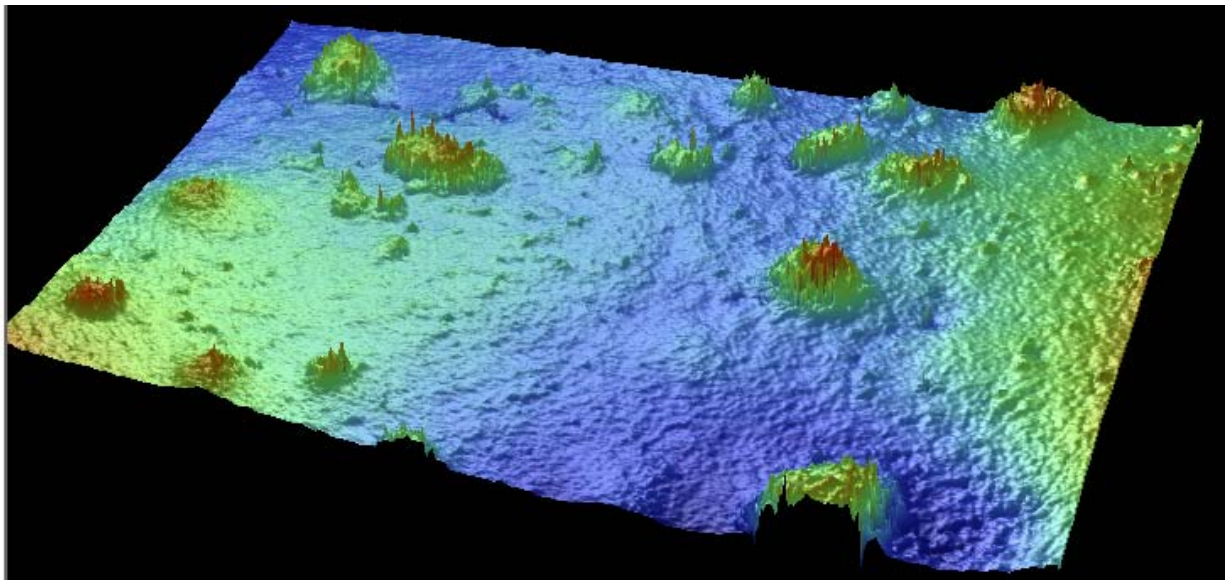

Hypalon ® 5x magnification

Surface Statistics:

Ra: 1.70 um

Rq: 2.15 um

Rz: 19.52 um

Rt: 21.57 um

Set-up Parameters:

Size: 640 X 480

Sampling: 1.93 um

Processed Options:

Terms Removed:

Tilt

Filtering:

None

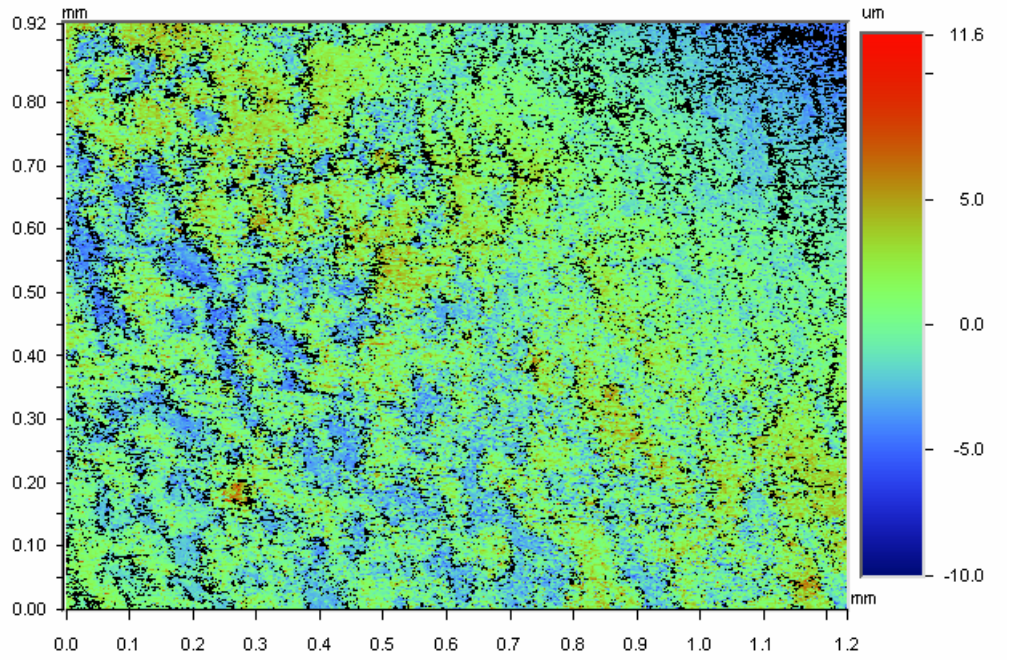

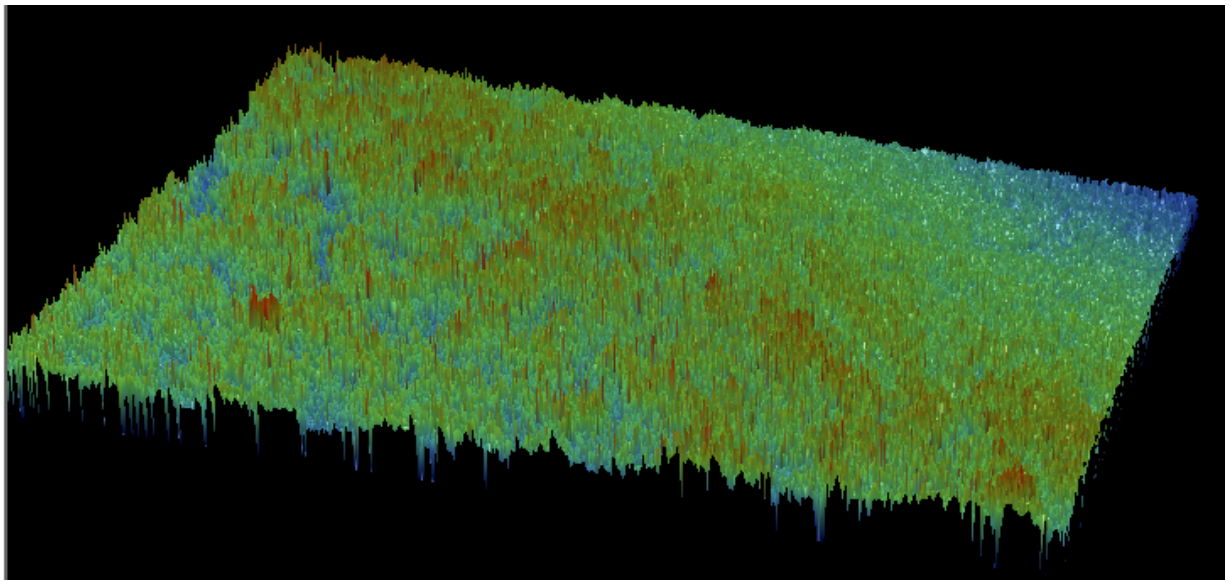

Hypalon ® 50x magnification

Surface Statistics:

Ra: 807.72 nm

Rq: 996.76 nm

Rz: 9.26 um

Rt: 11.48 um

Set-up Parameters:

Size: 640 X 480

Sampling: 193.36 nm

Processed Options:

Terms Removed:

Tilt

Filtering:

None

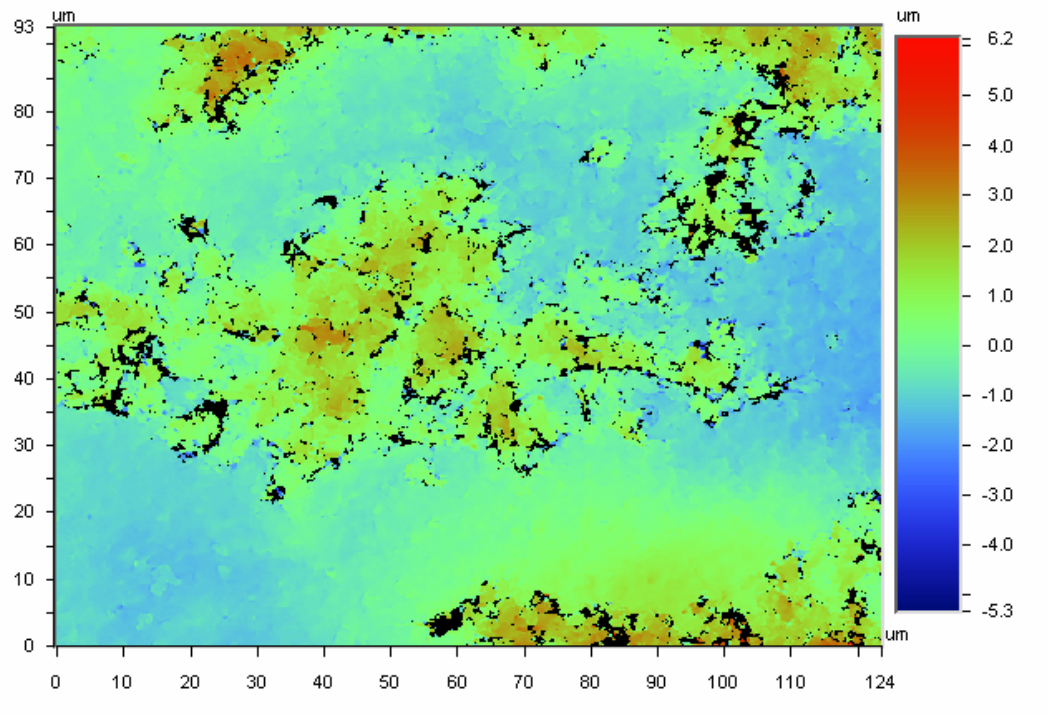

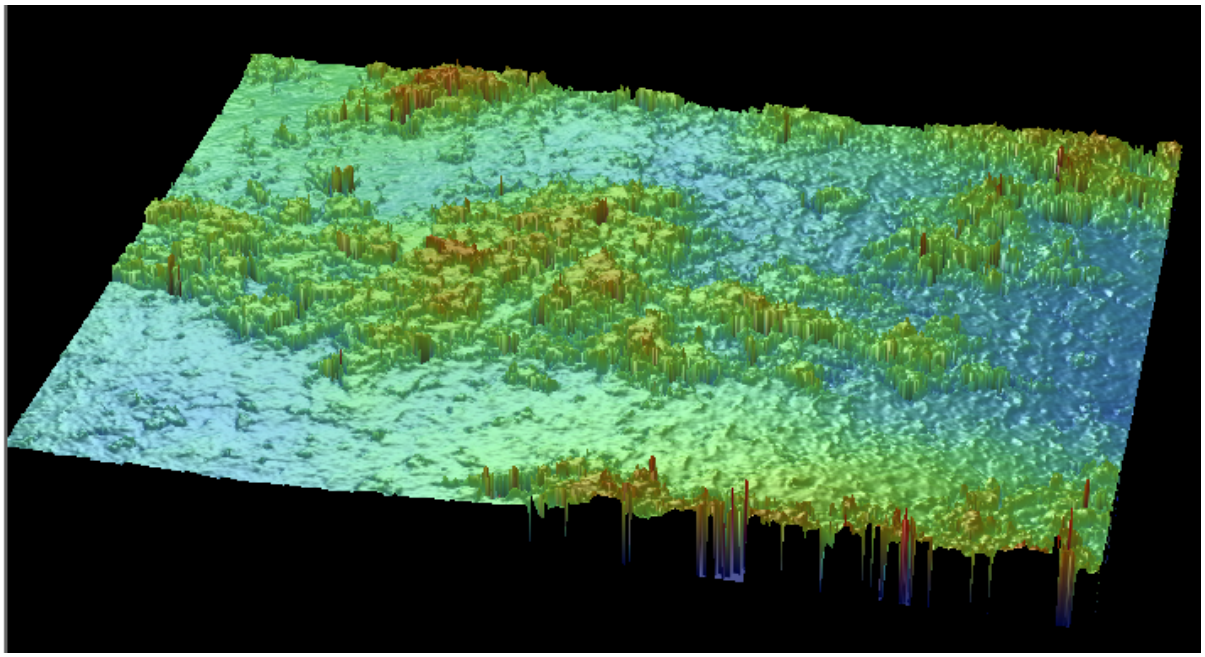

Neoprene® 10x

Surface Statistics:

Ra: 431.61 nm

Rq: 620.07 nm

Rz: 13.99 um

Rt: 26.60 um

Set-up Parameters:

Size: 640 X 480

Sampling: 966.80 nm

Processed Options:

Terms Removed:

Tilt

Filtering:

None

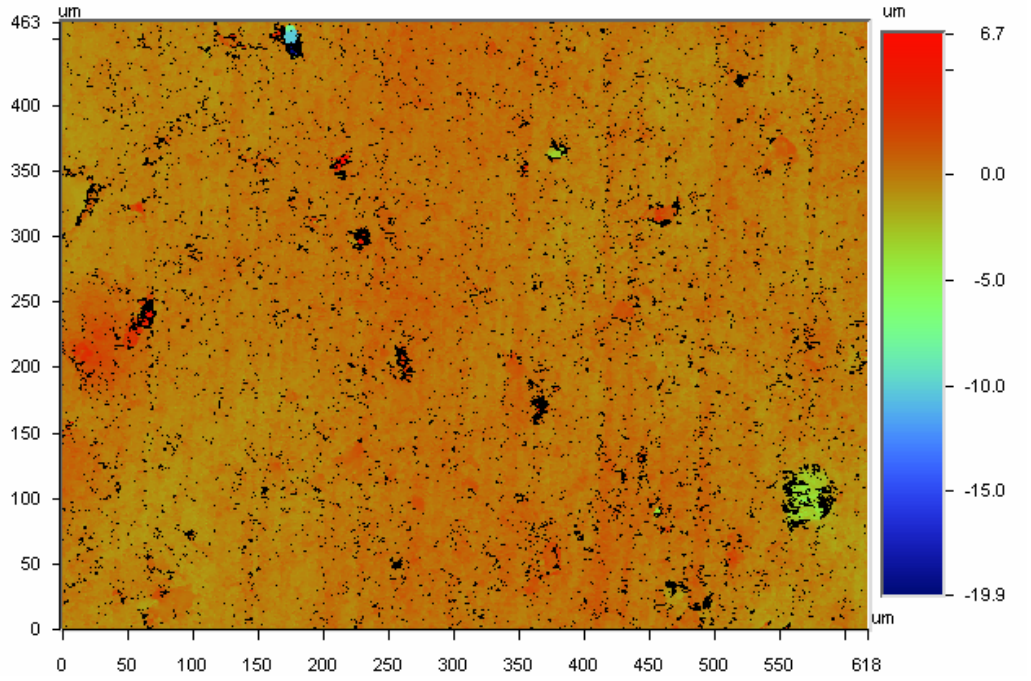

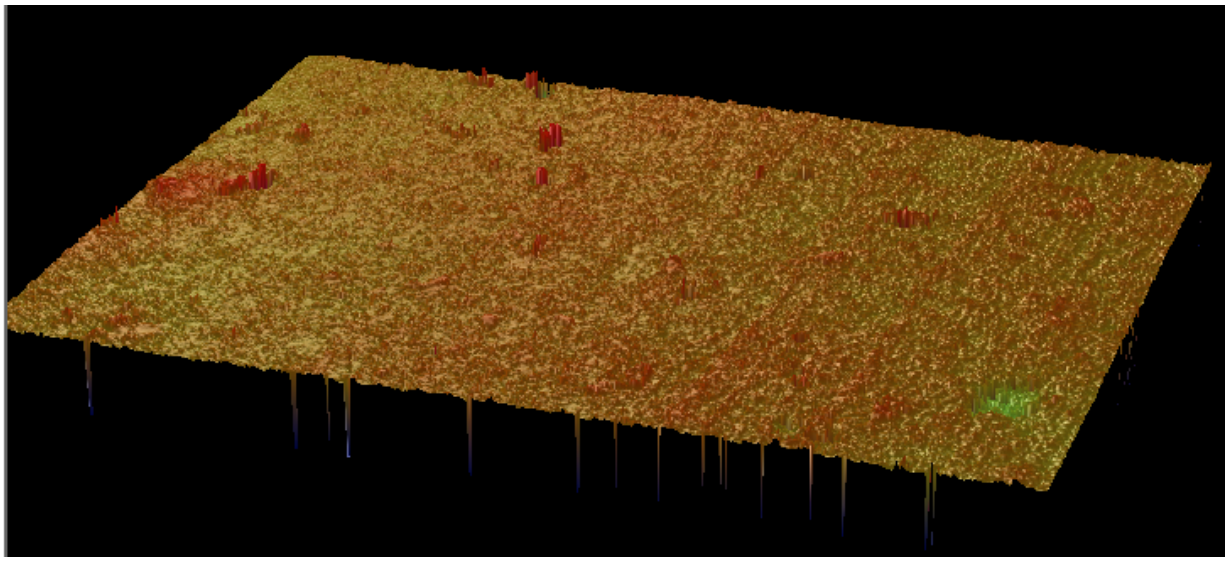

Neoprene® 50x

Surface Statistics:

Ra: 192.80 nm

Rq: 247.99 nm

Rz: 2.55 um

Rt: 2.88 um

Set-up Parameters:

Size: 640 X 480

Sampling: 193.36 nm

Processed Options:

Terms Removed:

Tilt

Filtering:

None

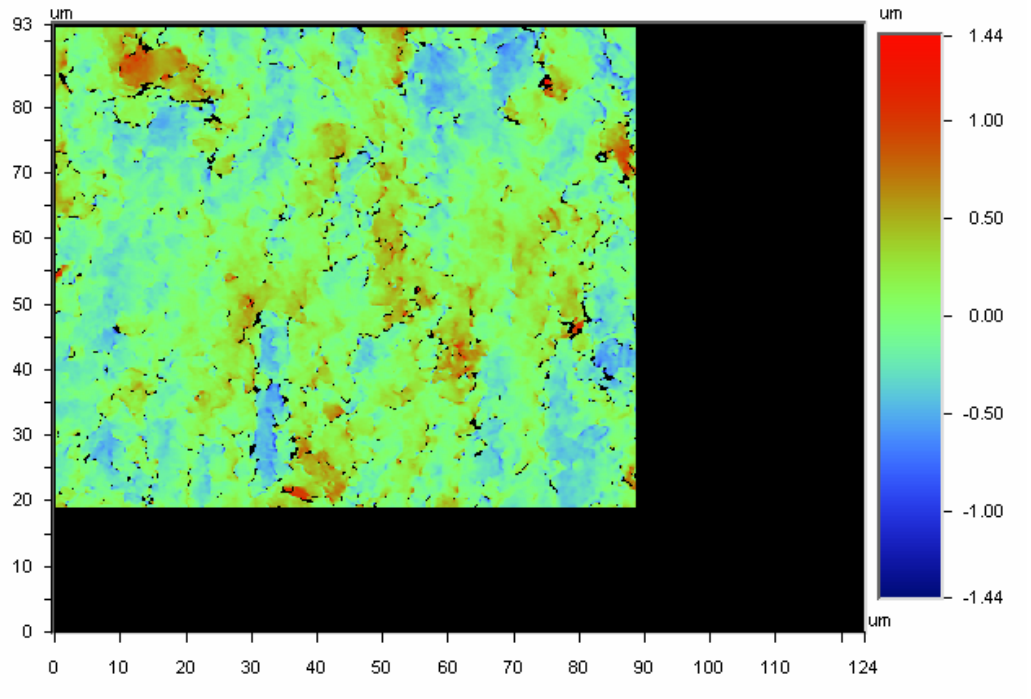

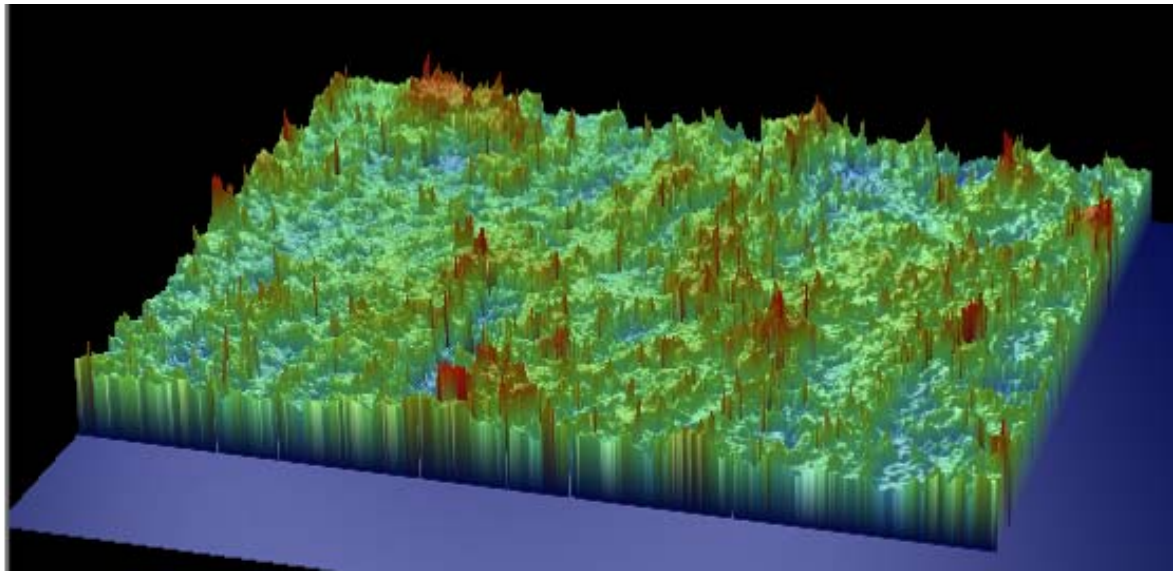

Polyethylene 10x magnification

Surface Statistics:

Ra: 29.68 nm

Rq: 63.13 nm

Rz: 2.77 um

Rt: 5.15 um

Set-up Parameters:

Size: 640 X 480

Sampling: 966.80 nm

Processed Options:

Terms Removed:

Tilt

Filtering:

None

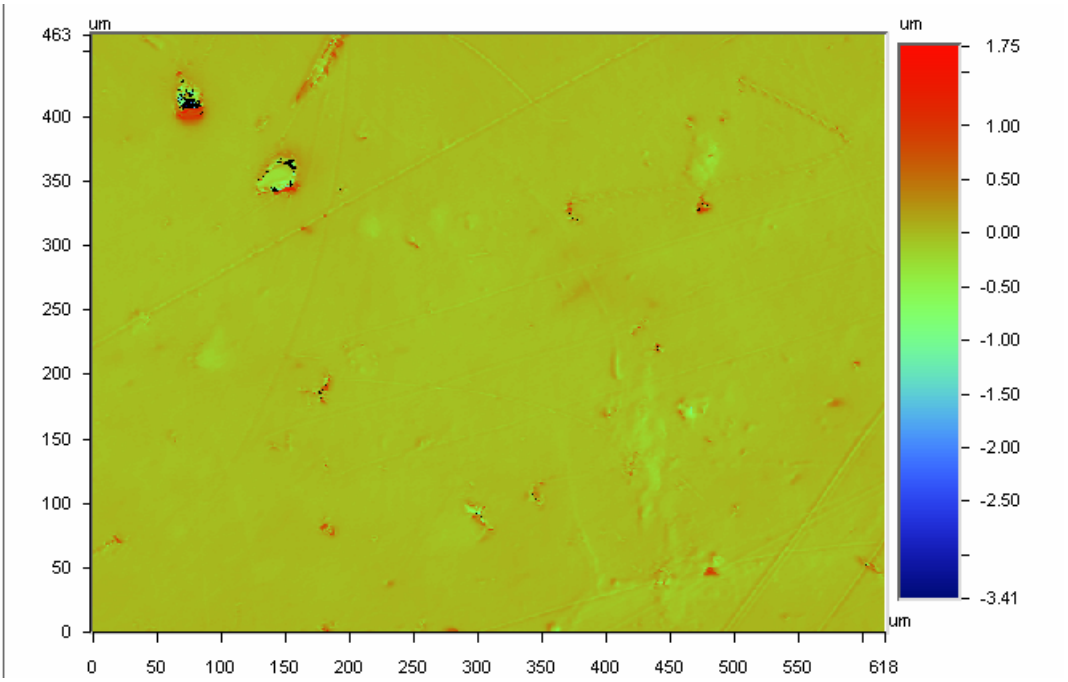

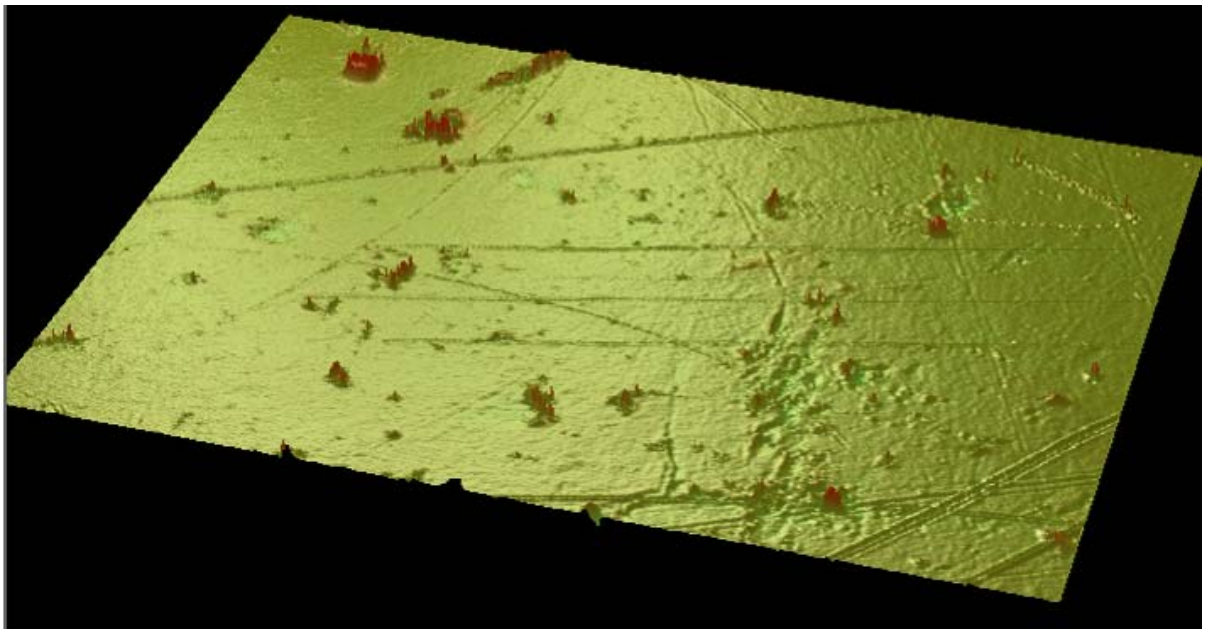

Polyethylene 50x magnification

Surface Statistics:

Ra: 11.98 nm

Rq: 16.52 nm

Rz: 278.29 nm

Rt: 914.83 nm

Set-up Parameters:

Size: 640 X 480

Sampling: 193.36 nm

Processed Options:

Terms Removed:

Tilt

Filtering:

None

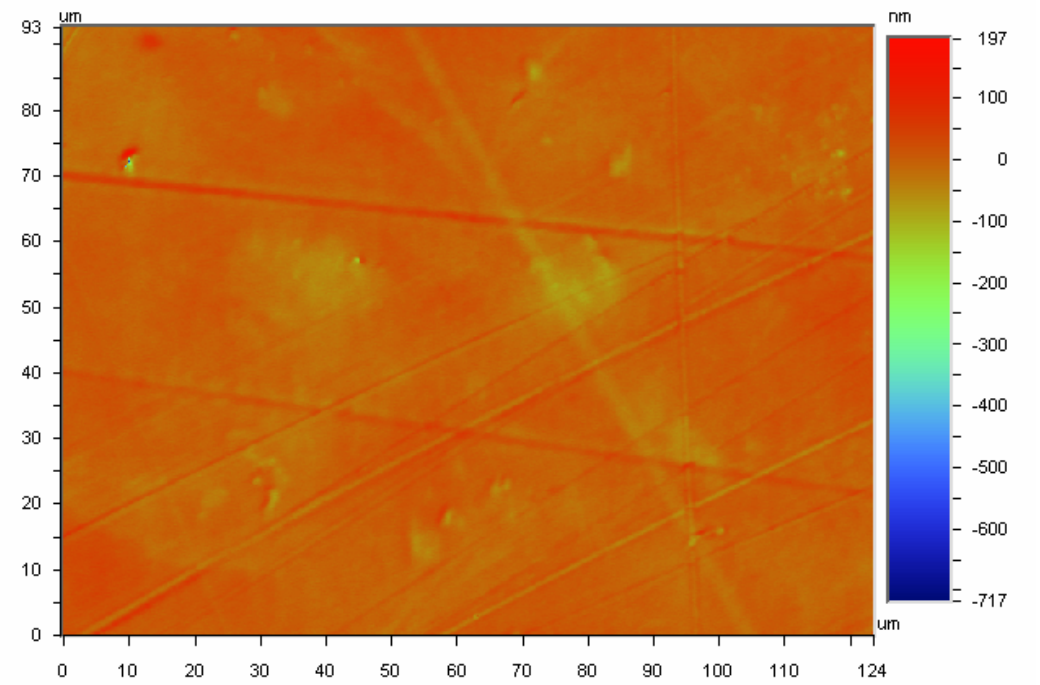

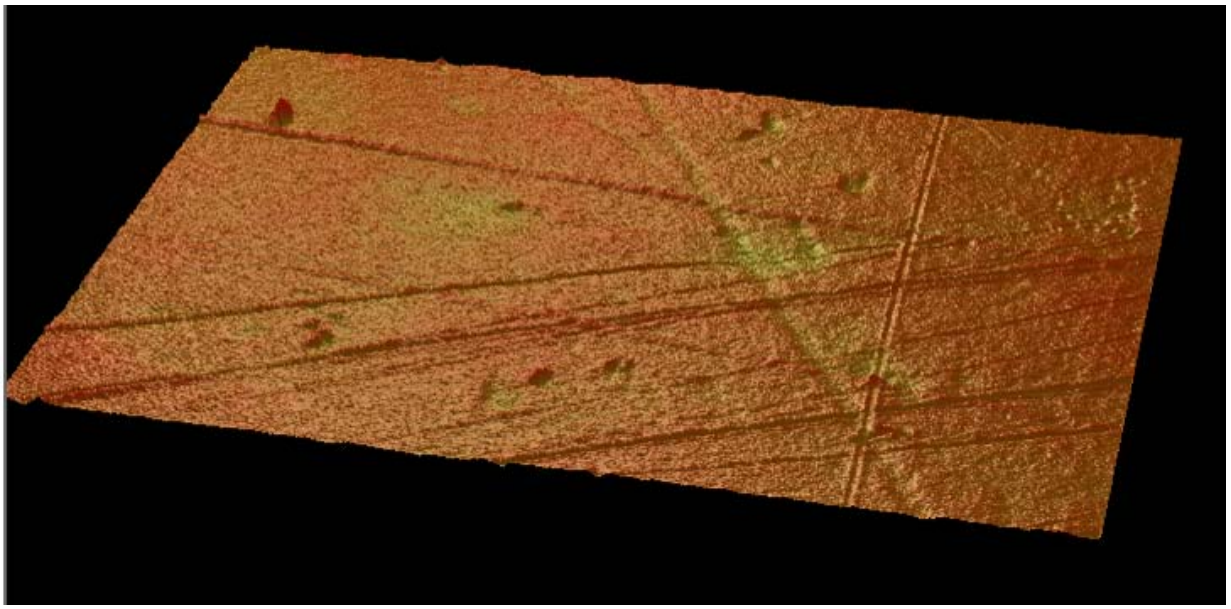

Polypropylene 10x magnification

Surface Statistics:

Ra: 104.74 nm

Rq: 142.82 nm

Rz: 1.81 um

Rt: 1.95 um

Set-up Parameters:

Size: 640 X 480

Sampling: 966.80 nm

Processed Options:

Terms Removed:

Tilt

Filtering:

None

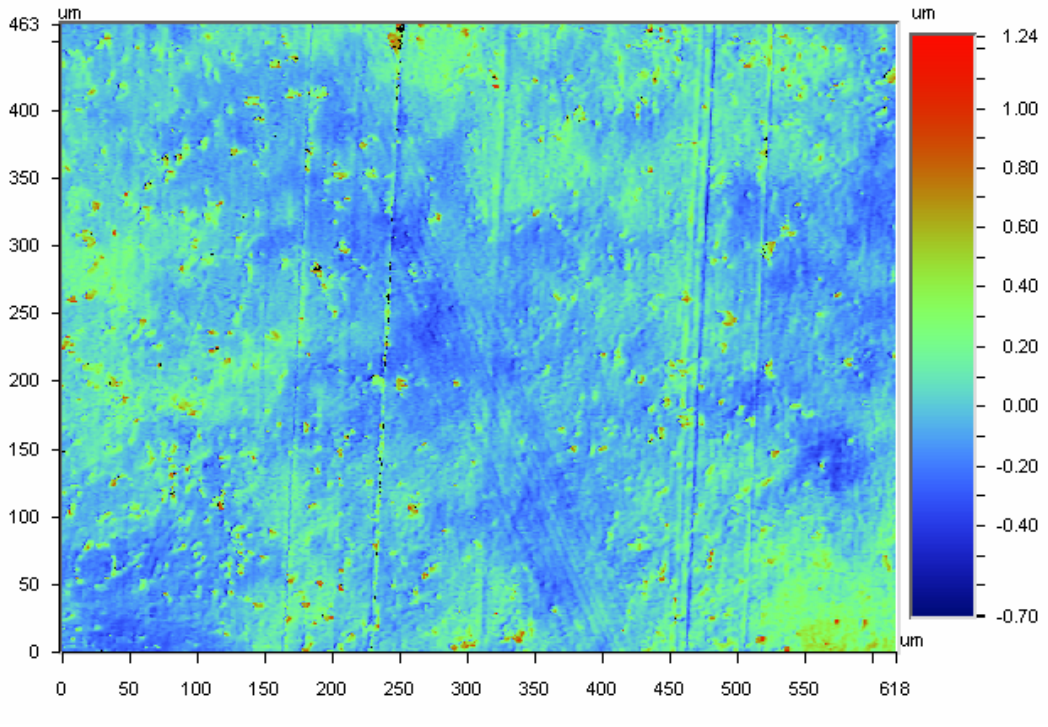

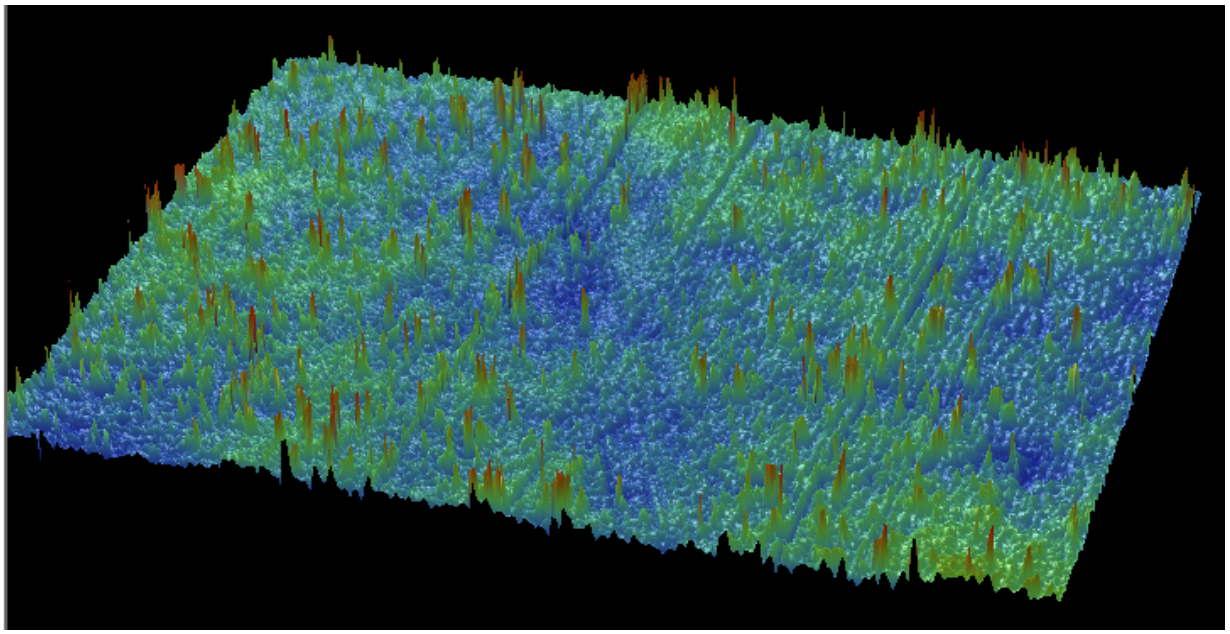

Polypropylene 50x magnification

Surface Statistics:

Ra: 53.77 nm

Rq: 75.61 nm

Rz: 1.40 um

Rt: 1.82 um

Set-up Parameters:

Size: 640 X 480

Sampling: 193.36 nm

Processed Options:

Terms Removed:

Tilt

Filtering:

None

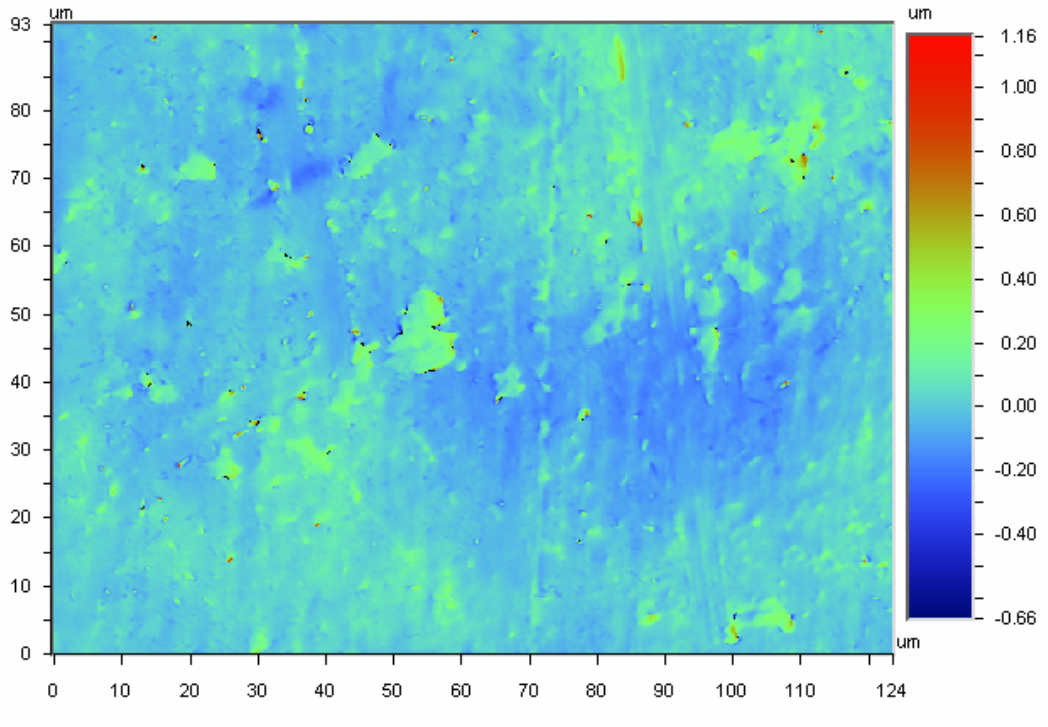

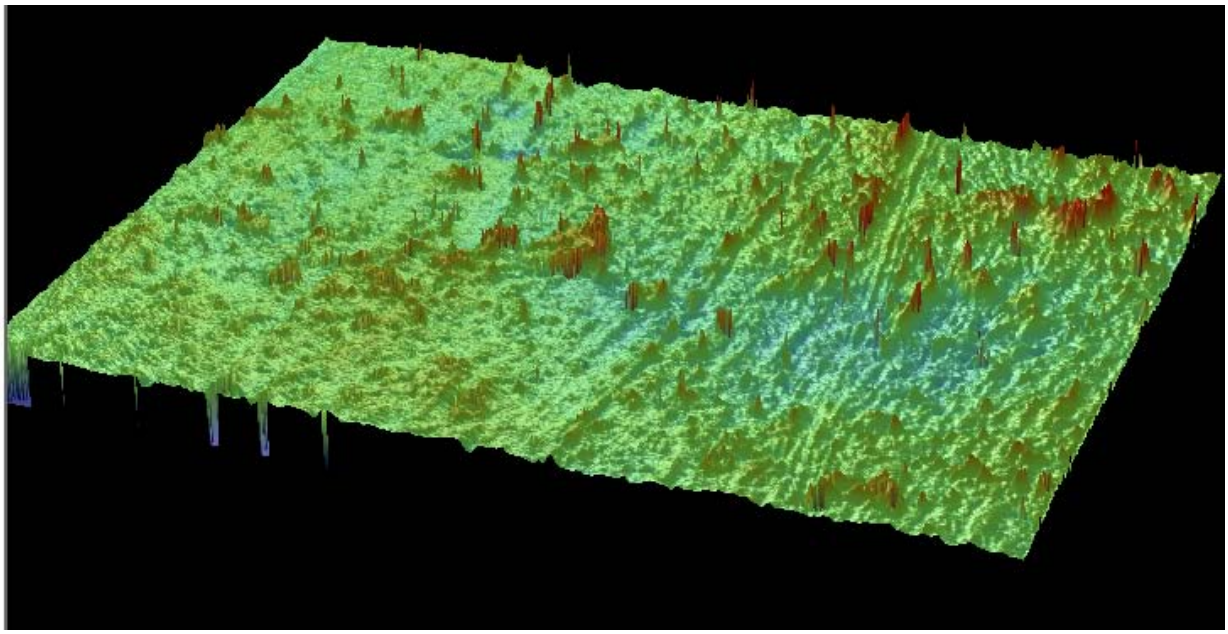

SBR 10x magnification

Surface Statistics:

Ra: 276.03 nm

Rq: 361.02 nm

Rz: 4.76 um

Rt: 6.22 um

Set-up Parameters:

Size: 640 X 480

Sampling: 966.80 nm

Processed Options:

Terms Removed:

Tilt

Filtering:

None

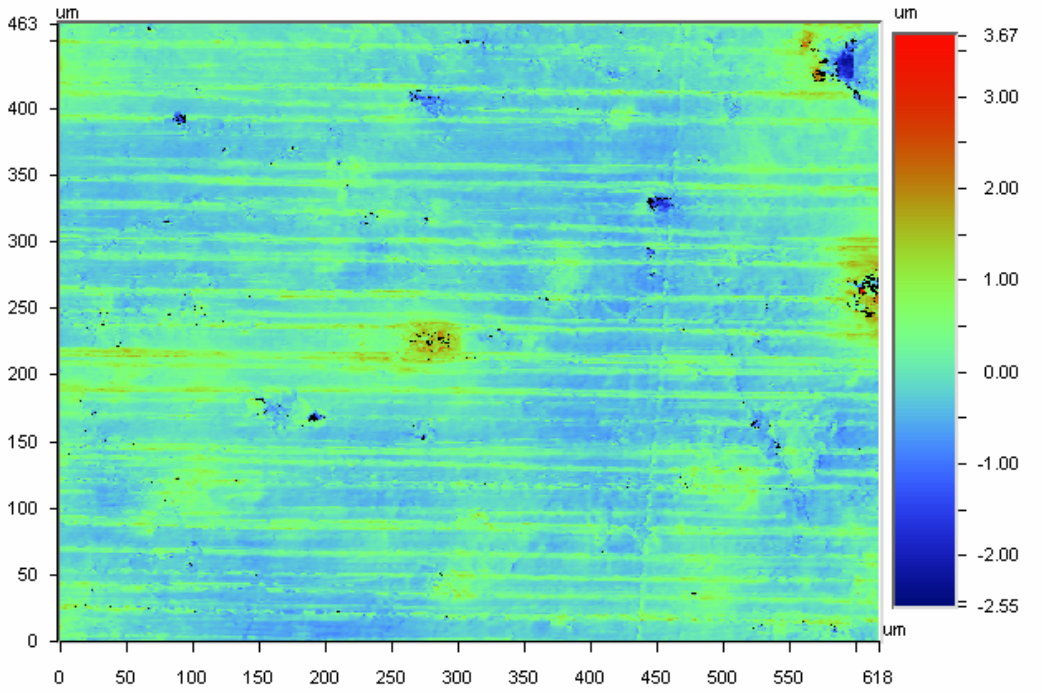

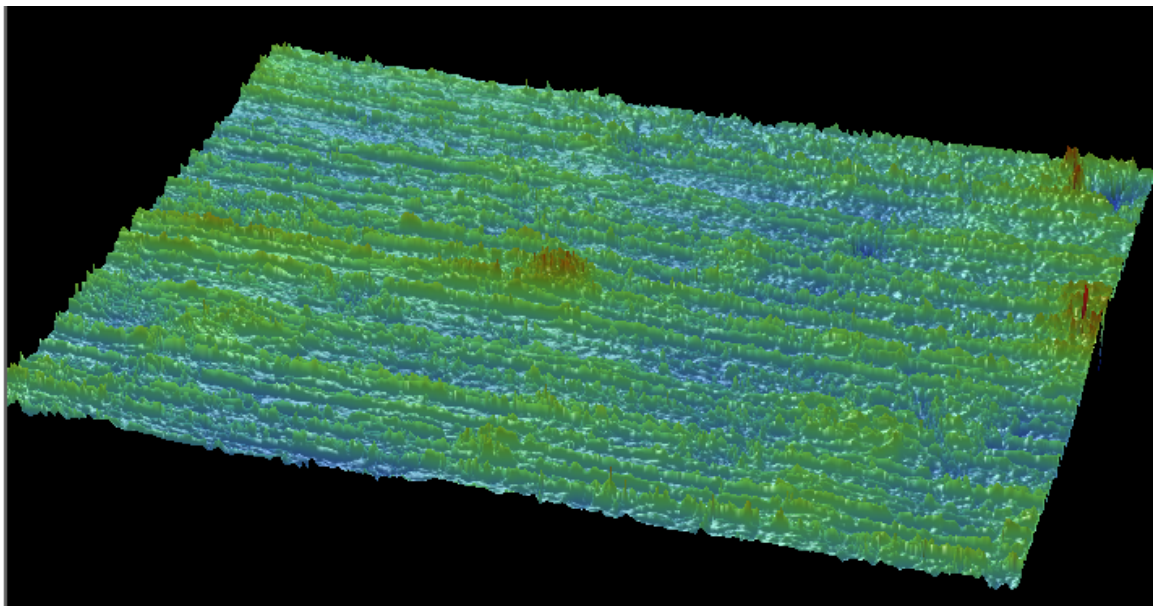

SBR 50x magnification

Surface Statistics:

Ra: 106.63 nm

Rq: 137.00 nm

Rz: 1.86 um

Rt: 2.19 um

Set-up Parameters:

Size: 640 X 480

Sampling: 193.36 nm

Processed Options:

Terms Removed:

Tilt

Filtering:

None

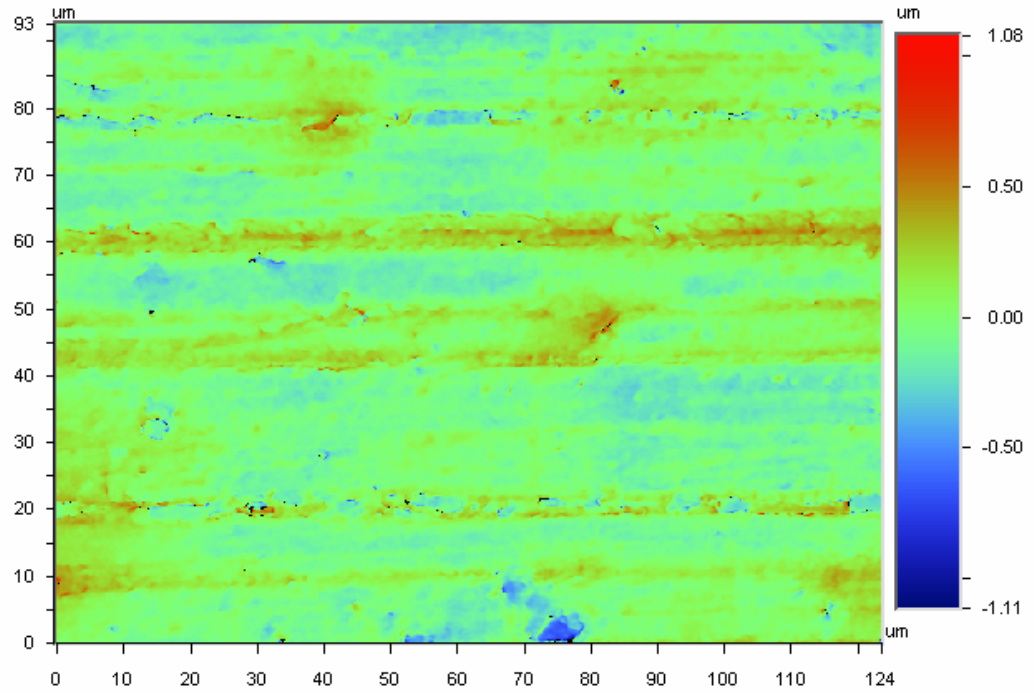

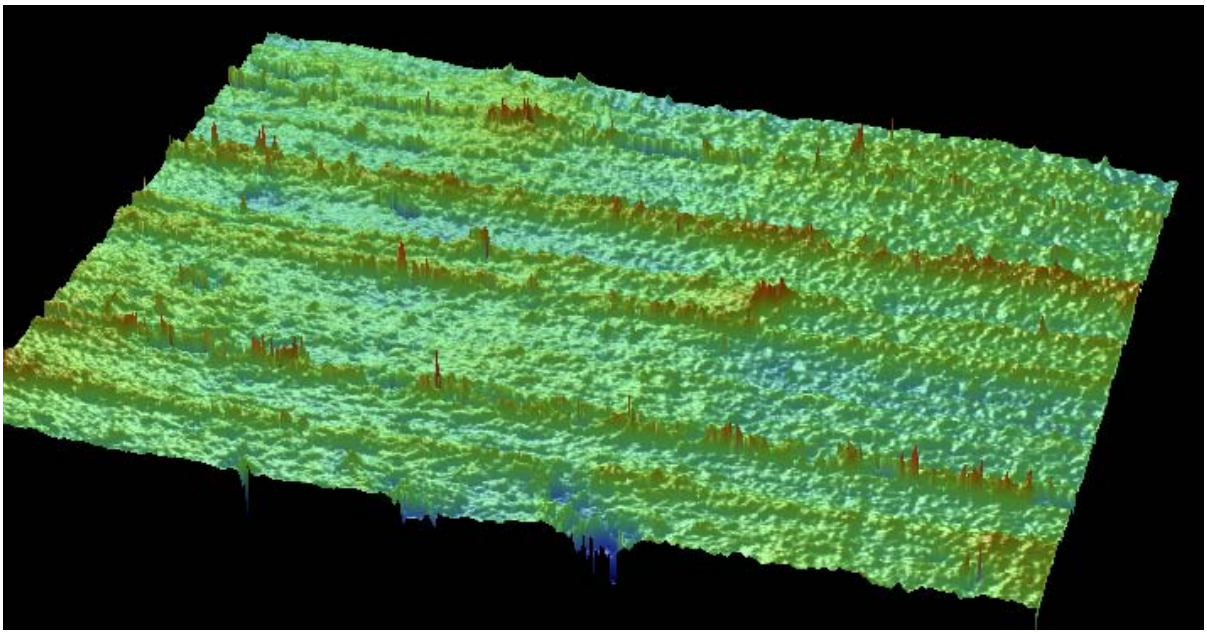

Steel 10x magnification

Surface Statistics:

Ra: 170.09 nm

Rq: 269.76 nm

Rz: 4.40 um

Rt: 5.44 um

Set-up Parameters:

Size: 640 X 480

Sampling: 966.80 nm

Processed Options:

Terms Removed:

Tilt

Filtering:

None

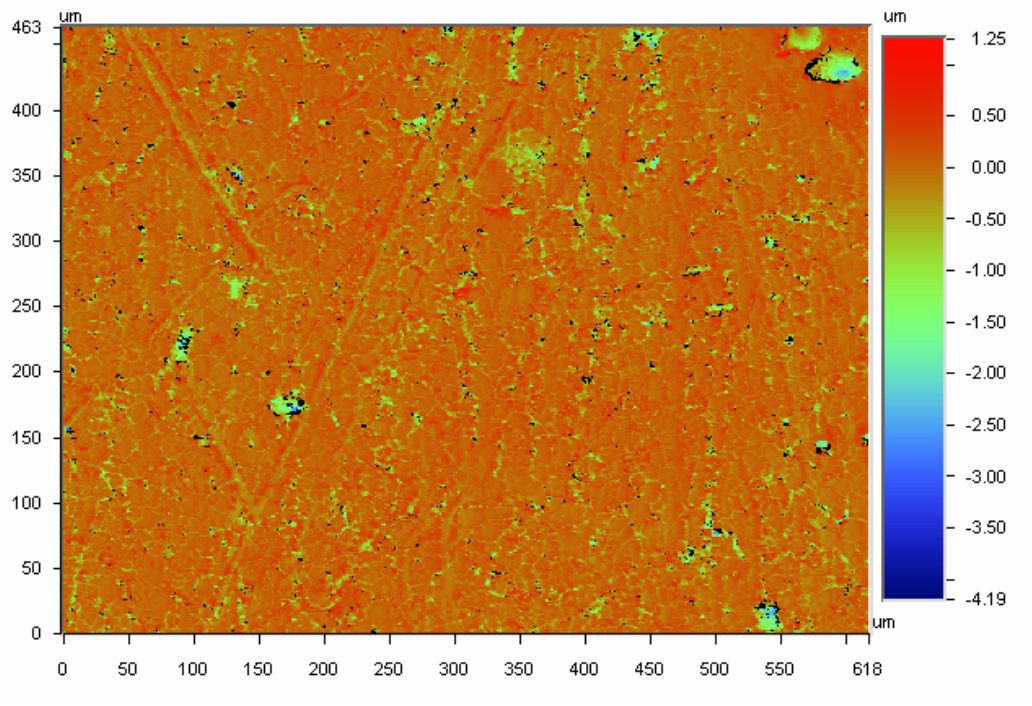

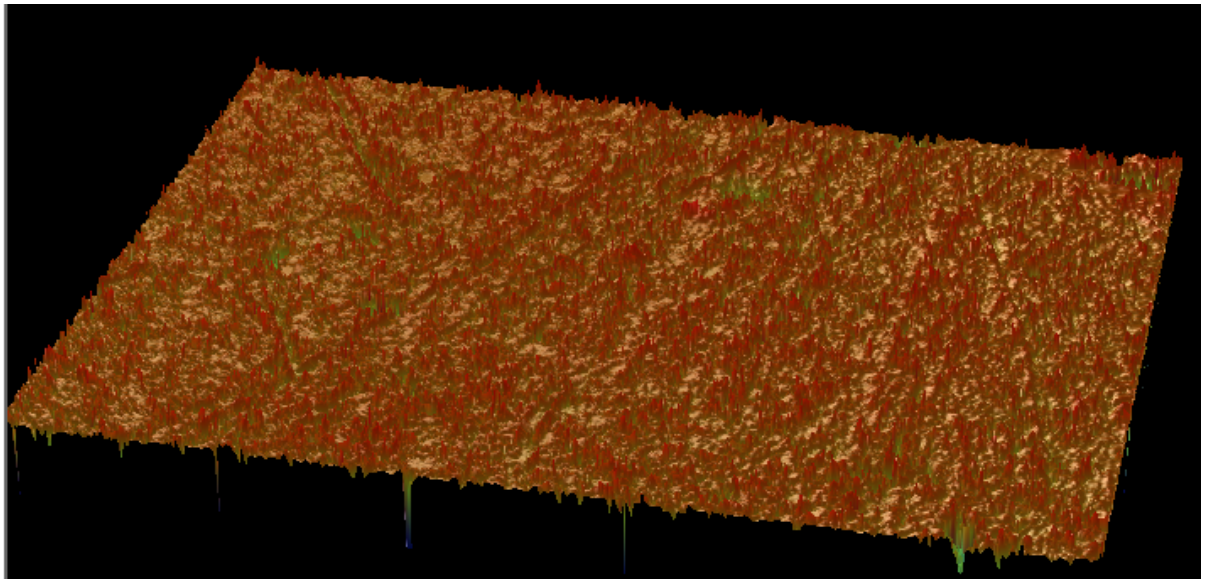

Steel 50x magnification

Surface Statistics:

Ra: 313.04 nm

Rq: 454.20 nm

Rz: 4.08 um

Rt: 4.53 um

Set-up Parameters:

Size: 640 X 480

Sampling: 193.36 nm

Processed Options:

Terms Removed:

Tilt

Filtering:

None

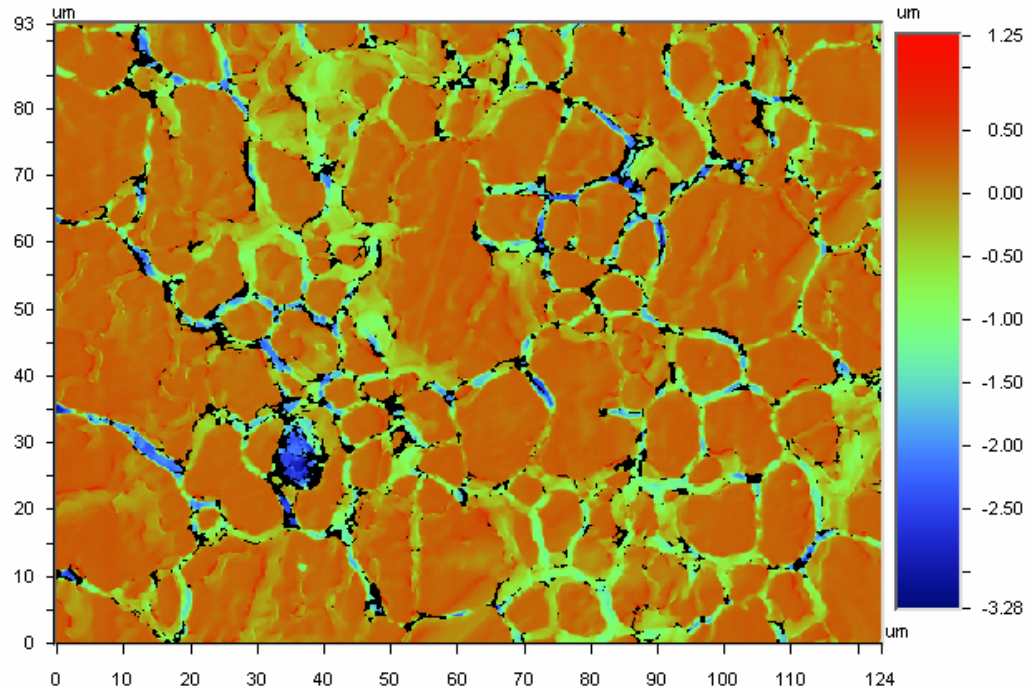

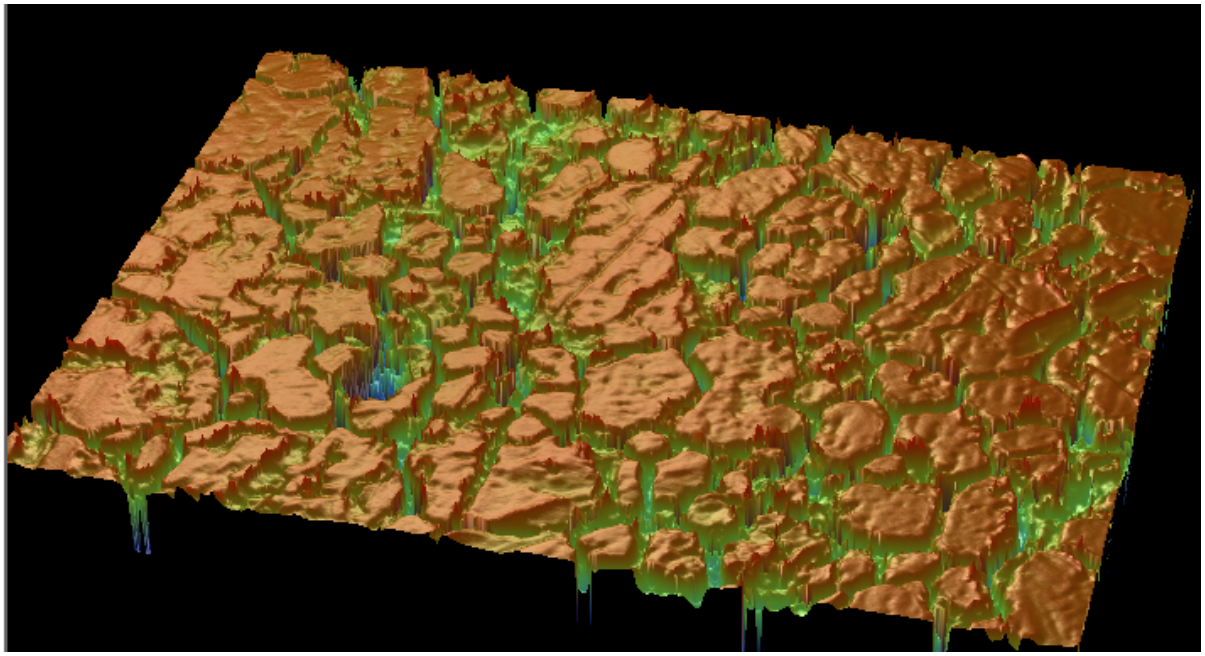

Appendix 3. Contact angle data.

Results of the experiments at 25ºC:

Pt. McIntyre

Material	Mass normalized by unit area	Cosine of Advancing angle by DCA	Cosine of Receding angle by DCA	Corrected cosine of advancing angle	Corrected advancing angle	Hysteresis in cosines
Buna - new	0.0104	0.840767	0.270233	0.7298	43	0.2702
Hypalon ®	0.020268	0.896375	0.214625	0.7854	38	0.2146
SBR	0.021114	0.776367	0.334633	0.6654	48	0.3346
Neoprene ®	0.016787	1.04122	0.06978	0.9302	22	0.0698
ECH	0.010336	1.014756	0.096244	0.9038	25	0.0962
LD Polyethylene	0.009726	1.0377	0.0733	0.9267	22	0.0733
Steel	0.007089	1.0581	0.0529	0.9471	19	0.0529
HD Polyethylene	0.008749	1.044825	0.066175	0.9338	21	0.0662
Aluminum	0.006979	1.0585	0.0525	0.9475	19	0.0525
Polypropylene	0.007995	1.0455	0.0655	0.9345	21	0.0655
ABS	0.008119	1.04892	0.06208	0.9379	20	0.0621
Delrin	0.007091	1.05854	0.05246	0.9475	19	0.0525
Acetal	0.009087	1.0372	0.0738	0.9262	22	0.0738
PVC	0.005464	1.0661	0.0449	0.9551	17	0.0449

HydroCal 300

Material	Mass normalized by unit area	Cosine of Advancing angle by DCA	Cosine of Receding angle by DCA	Corrected cosine of advancing angle	Corrected advancing angle	Hysteresis in cosines
Polypropylene	0.015551	0.888275	0.222725	0.7773	39	0.2227
HD Polyethylene	0.014601	0.92935	0.18165	0.8184	35	0.1817
LD Polyethylene	0.013411	0.958538	0.152463	0.8475	32	0.1525
Steel	0.013964	0.94745	0.16355	0.8365	33	0.1636
Aluminum	0.01365	0.950629	0.160371	0.8396	33	0.1604
Buna	0.013325	0.7572	0.3538	0.6462	50	0.3538
Neoprene®	0.020309	0.842322	0.268678	0.7313	43	0.2687
Hypalon ®	0.016758	0.746557	0.364443	0.6356	51	0.3644
SBR	0.01612	0.631186	0.479814	0.5202	59	0.4798
ECH	0.0142	0.748	0.363	0.6370	50	0.3630

IFO-120

Material	Mass normalized by unit area	Cosine of Advancing angle by DCA	Cosine of Receding angle by DCA	Corrected cosine of advancing angle	Corrected advancing angle	Hysteresis in cosines
Steel	0.026143	0.8501	0.2609	0.7391	42	0.2609
Aluminium	0.023937	0.847367	0.263633	0.7364	43	0.2636
Polypropylene	0.030378	0.725633	0.385367	0.6146	52	0.3854
HD Polyethylene	0.029272	0.77545	0.33555	0.6645	48	0.3356
LD Polyethylene	0.028737	0.76735	0.34365	0.6564	49	0.3437
Hypalon ®	0.0325	0.5856	0.5254	0.4746	62	0.5254
Neoprene®	0.036627	0.514143	0.596857	0.4031	66	0.5969
ECH	0.031989	0.584633	0.526367	0.4736	62	0.5264
SBR	0.035029	0.514143	0.596857	0.4031	66	0.5969
Buna	0.0303	0.5961	0.5149	0.4851	61	0.5149

Results of the experiments at 15ºC:

Cook's Inlet

Material	Mass normalized by unit area	Cosine of Advancing angle by DCA	Cosine of Receding angle by DCA	Corrected cosine of advancing angle	Corrected advancing angle	Hysteresis in cosines
ABS	0.0050	1.0605	1.1768	0.9495	18	0.0505
Aluminum	0.0050	1.0525	1.0469	0.9415	20	0.0585
LD Polyethylene	0.0045	1.0749	1.0710	0.9639	15	0.0361
Polypropylene	0.0060	1.0285	1.0651	0.9175	23	0.0825
Steel	0.0053	1.0526	1.0466	0.9416	20	0.0584
Neoprene®	0.0204	0.9205	1.1625	0.8095	36	0.1905
Hypalon ®	0.0194	0.9683	1.1358	0.8573	31	0.1427
SBR	0.0189	0.8754	1.1618	0.7644	40	0.2356
ECH	0.0071	0.8967	1.0540	0.7857	38	0.2143

Pt. McIntyre

material	Mass normalized by unit area	Cosine of Advancing angle by DCA	Cosine of Receding angle by DCA	Corrected cosine of advancing angle	Corrected advancing angle	Hysteresis in cosines
ABS	0.0086	1.0056	1.0454	0.8946	27	0.1054
Aluminum	0.0096	0.9496	1.0373	0.8386	33	0.1614
LD Polyethylene	0.0061	1.0526	1.1489	0.9416	20	0.0584
Polypropylene	0.0095	0.9656	1.1032	0.8546	31	0.1454
Steel	0.0091	0.9749	1.0487	0.8639	30	0.1361
Delrin	0.0091	1.0090	1.0286	0.8980	26	0.1020
Neoprene®	0.0150	0.8645	1.1746	0.7535	41	0.2465
SBR	0.0182	0.8560	1.1660	0.7452	42	0.2548
Hypalon ®	0.0226	0.8873	1.1303	0.7759	39	0.2241
Viton	0.0086	0.8070	1.1425	0.6962	45	0.3038

ECH	0.0121	0.8355	1.0732	0.7241	44	0.2759

HydroCal-300

Material	Mass normalized by unit area	Cosine of Advancing angle by DCA	Cosine of Receding angle by DCA	Corrected cosine of advancing angle	Corrected advancing angle	Hysteresis in cosines
ABS	0.0224	0.8623	1.1520	0.7513	41	0.2487
Aluminum	0.0224	0.8414	1.1307	0.7304	43	0.2696
LD Polyethylene	0.019145	0.908767	1.15105	0.7978	37	0.2022
Polypropylene	0.026209	0.762483	1.192833	0.6515	49	0.3485
Steel	0.022276	0.85006	1.12882	0.7391	42	0.2609
ECH	0.021321	0.580583	1.138017	0.4696	62	0.5304
Neoprene®	0.022844	0.631733	1.1841	0.5207	59	0.4793
SBR	0.022323	0.605733	1.16735	0.4947	60	0.5053
Hypalon ®	0.022386	0.644117	1.168633	0.5331	58	0.4669

IFO-120

Material	Mass normalized by unit area	Cosine of Advancing angle by DCA	Cosine of Receding angle by DCA	Corrected cosine of advancing angle	Corrected advancing angle	Hysteresis in cosines
ABS	0.0479	0.6305	1.3504	0.5195	59	0.4805
Aluminum	0.0477	0.6758	1.3110	0.5648	56	0.4352
LD Polyethylene	0.046447	0.740333	1.424833	0.6293	51	0.3707
Polypropylene	0.047789	0.5807	1.326	0.4697	62	0.5303
Steel	0.047497	0.67112	1.30802	0.5601	56	0.4399
SBR	0.059863	0.40918	1.39862	0.2982	73	0.7018
Hypalon ®	0.061526	0.420775	1.434975	0.3098	72	0.6902
Neoprene®	0.065484	0.49316	1.45114	0.3822	68	0.6178
ECH	0.048885	0.321225	1.318225	0.2102	78	0.7898

Cook's Inlet weathered (15% weight loss)

Material	Mass normalized by unit area	Cosine of Advancing angle by DCA	Cosine of Receding angle by DCA	Corrected cosine of advancing angle	Corrected advancing angle	Hysteresis in cosines
ABS	0.0078	1.0311	1.0458	0.9201	23	0.0800
Aluminum	0.010499	0.96964	1.00392	0.8586	31	0.1414
LD Polyethylene	0.009251	0.98845	1.01525	0.8775	29	0.1226
Polypropylene	0.009106	1.002567	1.0752	0.8916	27	0.1084
Steel	0.010324	0.954975	0.99135	0.8440	32	0.1560
ECH	0.01237	0.88876	1.03406	0.7778	39	0.2222
SBR	0.017212	0.847933	1.0752	0.7369	43	0.2631
Hypalon ®	0.015415	0.871075	1.08565	0.7601	41	0.2399
Neoprene ®	0.019707	0.869825	1.1626	0.7588	41	0.2412

Pt. McIntyre weathered (15% weight loss)

Material	Mass normalized by unit area	Cosine of Advancing angle by DCA	Cosine of Receding angle by DCA	Corrected cosine of advancing angle	Corrected advancing angle	Hysteresis in cosines
ABS	0.0125	0.9775	1.0554	0.8665	30	0.1335
Aluminum	0.013145	0.982	1.05645	0.8710	29	0.1290
LD Polyethylene	0.017814	0.9668	1.11205	0.8558	31	0.1442
Polypropylene	0.017315	0.968775	1.168775	0.8578	31	0.1422
Steel	0.015886	0.971575	1.091375	0.8606	31	0.1394
Polyethylene	0.019118	0.9635	1.14345	0.8525	32	0.1475
SBR	0.021569	0.74928	1.17864	0.6383	50	0.3617
Hypalon ®	0.019354	0.796174	1.163243	0.6852	47	0.3148
ECH	0.017312	0.818543	1.163514	0.7075	45	0.2925
Neoprene ®	0.020826	0.753333	1.142617	0.6423	50	0.3577

Results of the experiments at 5ºC:

Pt. McIntyre

Material	Mass normalized by unit area	Cosine of Advancing angle by DCA	Cosine of Receding angle by DCA	Corrected cosine of advancing angle	Corrected advancing angle	Hysteresis in cosines
Hypalon ®	0.019922	0.831438	1.22515	0.7204	44	0.2796
Neoprene ®	0.018975	0.80156	1.2459	0.6906	46	0.3094
SBR	0.026222	0.866967	1.31436	0.7560	41	0.2440
ECH	0.016505	0.7851	1.21658	0.6741	48	0.3259
LD Polyethylene	0.012245	1.0510	1.1361	0.9400	20	0.0600
Polypropylene	0.011486	1.0710	1.1629	0.9600	16	0.0400
Steel	0.013008	1.0223	1.1386	0.9113	24	0.0887
Aluminum	0.013318	0.9884	1.1220	0.8774	29	0.1226

HydroCal 300

Material	Mass normalized by unit area	Cosine of Advancing angle by DCA	Cosine of Receding angle by DCA	Corrected cosine of advancing angle	Corrected advancing angle	Hysteresis in cosines
Hypalon ®	0.040599	0.55475	1.36445	0.4438	64	0.5563
Neoprene ®	0.039265	0.468125	1.32365	0.3571	69	0.6429
SBR	0.040229	0.52906	1.31724	0.4181	65	0.5819
ECH	0.039009	0.446633	1.2849	0.3356	70	0.6644
LDPE	0.038653	0.749711	1.334878	0.6387	50	0.3613
Polypropylene	0.039279	0.66895	1.350975	0.5580	56	0.4421
Aluminum	0.038053	0.7881	1.2636	0.6771	47	0.3229
Steel	0.03711	0.840042	1.270325	0.7290	43	0.2710